**University of Urbino Carlo Bo**

Department of Biomolecular Sciences (DISB)

---

PhD COURSE IN: LIFE SCIENCES, HEALTH AND BIOTECHNOLOGY

CURRICULUM: BIOLOGY OF CELLS AND ORGANISMS

CICLO XXXIV

# EVs from *C. jejuni* CDT intoxicated-Caco-2 cells differently inhibit proliferation in tumour intestinal epithelial and myeloid cells: potential utility for antitumor strategies

**SSD: BIO/16**

**Coordinator:** Ch.mo Prof. Marco Bruno Luigi Rocchi

**Supervisor**: Ch.ma Prof.ssa Francesca Luchetti

**Co-Supervisor**: Ch.ma Prof.ssa Barbara Canonico

**PhD candidate**: Mariele Montanari

ACADEMIC YEAR 2021/2022

# INDEX

**ABSTRACT**

*Campylobacter jejuni* is a Gram-negative spiral-shaped bacterium that is the most prevalent cause of human's gastroenteritis, responsible for over 500 million cases of gastroenteritis in the world over each year. The Cytolethal Distending Toxin (CDT) represents an important virulence factor, it is a heterotrimeric complex composed of CdtA, CdtB, and CdtC. CdtA and CdtC constitute the regulatory subunits and CdtB the catalytic subunit exhibiting phosphatase and DNase activities, resulting in cell cycle arrest and cell death. Moreover, an important complication of *C. jejuni* enteritis is Guillain-Barré syndrome (GBS), an acute autoimmune inflammatory demyelinating polyneuropathy. Macrophages have been implicated in both initiation and resolution of Experimental Autoimmune Neuritis (EAN), the animal model of GBS. Effective functioning of these cells requires intercellular communication between myeloid cells, primary epithelial infected cells, and other types of immune cells. Mediators of intercellular communication are extracellular vesicles (EVs). They play important roles in normal cell-to-cell communications but can also spread pathogen- and host-derived molecules during infections to alter immune responses. The thesis focuses on multiple aspects:

A. The effects of CDT on U937 myeloid cells, drawing the involvement of lysosomal and endosomal compartment, ER-remodelling and mitochondria network. Rapamycin, an efficient inhibitor of the mammalian target of rapamycin (mTOR), acts as a mitigating factor of the intoxication.
B. Mitochondrial modifications, deep changes in lysosomal exocytosis, secretory autophagy and EV release were registered in intestinal epithelial Caco-2 cells, particularly induced by the wild-type strain, compared to the mutant strain. Caco-2 cells respond to stimuli by activating the crosstalk between the autophagic and the endosomal system, largely involved in bacterial infections. Through the co-culture model between Caco-2 and U937, we deduce that CDT-like effects are transferred by Caco-2 cells to uninfected U937 cells.
C. The role of EVs from *C. jejuni* Caco-2 infected cells in modulating the myeloid response during CDT treatment (mimicking the *in vivo* cellular interactions, possibly leading to GBS). Indeed, EVs represent a mechanism to spread the active CDT on both myeloid and intestinal cells revealing that in their cargo the active toxin is still present. Since CDT is an antiproliferative factor, these EVs act as antitumor agents, in our *in vitro* model.

In summary, CDT targets endo-lysosomal compartment, partially eluding lysosomal degradation and exploiting unconventional secretion (EV release). This scenario is observed in both intestinal epithelial and myeloid cells. EVs are the primary routes to spread the efficient CDT among homologous and heterologous cells, and, due to the typical arrest of proliferation, their possible use is envisaged in anticancer strategies, on which engineered CDTs are recently considered for targeted therapies.

# INTRODUCTION

## *1.1 Campylobacter jejuni*

To date, the genus *Campylobacter* includes 32 formally described species and 9 subspecies (Costa and Iraola, 2019). The most known species are *Campylobacter jejuni* and *Campylobacter coli* that are mainly associated with campylobacteriosis in humans (Møller Nielsen, Engberg and Madsen, 1997; Gillespie *et al.*, 2002).

*C. jejuni* is a flagellated Gram-negative bacillus with a characteristic spiral shape, has a variable length and thickness (0.2-5 x 0.2-0.5 μm) (**Figure 1**). It is a microaerophilic bacterium as it requires a concentration of $O_2$ equal to 3-15% and $CO_2$ equal to 3-5%, and is thermophilic with optimum growth temperature 37-42°C. The upper temperature reflects the adaptation to the temperatures found in the intestines of warm-blooded animals and in avians (Ketley, 1997; Harrer *et al.*, 2019).

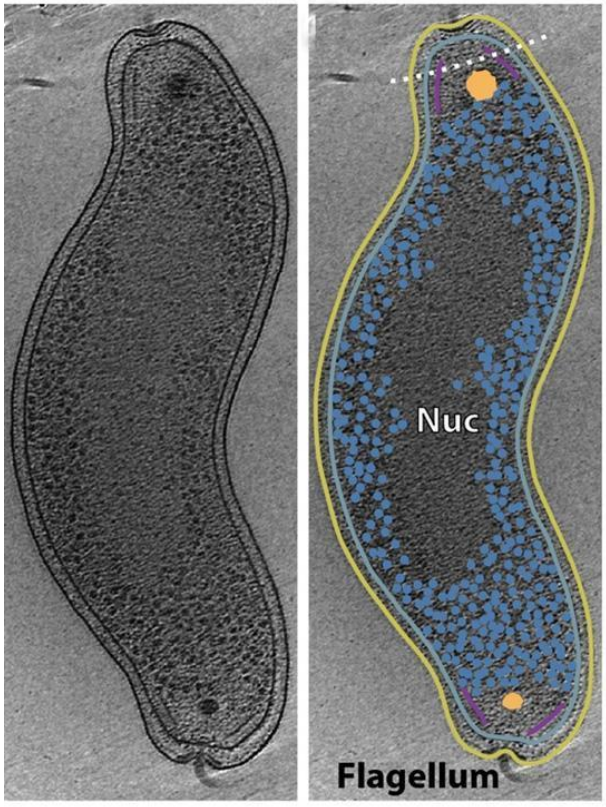


**Figure 1**: Ultrastructure of *C. jejuni* by electron cryotomography: in gold are highlight outer membrane, in light blue inner membrane, in purple chemoreceptors, blue spheres ribosomes, in orange storage granules, and nucleoid (Nuc) (Müller *et al.*, 2014).

## *1.2 Campylobacter jejuni: epidemiology*

Microorganisms of the genus *Campylobacter* are recognized as one of the main causes of gastroenteritis in humans. *C. jejuni* is currently one of the most common causes of human bacterial enterocolitis in Europe, often with more cases than other similar pathogens such as *Salmonella*, *Shigella* and *Escherichia coli* (European Food Safety Authority and European Centre for Disease Prevention and Control, 2019). The European Union reported 246,571 cases about *Campylobacter* contamination in 2018, and 83.9% were caused by *C. jejuni*, which accounts for the highest contamination rate compared to other *Campylobacter* species (**Figure 2**) (European Food Safety Authority and European Centre for Disease Prevention and Control, 2019). Sixty deaths due to campylobacteriosis were reported in 2018, resulting in an EU case fatality of 0.03%.

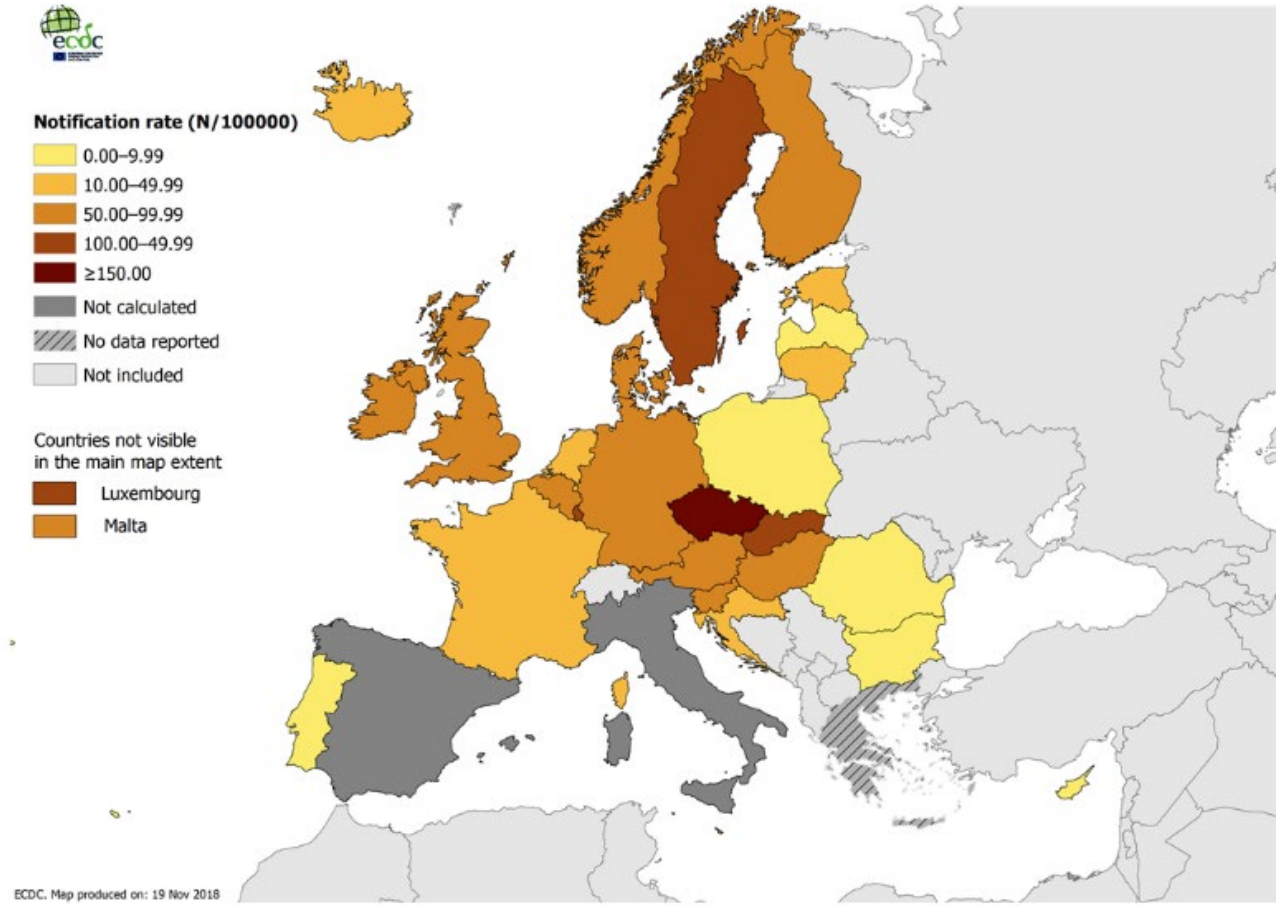


**Figure 2**: Distribution of confirmed campylobacteriosis cases per 100 000 population in Europe countries.(European Centre for Disease Prevention and Control, 2019).

*Campylobacter* has a seasonality characteristic, with a strong increase in the number of cases from late spring to early autumn (Skirrow, 1987; Sari Kovats *et al.*, 2005; Olson *et al.*, 2014). Between 2013 and 2017, the number of confirmed campylobacteriosis cases reveals a clear recurrent trend, reported in

Europe, with peaks in the summer months (**Figure 3**). Annual winter peaks, although with lower numbers compared with summer, were also observed in January annually from 2013 to 2017. Increased travel, the number of barbeque and uncooked meat during the holiday season might be an explanation of the increase in many countries (European Food Safety Authority and European Centre for Disease Prevention and Control, 2019). Despite comprehensive surveillance and national coverage in 25 countries, reported cases represent only a small proportion of *Campylobacter* infections occurring in Europe.

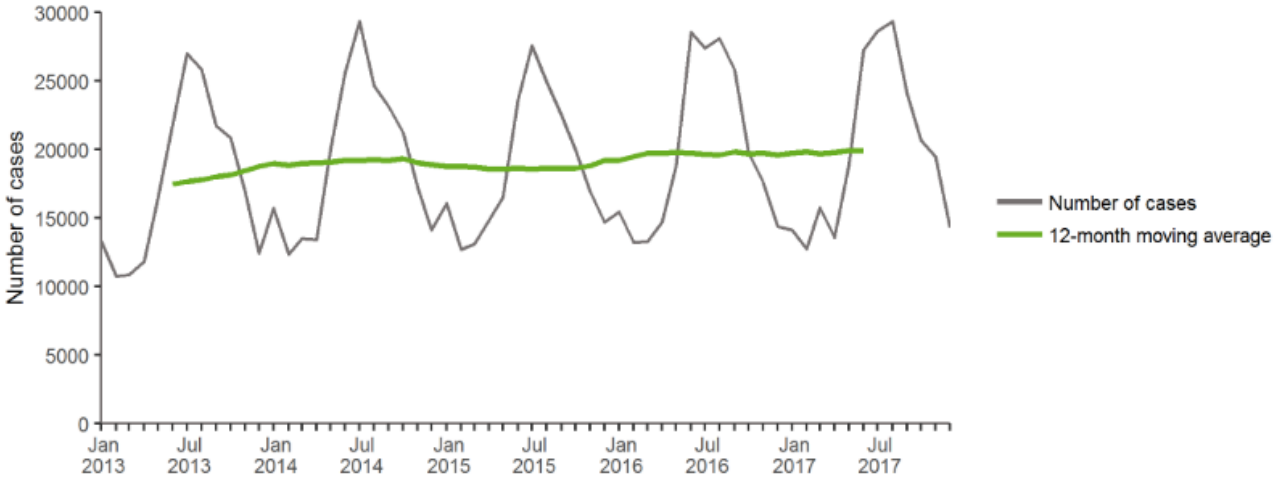


**Figure 3**: Distribution of confirmed campylobacteriosis cases by month from 2013 to 2017 in Europe (European Centre for Disease Prevention and Control, 2019).

### *1.3 Campylobacter jejuni: pathology*

*C. jejuni* is responsible of human enterocolitis, and typically after a 2 to 5 day incubation period, it causes diarrhoea, cramping, abdominal pain, and fever with a duration of up to a week and it is normally self-limiting in immunocompetent patients (Chen *et al.*, 2006; Schnee and Petri, 2017).

In low-resource areas, *Campylobacter* infections affect mainly children; this early infection, in children younger than 1 year, are correlated with stunted growth and therefore life-long physical and cognitive deficits (Amour *et al.*, 2016; Ijaz *et al.*, 2018). *C. jejuni* is distinct from other causes of dysentery in its association with post-infectious complications such as Guillain–Barré syndrome (GBS), reactive arthritis and post-infectious irritable bowel syndrome (PI-IBS) (Dempe *et al.*, 2013; Card *et al.*, 2018; Harrer *et al.*, 2019; Vojdani and Vojdani, 2019). Approximately 1/1000 people develop GBS following *C. jejuni* infection (Nyati *et al.*, 2013). GBS is a rare post-infectious neuropathy, characterised by acute or subacute symmetrical ascending motor weakness, areflexia and mild to moderate sensory abnormalities (Nyati *et al.*, 2013). GBS has become the most common

cause of acute flaccid paralysis in the post-polio era (Amon *et al.*, 2012; Wijdicks and Klein, 2017). GBS occurs a week or two after a gastrointestinal or a respiratory infection or other immune stimulus that triggers an atypical autoimmune response that affects the peripheral nerves and their spinal roots (Wachira, Peixoto and de Oliveira, 2019). The immune response depends on certain bacterial factors, such as the specificity of liposaccharide/lipooligosaccharide LPS/LOS and patient-related/host factors. Both humoral and cellular immune response associated with autoantibodies and activated lymphocytes work in coordination in the pathogenesis of *C. jejuni*-associated GBS. Antibodies to LPS/LOS can cross-react with specific nerve gangliosides and can activate the complement system (**Figure 4**) (Nyati et al., 2013).

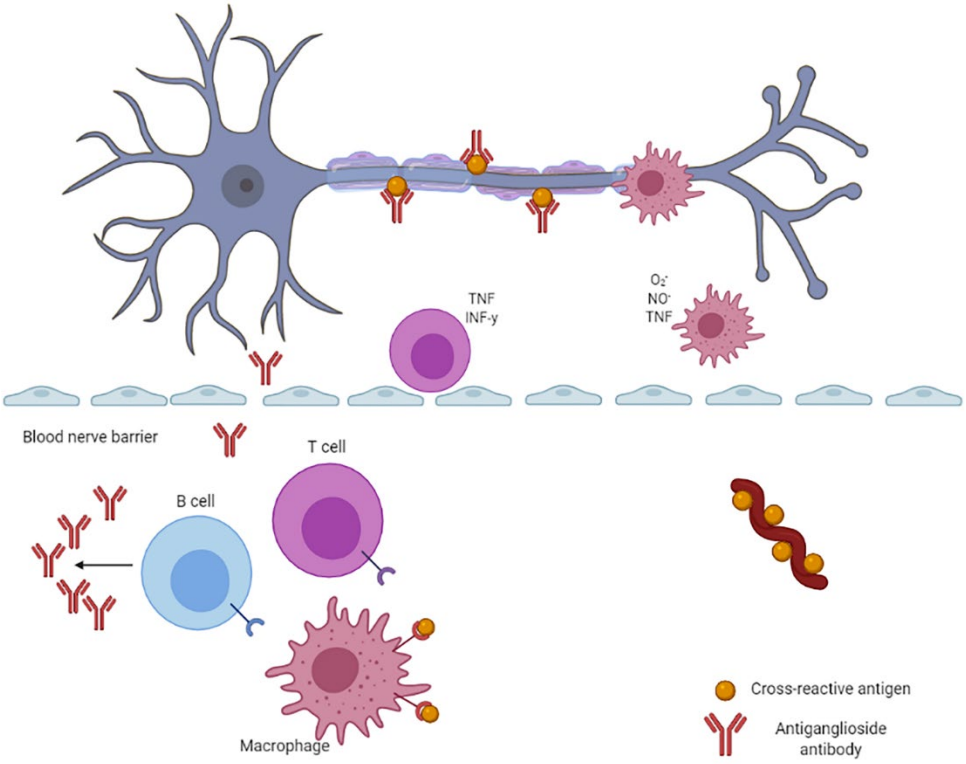


**Figure 4:** Origin and contribution of *C. jejuni* infection to Guillain-Barré syndrome pathogenesis. A bacterial cross-reactive antigen recognized by macrophages and T cells that help B cells to produce antiganglioside antibodies, which penetrate blood nerve barrier and activate complement. These antibodies bind with specific nerve gangliosides and *C. jejuni* antigen. Activated macrophages release cytokines and free radicals (nitric oxide), invade compact myelin, periaxonal space, and sometimes block nerve conduction or cause axonal degeneration. Activated T cells release proinflammatory cytokines and in the end produce dissolution of myelin. Image adapted from (Nyati *et al.*, 2013). Created in Biorender.com.

### *1.4 Campylobacter jejuni: mode of transmission*

*C. jejuni* is generally considered a commensal organism of avians and so, are considered an environmental reservoir. It colonises the gastrointestinal tract of the chicken, mainly in the mucous layer, and is transmitted to the chicks through the faecal-oral route. *C. jejuni* can infect humans directly through the consumption of contaminated food, especially derived from poultry, unpasteurized milk and water (**Figure 5**) (Kapperud et al. 1992; Neimann et al. 2003; Friedman et al. 2004). In humans, *C. jejuni* can invade the intestinal epithelial layer, causing inflammation and diarrhoea.

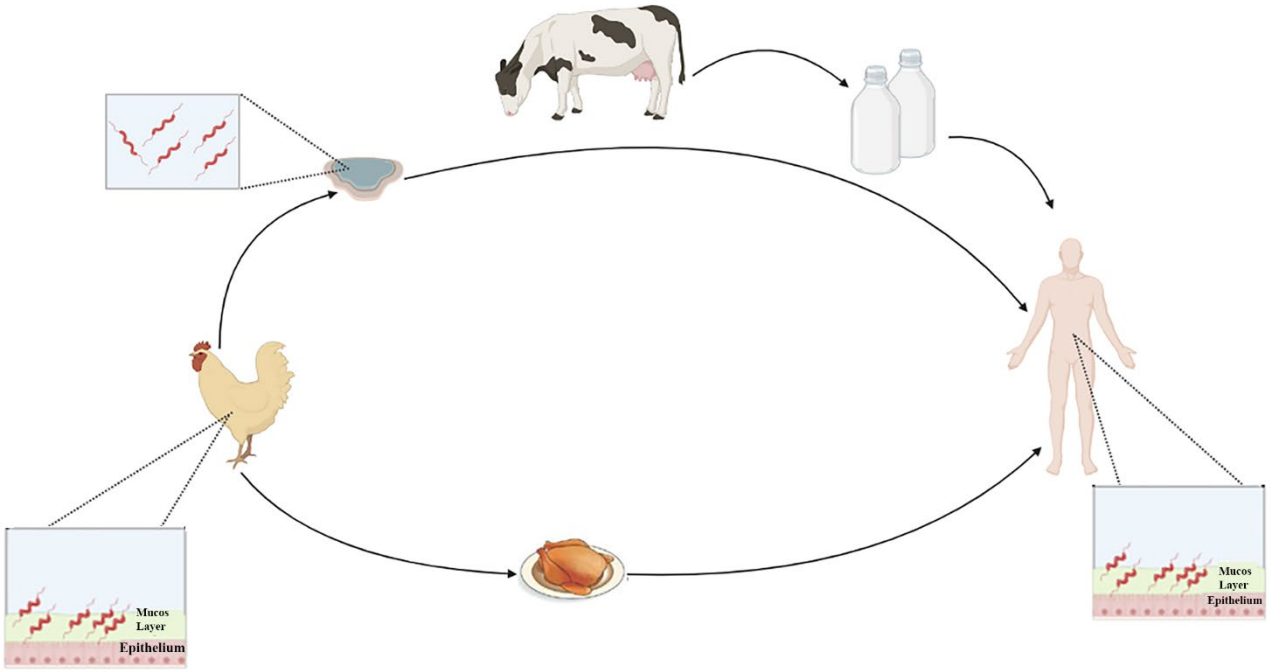


**Figure 5**: The sources and outcomes of *Campylobacter jejuni* infection. Several environmental reservoirs can lead to human infection by *C. jejuni*. It colonises the chicken gastrointestinal tract in high numbers. *C. jejuni* can infect humans directly through the drinking water or through the consumption of contaminated animal products, such as unpasteurized milk or meat, particularly poultry. In humans. Image adapted from (Young, Davis and DiRita, 2007). Created in Biorender.com

### *1.5 Campylobacter jejuni: pathogenesis*

*C. jejuni* harbours numerous virulence factors, such as an O-linked glycosylated flagella (Wassenaar, Bleumink-Pluym and Van Der Zeijst, 1991; Mertins *et al.*, 2013), Type VI Secretion System (Liaw *et al.*, 2019), a polysaccharide capsule and lipooligosaccharide (LOS) (Bacon *et al.*, 2001), various adhesins (Monteville, Yoon and Konkel, 2003), a cytolethal distending toxin (CDT) (Whitehouse *et*

*al.*, 1998; Lara-Tejero and Galán, 2001), and multiple proteases (Elmi *et al.*, 2016, 2018). The helical shape of *C. jejuni* cell and its flagella are postulated to contribute to the colonisation of the intestine and the natural motility observed in viscous environments (Ferrero and Lee, 1988; Szymanski *et al.*, 1995; Shigematsu *et al.*, 1998). The polysaccharide capsule covers the surface of *C. jejuni* and is described in several bacterial species (Cress *et al.*, 2014), being responsible for various functions related to virulence, such as protection to desiccation, adherence, colonisation and resistance to host immune system (Maue *et al.*, 2013; Lopes *et al.*, 2021). LPSs and LOSs are families of phosphorylated lipoglycans and glycolipids that are considered toxic with potent immunomodulating and immune stimulating properties. LOS is located on the *Campylobacter* surface and is related to adhesion and invasion of epithelial cells (Hameed *et al.*, 2020). However, the analogy between the LOS structure of some *C. jejuni* strains and the neuronal gangliosides can cause a cross-reactive antibody response, maybe implicated in GBS manifestation (Islam *et al.*, 2012).

Most recently, the Type VI Secretion System (T6SS) of *C. jejuni* was discovered as a factor which might be involved in virulence. This system enables the contact-dependent secretion of effector proteins into host cells and even other bacteria. However, the function and variability of T6SSs and effectors among *C. jejuni* strains is still poorly understood (Ugarte-Ruiz *et al.*, 2015; Liaw *et al.*, 2019; Robinson *et al.*, 2021).

An alternative machinery to deliver potential virulence determinants are outer membrane vesicles (OMVs), which can act as a general secretion pathway among Gram-negative bacteria and are of particular importance for *C. jejuni* virulence and survival. OMVs are spherical proteasomes, with a diameter of 10-500 nm (Mashburn-Warren, McLean and Whiteley, 2008). These structures are formed by phospholipids, membrane proteins, lipooligosaccharides but are also enriched by virulence factors and toxins. OMV identifiable in the supernatant of *C. jejuni* cultures contain a biologically active toxin: Cytolethal Distending Toxin (CDT) a nuclease that causes DNA damage and therefore the arrest of the cell cycle in the host. OMVs were first studied in *C. jejuni*, strain 81-176, in which it was clear that these vesicles are not used by the bacterium exclusively for the delivery of virulence factors but also to infect the host cell, making it possible to spread the CDT toxin contained in them (Lindmark *et al.*, 2009; Davies *et al.*, 2019).

### *1.6 Campylobacter jejuni: Cytolethal distending toxin*

CDT is produced by a range of Gram-negative pathogenic bacteria, such as the *Pasteurelaceae* family, the *Enterobacteriaceae* family, and the *Campylobacterales* order, including *Campylobacter* and *Helicobacter* species (Faïs *et al*., 2016).

CDT is a heterotrimeric holotoxin belonging to the AB family toxins. CDT (**Figure 6**) consists of three subunits (A, B and C; 23, 29 and 21 kDa respectively) encoded from the cluster of *cdtA, cdtB* and *cdtC* genes. Compared to the CdtA and CdtC sequences, which show a higher degree of variability, the CdtB sequence is more conserved (Jinadasa *et al.*, 2011). The CdtB subunit, possesses a cation-dependent metalloenzyme activity *in vitro* typical of endonuclease (Elwell and Dreyfus, 2000; Lara-Tejero and Galán, 2000), phosphatidylinositol-3,4,5-triphosphate (Dlakic, 2001; Shenker *et al*., 2007) and sphingomyelinase (Hofmann *et al*., 2000). CDT toxicity is mainly dependent on CdtB nuclease activity, while phosphatase activity may be involved in CdtB intracellular trafficking (Pons *et al*., 2020). The CdtA and CdtC act as carriers to transport the catalytic subunit, CdtB, within host cells (Smith and Bayles, 2006). CdtB can reach the nucleus through either ERAD pathway (protein degradation associated with the endoplasmic reticulum) or through the translocation of the nuclear membrane.

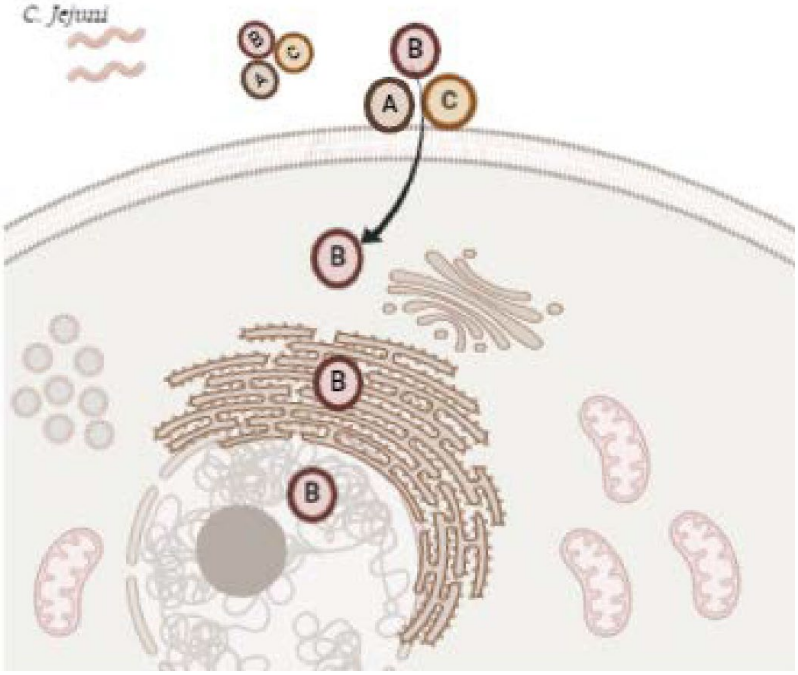


**Figure 6: Heterodimeric complex of CDT.** CdtA and CdtC bind to cell membranes and facilitate CdtB entry into cells. Following internalisation, CdtB translocates to the cytosol, into the endoplasmic reticulum and to the nucleus. Once in the nucleus, CdtB induces DNA double-strand breaks, which lead to cell-cycle arrest. Created in Biorender.com

Inside the nucleus, CdtB exhibits a DNase I type activity capable of causing damage to the double strand (Elwell and Dreyfus, 2000), these will cause the activation of DNA repair complexes by inducing a blockage of the cell cycle in G2/M before cell division (Lara-Tejero and Galán, 2000; Canonico *et al.*, 2014, 2020). In the eukaryotic cell, first there will be a cytoplasmic distension and then cell death, through mechanisms not yet clarified (Whitehouse *et al.*, 1998; Lara-Tejero and Galán, 2001; Canonico *et al.*, 2020). CDT toxin exerts multiple effects such as: the release of IL-8 by intestinal epithelial cells (IECs) (Hickey *et al.*, 2000), the promotion of DNA repair in the host cell (Hassane, Lee and Pickett, 2003), gastroenteritis in NF-kB deficient mice (Gantier *et al.*, 2010) as well as cell death of human monocytes (Ge, Schauer and Fox, 2008; Canonico *et al.*, 2018). In humans, the symptoms of the disease could be due to CDT-induced cell death and the resulting inflammatory response (Jeon, Itoh and Ryu, 2005; Guerra *et al.*, 2011). It is therefore deduced that the effects of the toxin will vary depending on the type of eukaryotic cell infected. Generally, in humans it can inhibit both humoral and cellular immunity by inducing apoptosis in immune cells as well as necrosis in the epithelial cells of the intestine, which first act as a barrier against pathogenic enterobacteria (Pickett and Whitehouse, 1999; Shenker *et al.*, 1999).

Therefore, CDT had potential to be used as an anti-tumor agent. Currently, cancer therapy employs all subunits of CDT, or only the enzymatic subunit CdtB in combination with some targeted portions. Bachran et al. (Bachran *et al.*, 2014) reported that conjugation of CdtB of *Haemophilus ducreyi* with the N-terminal 255 amino acids of *Bacillus anthracis* toxin lethal factor, has potential as an anticancer treatment. Additionally, Chen and colleagues delivered nanoparticles based on hyaluronic acid for delivering CdtB to prostate cancer (Chen *et al.*, 2021). They show that this composition has activity like CDT whole toxin, but with the difference that the CdtB can be delivered specifically to cancer cells and enhance the effect of ionising radiation in radio-resistant prostate cancer cells (Chen *et al.*, 2021). In another work by Vafadar and co-workers (Vafadar *et al.*, 2020), the new immune-toxin based on Single-chain variable fragment associated with CDT (ScFv-CdtB) were designed and evaluated against breast cancer. Therefore, Keshtvarz et al. 2021 produced an engineering of CdtB to reduce immunogenicity and maintain stability as a new drug candidate for tumour therapy (Keshtvarz *et al.*, 2021).

### *1.7 Co-culture*

*C. jejuni*, as already described, is a widespread zoonotic pathogen, infection studies showed disruption of intercellular contacts, induction of epithelial apoptosis and immune activation (Butkevych *et al.*, 2020). This triggering could lead to severe postinfectious complications, including GBS and reactive arthritis (Nyati *et al.*, 2013; Huizinga *et al.*, 2015; Sirirak *et al.*, 2019). Myeloid cells have been implicated in both initiation and resolution of the animal model of GBS (Du *et al.*, 2020). Effective functioning of these cells requires intercellular communication between myeloid cells and primary epithelial infected cells (Du *et al.*, 2020). The gastrointestinal tract epithelium is a single-cell layer that forms the largest and most important barrier against the external environment. It regulates the absorption of nutrients, electrolytes, water and maintains an effective defence against intraluminal toxins, antigens, and enteric flora (Groschwitz and Hogan, 2009; Kvietys and Granger, 2010). To fulfil this ambivalent role, IECs and the gut-associated lymphoid tissue (GALT) have established a finely tuned cohabitation (Kämpfer *et al.*, 2017). Cell monocultures are, however, not capable of mimicking the complex structure of intestine. Whereas monocultures are valued to study specific endpoints such as cytotoxicity, their ability to predict downstream impacts in relation to the biokinetics and metabolism of substances is limited (Lilienblum *et al.*, 2008; Duell *et al.*, 2011). An *in vitro* alternative to monoculture is co-culture of multiple cell types including most commonly epithelial cells. This approach is being used with increasing frequency as a solution to bridge the gap between overly simplistic single lineage *in vitro* models and the dynamic biological processes that occur *in vivo*. Co-culturing epithelial cells with other cell types in proportional levels approximated to known tissue constituency have been used to mimic the *in situ* interactions of various body systems. One benefit of co-culture compared to monoculture is their capacity to better reflect the *in vivo* biology of cytokines, growth factors, transcriptional regulators activated or repressed in response to disease and altered signalling by extracellular vesicles. Epithelial cell co-cultures, such as IECs, are increasingly being used to study host responses to infection (Lea, 2015; Yoshimoto, Okada and Hayashi, 2019). These models are typically based on co-cultures of two host cell types and subsequent challenge with a microbial component such as membrane proteins or cytotoxins, such as CDT to study virulence and pathogenesis (**Figure 7**).

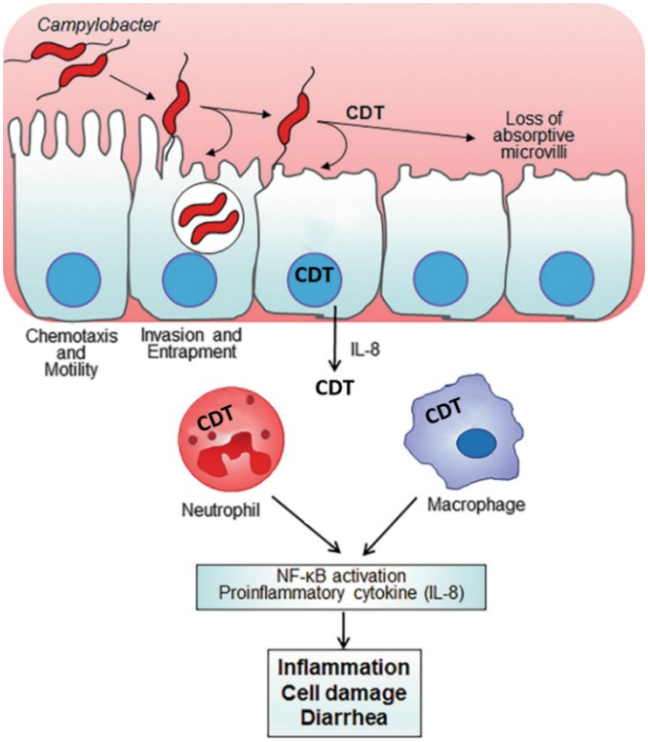


**Figure 7:** Scheme of interaction between epithelial cells and immune cells during *C. jejuni* infection. Image adapted from (Bhunia, 2018).

Epithelial cell-macrophage co-cultures are particularly helpful where there is known *in situ* proximity of these two cell types *in vivo* such as in the gut. Different roles between macrophages and epithelial cells in tissues such as the kidneys (Patel *et al.*, 2009), urogenital tissues (Wira *et al.*, 2005), and intestinal epithelium (Bull and Bookman, 1977; Bockman, Boydston and Beezhold, 1983; Sansonetti, 2001; Duell *et al.*, 2011) have been highlighted through different responses to cytotoxic and infectious agents. The application of these increasingly complex cell models generated new insights regarding the regulation of intestinal homeostasis (Nathens *et al.*, 1995; Parlesak *et al.*, 2004) and confirmed the influence of immune cells on IEC responsiveness to stressors (Wottrich, Diabaté and Krug, 2004; Moyes, Morris and Carr, 2010; Susewind *et al.*, 2016). Most of these models, however, were established using primary cells (Bisping *et al.*, 2001; Leonard, Collnot and Lehr, 2010), which can negatively affect the reproducibility and the inter-laboratory comparability of the results (Corazza S. and Wade E.J., 2010), or using cell lines of non-human origin (Tanoue *et al.*, 2008).

### *1.8 Extracellular Vesicles*

Extracellular vesicle (EV) secretion appears to be an evolutionarily preserved process present throughout all kingdoms (Woith, Fuhrmann and Melzig, 2019). EV research focuses on understanding the biogenesis and release of these natural carriers and their destiny upon interaction with target cells. This also comprises the genotypic and phenotypic responses that EVs induce and the mechanisms by which EVs mediate cell-to-cell communication (Mathieu *et al.*, 2019; Kalluri and LeBleu, 2020; Herrmann, Wood and Fuhrmann, 2021). EVs are known as cell-derived membranous structures that can transport various active biomolecules from creator cells to target cells, thereby changing the physiology of the target cells (Antonyak and Cerione, 2018; Ofir-Birin *et al.*, 2018; Elsharkasy *et al.*, 2020). EVs have been isolated from various sources, including mammalian and prokaryotic cell cultures, blood plasma, bovine milk and plants (Woith, Fuhrmann and Melzig, 2019). EVs make up a heterogeneous population of particles that are generally classified into three distinct populations based on their biogenesis: microvesicles, apoptotic bodies and exosomes (Elsharkasy *et al.*, 2020). Each EV subpopulation may be derived via distinct biogenesis pathways, and because their precise biogenic origin is impossible to ascertain in most cases, a comprehensive characterization of the vesicles is crucial.

Microvesicles arise from direct outer budding of the plasma membrane, producing a population of EVs that are heterogeneous in size. Apoptotic bodies are also generated from the cell surface, although they are only released by dying cells during cell fragmentation (Bebelman *et al.*, 2018; Hessvik and Llorente, 2018). Exosomes are formed because of inward budding of the limiting membrane of endosomes to form multivesicular bodies (MVBs). Subsequently, exosomes are released into the extracellular space by fusion of MVBs with the plasma membrane. Following release from the cell surface, exosomes can interact with the extracellular matrix, or elicit a response in cells within the microenvironment or at a distance. Exosomes have a size ranging from 40 to 120 nm, while microvesicles have a size of 50–1000 nm (Zaborowski *et al.*, 2015; Willms *et al.*, 2018). As a result of their overlapping sizes, surface markers, and the absence of proteins that are restricted to specific populations, it has been challenging to distinguish between exosomes and microvesicles; therefore, all different types of vesicles are referred to as EVs. Moreover, EVs may have the capacity to cross biological barriers (Alvarez-Erviti *et al.*, 2011; Cooper *et al.*, 2014; Liu *et al.*, 2015), exploit endogenous intracellular trafficking mechanisms and trigger a response upon uptake by recipient cells (Murphy *et al.*, 2019). In addition, they may display inherent targeting properties that are

dictated by their lipid composition and protein content (Murphy *et al.*, 2019). Studies have shown that specific progenitor cell derived EVs convey biological cargo that promotes angiogenesis and tissue repair and modulates immune functions (Turturici *et al.*, 2014) (**Figure 8**).

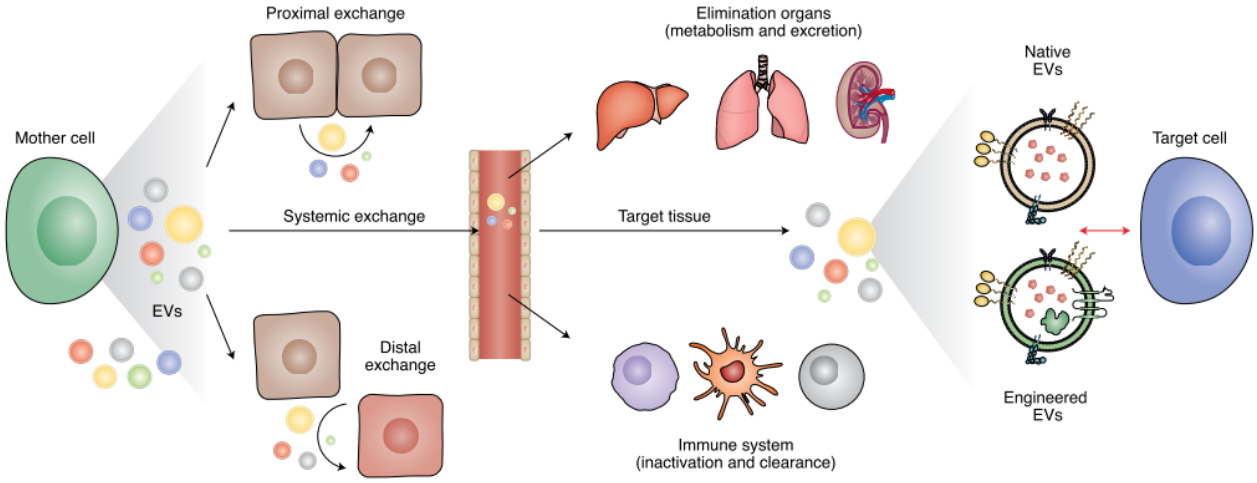


**Figure 8:** Illustration of EV-mediated cell crosstalk, clearance mechanisms and immune responses. EVs are produced as heterogeneous mixtures of different subpopulations, and they may participate in proximal and distal communication between cells. After entering the systemic circulation, they must avoid elimination organs, such as the liver, lungs and kidneys, as well as immune cells. Their target-tissue efficiency depends on the degree of functionalization and target-cell interaction. (Herrmann, Wood and Fuhrmann, 2021).

EVs contain numerous biomolecules like proteins, miRNAs, mRNAs, Long non-coding RNAs, DNA strands, lipids, and carbohydrates from parental cells, which deliver them to target calls and reprogram the fate, function, and morphology of target cells (Kowal, Tkach and Théry, 2014; Statello *et al.*, 2018). The secretion of EVs was initially designated as a tool for removing unwanted compounds from the cells (Pan *et al.*, 1985). Nonetheless, we currently know that EVs are more than just waste transporters, and the significant interest in the EVs field is now engrossed in their ability to exchange biomolecules between cells (Kowal, Tkach and Théry, 2014). EVs play critical roles in the progression of different pathological conditions (Yuana, Sturk and Nieuwland, 2013). For example, in infectious diseases and cancer, EVs can promote pathogenesis of diseases (Fleming *et al.*, 2014; Han, Lam and Sun, 2019). EVs from infected cells contain virus particles that induce virus infection in healthy cells and modulate immune responses of the host (Fleming *et al.*, 2014; Hassanpour *et al.*, 2020). EVs released by host cells infected with *Helicobacter pylori* contained the virulence factor CagA and could reached macrophages that contribute significantly to inflammation, and in doing so promote the development of disease (**Figure 9**) (González *et al.*, 2021). Such abilities

have drawn a great deal of attention towards EVs for therapeutic application, and as a prospective vehicle for the delivery of therapeutics that could overcome issues related to liposomes and other synthetic drug delivery systems (Pant, Hilton and Burczynski, 2012; Elsharkasy *et al.*, 2020).

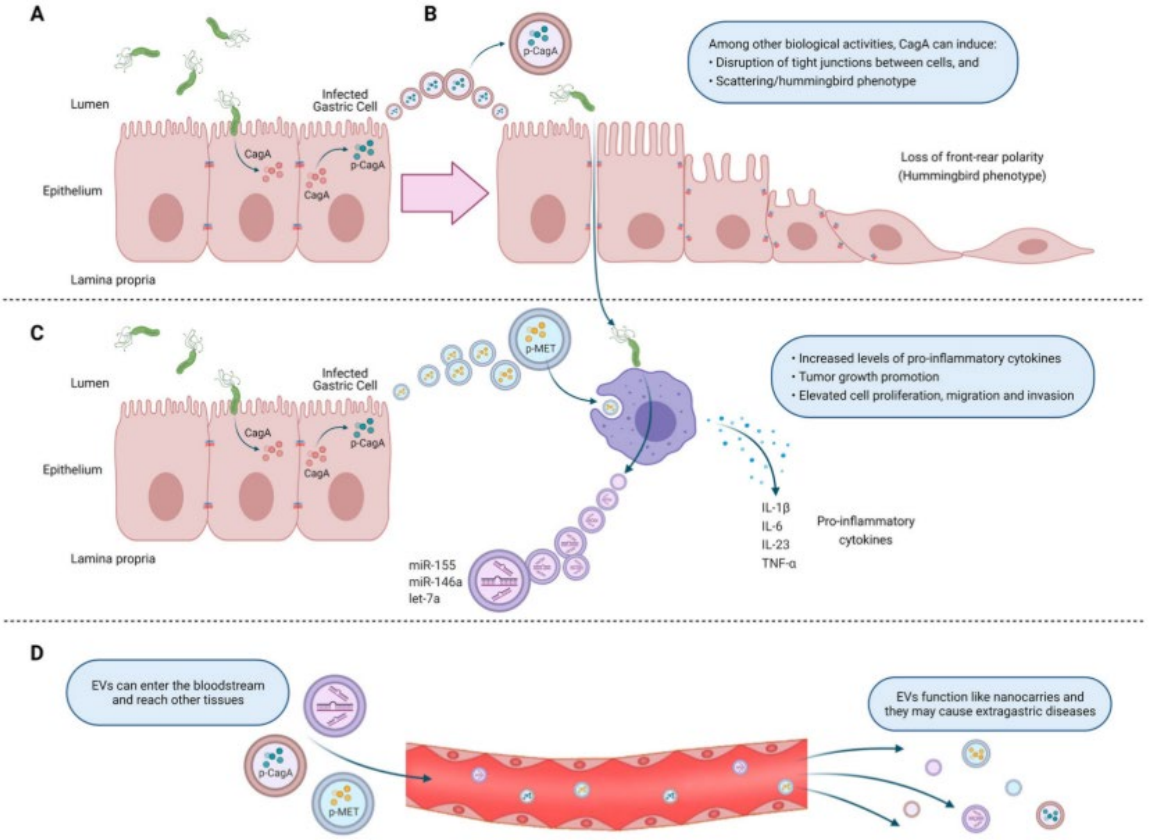


**Figure 9: Extracellular vesicles (EVs) from *H. pylori* infected-host cells are associated with gastric cancer development**. (A) During *H. pylori* infection, the virulence factor CagA is delivered into gastric epithelial cells. (B) EVs released from *H. pylori*-infected gastric epithelial cells contain CagA in its phosphorylated form (p-CagA), which induces morphological changes in host cells, causing gastric epithelial cells to elongate and spread. (C) Likewise, after *H. pylori* infection, EVs containing phosphorylated mesenchymal epithelial transition factor are released. These are internalised by macrophages, which release pro-inflammatory cytokines that promote tumour growth and increase cell proliferation, migration, and invasion. On the other hand, *H. pylori*-infected macrophages release EVs containing high levels of microRNAs, which either inhibit *H. pylori* proliferation or exert pro-inflammatory effects, depending on the microRNA type. (D) Finally, EVs can enter the bloodstream and reach other tissues, where they can cause extra-gastric diseases. (González *et al.*, 2021)

## AIMs OF THE STUDY

The aim of this work was to investigate the effects of CDT *C. jejuni* in human cells focusing the attention on cellular pathways that the toxin might activate or deactivate and the ways of CDT can spread to other cells. For this purpose, the effects induced by lysates of *C. jejuni* wild-type strains was compared with *C. jejuni* CdtA mutant strain in two different cell lines: tumour myeloid cells (U937) and human intestinal epithelial cells (Caco-2). Although it is well known that IECs are typical *C. jejuni* target cells, much less is known about the relationship between *C. jejuni* and myeloid cells. This topic was particularly investigated in this work since in the last two decades it was assumed a possible critical role of monocytes and macrophages in GBS onset.

In particular, the study presented in this Thesis is organised as the following:

- The first chapter is the published article (Canonico, B., Cesarini, E., Montanari, M., Di Sario, G., Campana, R., Galluzzi, L., Sola, F., Gundogdu, O., Luchetti, F., Diotallevi, A., Baffone, W., Giordano, A., & Papa, S. (2020). **Rapamycin Re-Directs Lysosome Network, Stimulates ER-Remodeling, Involving Membrane CD317 and Affecting Exocytosis, in *Campylobacter Jejuni*-Lysate-Infected U937 Cells**. International Journal of Molecular Sciences, 21(6), 2207. https://doi.org/10.3390/ijms21062207). In this work the effects of *C. jejuni* ATCC 33291 wild-type strains and *C. jejuni* 11168H *cdtA* mutant strain were described in human tumour myeloid cells (U937), focusing the apoptotic and autophagic pathways, and specifically attributing certain effects to the toxin, thanks to comparisons with the mutant strain. Then the ability of rapamycin to protect (at least in part) myeloid cells against *C. jejuni* CDT was elucidated.
- The second chapter entitled: **Deeply investigating the multiple ways of damage to the target cells and the routes that bring the infection/inflammation to persist and spread,** proceeds to investigate the mechanisms of CDT-caused damages at subcellular and nuclear level in the two cell lines of the Study (U937 and Caco-2 cells) to delineate the importance of both the source of the toxin and the target cell. The "*in vitro co-culture model*" of Caco-2 and U937 cells aims to mimic the "*in vivo*" interactions between epithelial intestinal cells and myeloid cells.
- The third chapter focuses on the relevance of EVs in this intoxication-driven crosstalk. Briefly, EVs derived from intoxicated Caco-2-cells were added to homologous Caco-2 and heterologous U937 cells to test the onset of the known toxin induced effects (cell distension, cell cycle block, alterations on mitochondria, lysosomes, and ROS production). The second and the third chapter will represent the future work: **EVs from *C. jejuni* CDT intoxicated-Caco-2 cells differently**

**inhibit proliferation in tumour intestinal epithelial and myeloid cells: potential utility for antitumor strategies**

**CHAPTER ONE**

*Article*

# *Rapamycin Re-Directs Lysosome Network, Stimulates ER-Remodeling, Involving Membrane CD317 and Affecting Exocytosis, in Campylobacter Jejuni-Lysate-Infected U937 Cells*

Barbara Canonico [1,*], Erica Cesarini [1], Mariele Montanari [1], Gianna Di Sario [1], Raffaella Campana [1], Luca Galluzzi [1], Federica Sola [1], Ozan Gundogdu [2], Francesca Luchetti [1], Aurora Diotallevi [1], Wally Baffone [1], Antonio Giordano [3,4] and Stefano Papa [1]

[1] Department of Biomolecular Sciences, University of Urbino Carlo Bo, 61029 Urbino, Italy; erica.cesarini@uniurb.it (E.C.); mariele.montanari@uniurb.it (M.M.); gianna.disario@uniurb.it (G.D.S.); raffaella.campana@uniurb.it (R.C.); luca.galluzzi@uniurb.it (L.G.); f.sola@campus.uniurb.it (F.S.); francesca.luchetti@uniurb.it (F.L.); aurora.diotallevi@uniurb.it (A.D.); wally.baffone@uniurb.it (W.B.); stefano.papa@uniurb.it (S.P.)

[2] Department of Pathogen Molecular Biology, London School of Hygiene & Tropical Medicine, London WC1E 7HT, UK; Ozan.Gundogdu@lshtm.ac.uk

[3] Sbarro Institute for Cancer Research and Molecular Medicine, Center for Biotechnology, Temple University, Philadelphia, PA 19122, USA; giordano@temple.edu

[4] Department of Medical Botechnologies, University of Siena, 53100 Siena, Italy

* Correspondence: barbara.canonico@uniurb.it; Tel.: +39-0722-304280

Received: 30 January 2020; Accepted: 18 March 2020; Published: 23 March 2020

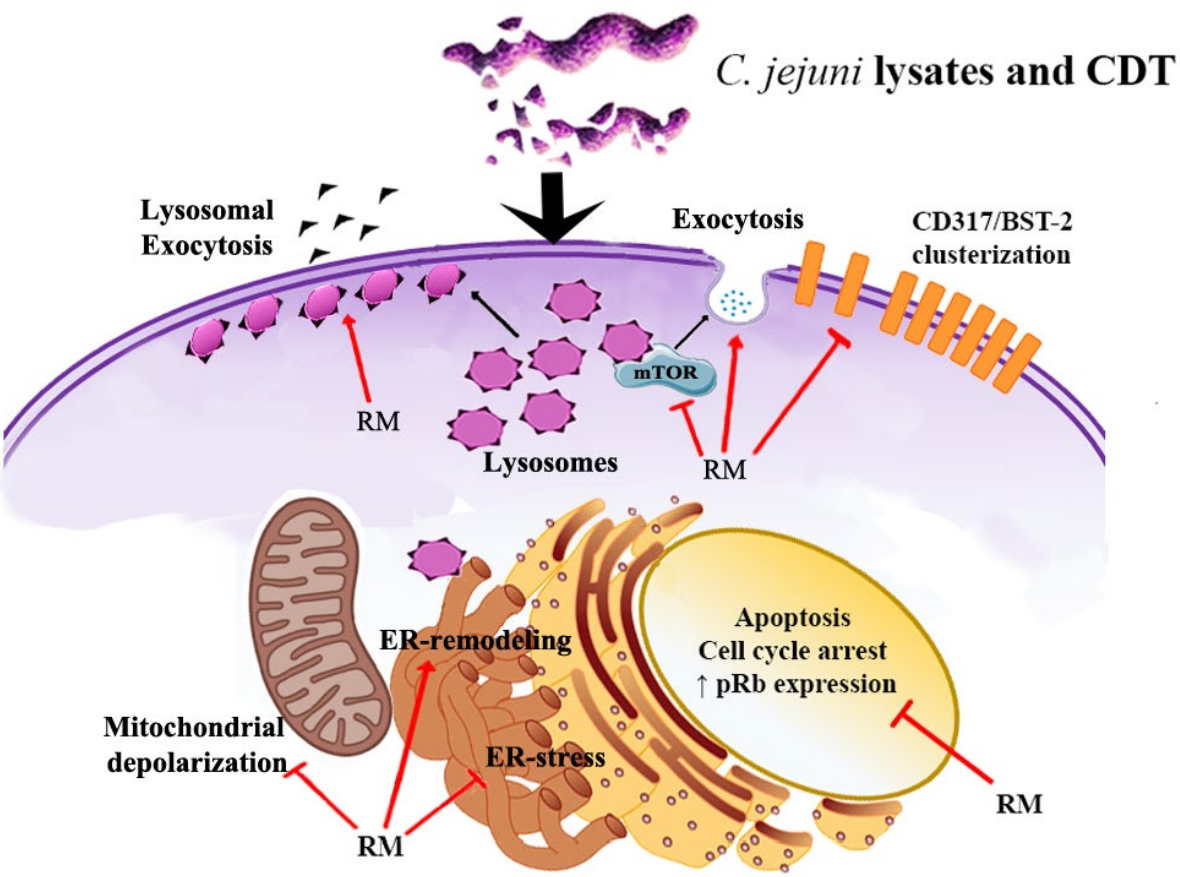


**Abstract:** The Gram-negative *Campylobacter jejuni* is a major cause of foodborne gastroenteritis in humans worldwide. The cytotoxic effects of *Campylobacter* have been mainly ascribed to the actions of the cytolethal distending toxin (CDT): it is mandatory to put in evidence risk factors for sequela development, such as reactive arthritis (ReA) and Guillain–Barré syndrome (GBS). Several research are directed to managing symptom severity and the possible onset of sequelae. We found for the first time that rapamycin (RM) is able to largely inhibit the action of *C. jejuni* lysate CDT in U937 cells, and to partially avoid the activation of specific sub-lethal effects. In fact, we observed that the ability of this drug to redirect lysosomal compartment, stimulate ER-remodelling (highlighted by ER–lysosome and ER–mitochondria contacts), protect mitochondria network, and downregulate CD317/tetherin, is an important component of membrane microdomains. In particular, lysosomes are involved in the process of the reduction of intoxication, until the final step of lysosome exocytosis. Our results indicate that rapamycin confers protection against *C. jejuni* bacterial lysate insults to myeloid cells.

**Keywords:** *Campylobacter jejuni*; rapamycin; ER-remodeling; lysosome positioning and exocytosis; CD317/tetherin

## 1. Introduction

The lysosome is the terminal component of the endocytic pathway, which possesses a series of biological functions including endocytosis, exocytosis, macropinocytosis, plasma membrane repair, defence against pathogens, cell death, signal transduction, and autophagy [1]. Autophagy has been proposed to be a component of the innate immune response against several types of intracellular microorganisms [2]. In physiological conditions, autophagosomes form and successfully fuse with lysosomes at baseline rates, underling the ability of autophagy to support normal cellular functions. In the presence of an autophagic stimulus, the rate of autophagosome formation, autophagosome–lysosome fusion, and lysosomal degradation increases, resulting in accelerated degradation of autophagic substrates [3]. In fact, autophagy stands out as a key process for the lysosomal degradation of cytosolic entities that is highly interconnected with several other biological functions. Although in many cases autophagy contributes to cell death, it has a protective and pro-survival function. Autophagy and apoptosis are two fundamental biological mechanisms that may cooperate or be antagonistic, and both are involved in deciding the fate of cells in physiological or pathological conditions.

The functional relationship between apoptosis ('self-killing') and autophagy ('self-eating') is intricate. Under certain circumstances, autophagy constitutes a stress adaptation that avoids cell death and suppresses apoptosis, whereas in others, it represents an alternative killing mechanism which is activated when apoptosis cannot be executed [4,5]. It is essential to determine which mechanism has to be activated as we try to either protect the cells from cell death, as in neurodegenerative diseases, or induce cell death, as in cancer treatment [6]. Other studies linked autophagy to facilitating the mitochondrial permeability transition: both apoptosis and autophagy could permit this process to cause cell death [7]. Depending on the upstream signals and the different instances, cells activate apoptosis or autophagy, or both, by combining or switching between them in a mutually exclusive manner [8] It is difficult to predict if autophagy is positive or negative: it depends on what gets degraded under different circumstances. Rapamycin, an antibiotic discovered as an anti-fungal agent in the 1970s, is an efficient inhibitor of mammalian target of rapamycin (mTOR) resulting in autophagic induction [9]. In mammals, mTOR is the central player in autophagy signalling. It is a serine/threonine kinase which inhibits autophagy by controlling both translation and transcription of autophagy-related (Atg) proteins, therefore interfering with the formation of autophagosomes. Recent studies showed that mammalian target of rapamycin complex 1 (mTORC1) signalling acts with the ER stress response and contributes to the cell fate decision [10–12].

Furthermore, the host cell plasma membrane is a central element in pathogen–host associations with interaction at the cell surface leading to internalization, while intracellular membranes play a critical role in subsequent pathogen trafficking. Ultimately, such pathogen–membrane lipid interactions work co-ordinately to mediate cytotoxicity [13]. CD317/tetherin (also called tetherin, BST2 or HM1.24) is a lipid raft-associated protein with several protective and deleterious roles. Despite its localization to lipid rafts, CD317/tetherin is internalized via clathrin-dependent endocytosis [14]. Mature CD317/tetherin recycles between the plasma membrane, endosomes, and trans-Golgi network (TGN) [15,16]. Regulation of virus restriction and tumor aggressiveness are the most studied aspects of CD317/tetherin function, where CD317/tetherin is expressed in airway and mucosal epithelia in response to viral infection [17]. Research has focused on the involvement of CD317/BST2 in cancer cells and cancer biology re-evaluation of the overall role of CD317/tetherin in host protection, as it appears that CD317/tetherin has pleiotropic effects in the host. In addition, it has been recently demonstrated [18] that BST2-mediated signalling may be involved in the balance of apoptosis and autophagy: the latter is a process representing a critical mechanism that regulates the fate of infected cells. CD317 might attach exosomes both to the plasma membrane and to each other: it acts to inhibit the spread of certain enveloped viruses, by cross-linking the virions and holding them together at the plasma membrane [19]. Edgar et al. have demonstrated that tetherin might act in a similar manner on exosomal vesicles [20], decreasing CD317's ability to reduce the number of exosomes associated with the plasma membrane of HeLa cells, with a concomitant increase in exosomes released into the medium.

*Campylobacter jejuni* is the most common causative agent of foodborne infectious illnesses in humans [21]. This Gram-negative bacterium is able to establish commensalism in several animal hosts and promote human diarrheal disease, and *C. jejuni*-associated enterocolitis is typically linked with a local acute inflammatory response that involves intestinal tissue damage [22].

*C. jejuni*, like several other Gram-negative bacteria, produces the cytolethal distending toxin (CDT), which is an important virulence factor that has been characterized in detail [23–29]. CDT is encoded by the *cdt*ABC operon and has three components: CdtA, CdtB, and CdtC. CdtB is a DNAse I that leads to DNA double-strand breakage in the nucleus, resulting in cell cycle arrest at the G2/M phase, thereby inducing cell distension [30], target-cell death, and/or autophagy. CdtA and CdtC assemble a tripartite complex with CdtB, and act as carriers for delivering CdtB into the cell [31].

*C. jejuni* CDT is released through outer membrane vesicles [32], which fuse with the host plasma membrane via lipid rafts [26], leading to its internalization within the host cells [33]. CdtA and CdtC

subunits are only able to bind these cholesterol-rich microdomains on the cytoplasmic membrane, allowing the delivery of the active subunit to cells [34–36]. Recently, the carcinogenic potential of*C. jejuni* and the key role of CDT in this process have been demonstrated [37]. CDT is also produced by*S. typhi* [38,39], in addition to *Escherichia coli* [23] and other causative agents of chronic infection, such as *Haemophilus ducreyi* [26], *Shigella dysenteriae* [28], *Actinobacillus actinomycetemcomitans* [40], *Helicobacter hepaticus* [27], and other species [41,42]. The damage to the host cells can be mediated either [39,43]: (1) directly by (a) enzymatic attack, (b) DNA damage, or (c) by affecting DNA damage repair mechanisms, or (2) indirectly, by (a) provoking a chronic inflammatory reaction, or (b) producing free radicals. These changes might be associated with carcinogenesis and might stimulate cellular aberrations, modify the immune response, or inhibit normal cell controls. Several studies have indicated that pRb proteins exhibit tumor suppressor activities, and play a central role in cell cycle regulation. In fact, recent data [44] have shown that this protein, although owing to its role in G1/S cell cycle checkpoint, participates in many other cellular functions, including, counterintuitively, the negative regulation of apoptosis cell-cycle activation, and apoptotic inhibition can be directly related to autophagy induction. We have previously demonstrated that lysates containing CDT from all strains are able to induce endoplasmic reticulum (ER) stress in monocytes, suggesting that ER stress was not associated with CDT, but with other *C. jejuni* virulence factors [45]. In the present study, ER was investigated in U937 cells treated by lysates and with the addition of rapamycin (RM), in association with lysosomes, in the mechanisms of escape from lysate intoxication. U937 cells were adopted secondarily to monocytes [45]. In fact, as they are known to be effective producers of both pro- and anti-inflammatory cytokines, monocytes play a major role in innate immunity and in non-specific host response against both exogenous pathogens—primarily by phagocytosis—and endogenous substances created by tissue damage [46]. Furthermore, other researchers [47–49] adopted U937 monocytic cells as a model to study the effects of bacterial infection, particularly for CDT intoxication. Here, we describe the evidence that rapamycin reduces CDT effects by the involvement of membrane CD317/tetherin. Furthermore, RM deeply delays the proliferation of intoxicated U937 cells and rescues them from apoptosis, redirecting the lysosomal compartment and their positioning. Finally RM stimulates ER-remodelling, concomitantly to the impairment of the usual progression of apoptosis and proliferation, with all events induced by the presence of lysates containing CDT.

## 2. Results

To investigate the efficacy of the CDT lysates isolated from the *C. jejuni* wild-type and mutant strains in U937 cells, cytometric and confocal analyses were conducted. In the first part of the work, we report specific results able to highlight CDT activity and to underline cell processes subsequently modified by rapamycin. In the second and wider part of the article, RM mechanistic effects on *Campylobacter jejuni*-lysate-infected U937 cells were evaluated, pointing out the processes and cellular compartments involved.

Although the mTOR inhibitor rapamycin does not exert the complete inhibition of mTORC1 downstream targets [50], we adopted this drug, because it is a macrocyclic triene antibiotic that is produced by fermentation of *Streptomyces hygroscopicus*. It is commercially available, and the United States (US) Food and Drug Administration (FDA) approved its employment in the United States. It is used alone or in combination with other drugs in cancer [51], autoimmune diseases [52] and, recently, [53] in bacterial infections.

*Morphological Features, Cell Death, Absolute Count, and Evaluation of Cellular Division*

As previously observed in monocytes, morphologic appearance was studied by microscopic and cytometric investigations. Also in U937 cells, *C. jejuni* wild-type lysate caused the typical CDT-dependent cellular distension, compared with untreated control cells and cells treated with the mutant strain lysate. Different sub-populations are visible on the basis of cellular scatter characteristics: we can distinguish normo-sized cells (red events—P1), distended/enlarged cells (pink events—P2), shrunken cells (blue events—P3) (Figure 1A), since one of the main effects of CDT is indeed cell distension/enlargement. Trypan blue viability test and absolute counting beads were applied, revealing that the wild-type strain caused a reduction in cell number in U937 cells (as well as for monocytes and HeLa cells [45,54]). In addition, Annexin V–propidium iodide (AnxV-PI) double staining revealed that AnxV-PI positive cells, which represent the apoptotic cells, were particularly present in U937 cells preincubated with the

*C. jejuni* ATCC 33291 lysate (Figure 1B,C).

As shown in (Figure 1D–H), efficiency of CDT in G2-M blocking was investigated by means of carboxyfluoresceinsuccinimidyl ester (CFSE), a fluorescent dye that can measure cell proliferation using flow cytometry. Results at 48 h showed that the *C. jejuni* ATCC 33291 lysate exerted maximally this blocking-effect, showing percentages of undivided cells higher than cells treated with the lysate from the mutant strain. Moreover, via CFSE fluorescence cytometric evaluation, the efficiency of CDT in G2-M blocking was calculated at 72 h (Figure 1F–H)). Bar graphs regarding the first, second,

and third division indicated that the typical CDT effect on DNA not only persisted after 72 h from lysate administration, but also became more evident, particularly for the *C. jejuni* ATCC 33291 lysate.

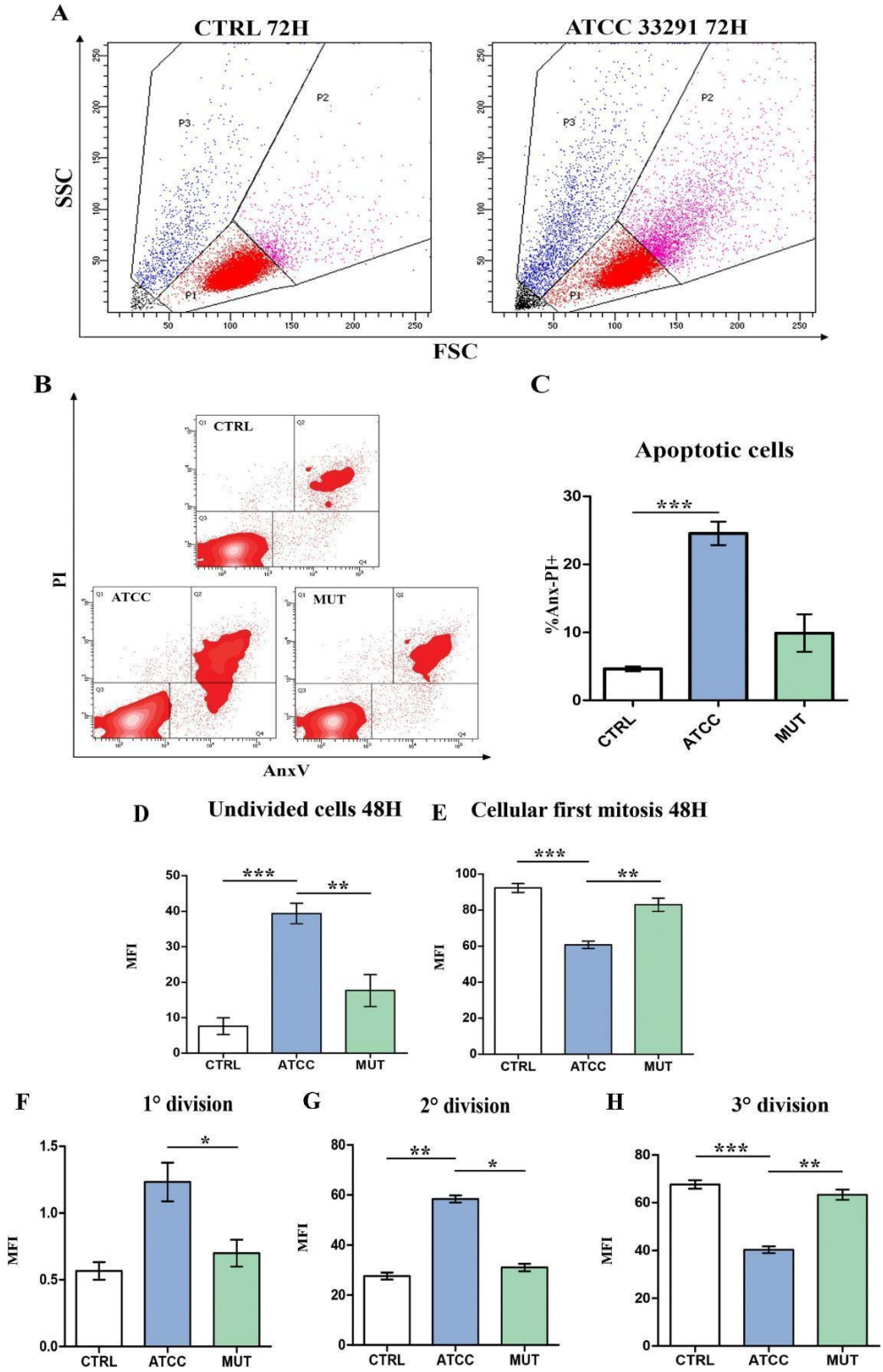


**Figure 1.** Evaluation of cell death induced by lysates and verification of the efficiency of the toxin, verified only in the ATCC33291-treated cells (**A**) U937 were split into different sub-populations depending on the morphologic parameters: blue gate shows dead cells, pink gate shows distended cells, and red gate shows viable cells. Total cells were the summary of red, pink, and blue gates. Black represents debris which were

excluded for the analysis. Dot plots in the picture show control (CTRL) untreated cells and cells treated with the *C. jejuni* ATCC 33291 lysate for 72 h. (**B**) Density plot of propidium iodide (PI) vs. Annexin V (AnxV) of all experimental conditions. Q1 shows PI positive cells, Q4 shows AnxV positive cells, Q2 shows AnxV-PI positive cells, Q3 shows AnxV-PI negative cells and debris. (**C**) Statistical histograms of the percentage of AnxV-PI positive cells calculated after 72 h from lysate administration in total cells. Each value is expressed as a percentage ± SD (results from $n \geq 3$ independent experiments). Asterisks denote a statistically significant difference (*** = $p < 0.001$) between strains. Statistical histograms related to CFSE dye dilution assay used to determine the number of divisions a given CFSE-labeled cell has undergone. (**D**) Statistical histogram of undivided cells calculated via CFSE staining at 48 h. (**E**) Statistical histogram of dividing cells calculated in cytometry via CFSE staining at 48 h. (**F–H**) Statistical histogram of cells in 1st, 2nd and 3rd division, at 72 h. Each value is expressed as a mean ± SD (results from $n \geq 3$ independent experiments). Asterisks denote a statistically significant difference (* = $p < 0.05$, ** = $p < 0.01$, *** = $p < 0.001$) between strains.

### *2.1. ER Stress Evaluation*

The ER is a critical stress-responsive organelle, where ER stress leads to the production of nuclear C/EBP-homologous protein (CHOP), which has been implicated as a key mediator of ER stress-mediated cell damage [55]. Unfolded protein response (UPR) is indeed a stress response pathway that promotes the inflammatory response and plays a critical role in a wide range of cellular pathologies [56]. At first, in order to investigate ER stress induced by lysates, U937 cells were stained with ER-Tracker (a live cell stain highly selective for the ER) and analysed in both cytometry and confocal microscopy. The results reported in Figure 2A–C show that ER stress occurred in U937 cells particularly after 24 h. In addition, having observed significant variations in ER Tracker MFI (Mean Fluorescence Intensity) at 24 h in cells preincubated with the *C. jejuni* ATCC 33291 lysate, CHOP gene expression was quantitated at the same time. As shown in Figure 2C, CHOP expression was significantly induced after 24 h treatment with
*C. jejuni* ATCC 33291 lysate.

### *2.2. Prb Detection*

Retinoblastoma protein (pRB) has been shown to regulate glucose tolerance, mitogenesis, glutathione synthesis, and the expression of genes involved in central carbon metabolism [57]. Several studies have indicated that pRb proteins exhibit tumor suppressor activities, and play a central role in cell cycle regulation [58]. In fact, recent data [44] have shown that this protein, although owing to its role in the G1/S cell cycle checkpoint, participates in many other cellular functions, including, counterintuitively, negative regulation of apoptosis.

Changes in pRb (Figure 2D-E) highlight a significant increase between ATCC and mutant-treated cells. Our data show an overexpression of pRb in cells after an incubation of 72 h with the wild-type lysate, compared with the control and the mutant. Confocal analyses focused on the nuclear localization of pRb, well evident after the ATCC 33291 lysate administration. We can consider a pRB-dependent $G_2$ arrest (induced by toxins), accordingly to data from the literature [59]. This process has features of noncanonical cell cycle blocker function, normally explicited in the G1/S cell cycle checkpoint, able to reduce proliferation and apoptosis in *C. jejuni* infected cells [45].

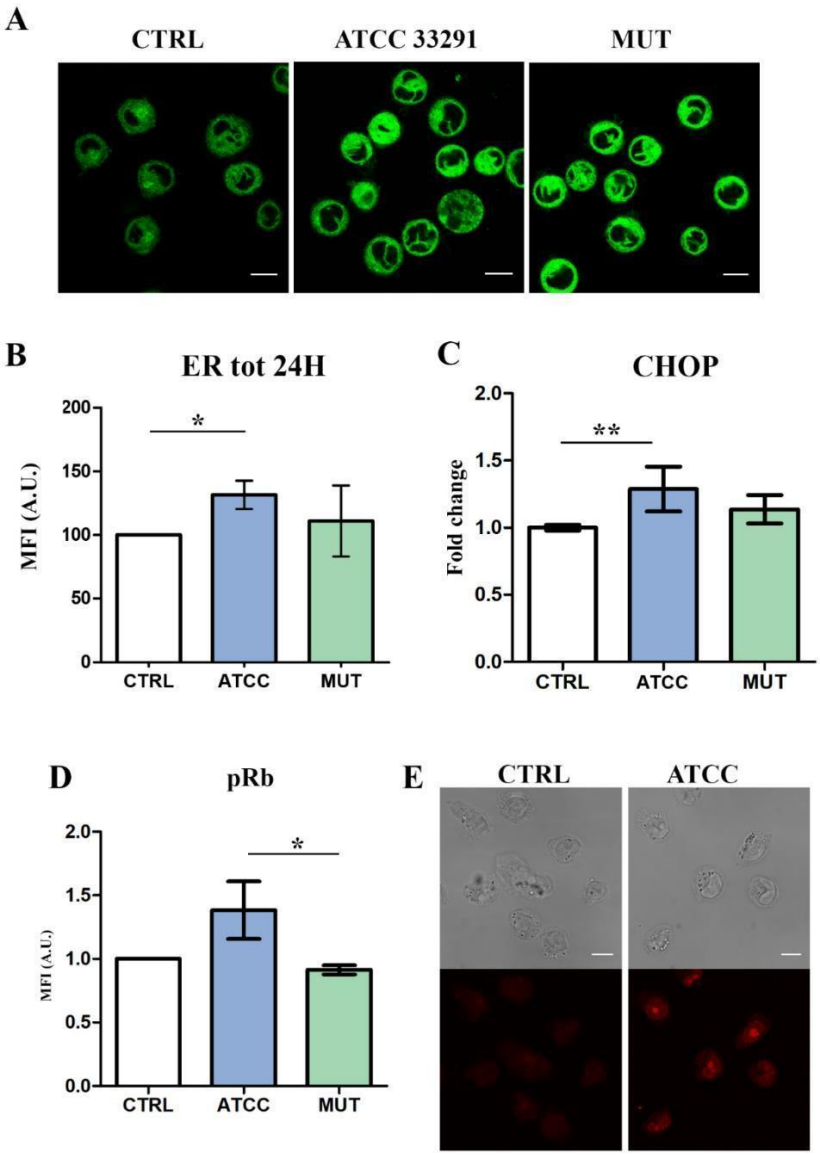


**Figure 2.** Evaluation of ER involvement by confocal microscopy, flow cytometry, and RT-PCR analyses. Single confocal optical sections of ER Tracker MFI of untreated cells and treated U937 at 24 h. Bars: 10 μM. (**B**) Statistical histograms of ER Tracker MFI at 24 h, quantitated by flow cytometry. Each value was converted to arbitrary units (A.U.), setting the control as 100. Each value is expressed as a mean ± SD (results from $n \geq 3$ independent experiments). (**C**) Evaluation of C/EBP-homologous protein (CHOP) expression in U937 cells

after 24 h from lysate administration. Welch's unpaired *t* test revealed: ** $p = 0.009$ for CTRL vs. ATCC 33291. Evidence of pRb modulation by flow cytometry and confocal microscopy. (**D**) Statistical histograms of pRb intracellular content in U937 cells at 72 h. Each value was converted to arbitrary units (A.U.), setting the control as 1. Each value was expressed as a mean ± SD (results from $n \geq 3$ independent experiments). The asterisk denotes a statistically significant difference (* = $p < 0.05$) between strains. (**E**) Single confocal optical sections of pRb MFI of untreated cells and U937 cells preincubated with the *C. jejuni* ATCC 33291 lysate for 72 h. Bars: 10 μM.

### *2.3. Rapamycin Inhibition of MTORC1 Signalling Reduces CDT-Induced Distension, Cell Death and Proliferation*

RM administration can reduce or eliminate important, CDT-induced effects, such as cell size enlargement, degree of apoptosis, and cell cycle perturbation (Figure 3). In particular, this last effect is due to the deep impact of RM in cell growth: It is known [60] that growth is decreased, and also our results on cell count underlined this evidence (Figure 3A), accordingly to pRb data (Figure 4D) Furthermore, RM administration leads to a decrease in apoptotic events, as stated by PI uptake results (Figure 3B). Intriguingly, since mTOR regulation of cell growth and cell size is complex, involving tight regulation of both anabolic and catabolic processes, RM appears to limit the cell enlargement induced by CDT (Figure 3C,D). To exclude that the prevalence of catabolic over anabolic pathways represents the main cause of cell size reduction, we performed the same analytic approach on RM+ and RM- control cells (S1-I): at 24 h and 48 h, RM+ cells demonstrated a slight and not relevant cell size decrease, if compared with RM- control cells. Of note, at the 72-h time point, RM-treated control cells highlighted a moderate increase in cellular dimension (Figure S1-I), whereas in ATCC 33291-treated cells, RM still continued to limit CDT-induced cell distension. (Figure 3C,D). The trend of cell distension/enlargement, evaluated on the basis of the forward light scatter (FSC) cytometric parameter, was also checked by measuring cell size in several single confocal optical sections (Figure S1-II, III). The above-mentioned effects are evident in ATCC 33291 lysate-treated cells, showing that RM specifically antagonizes the efficient CDT produced by this strain.

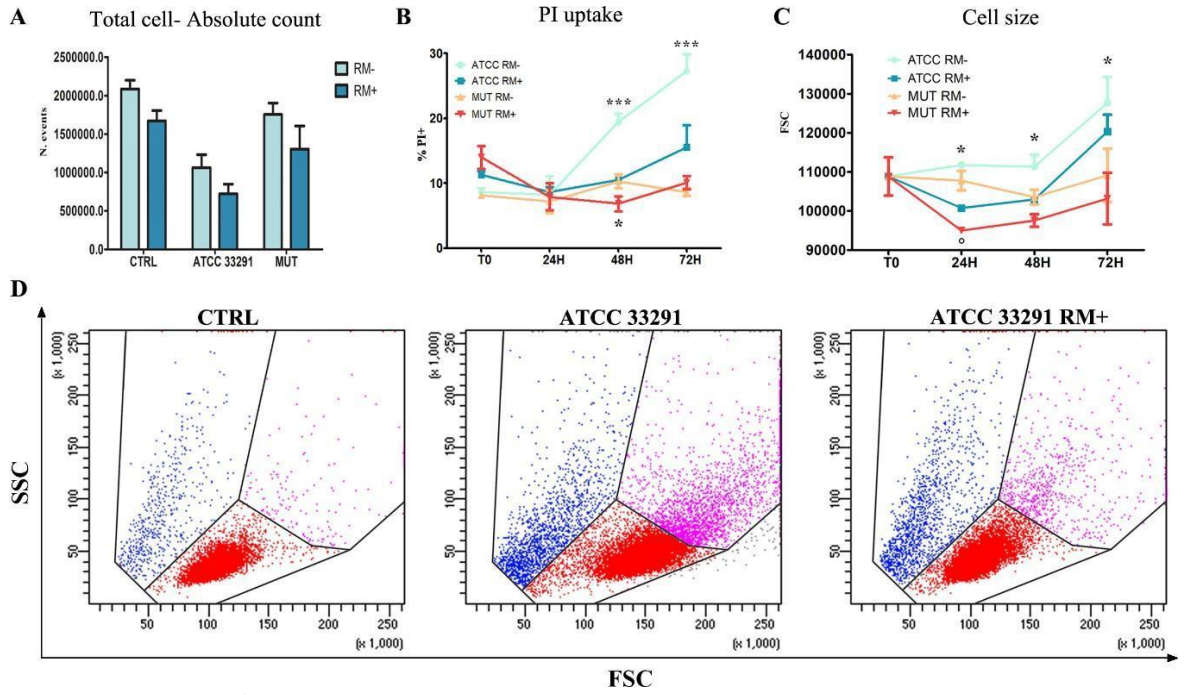


**Figure 3.** Evaluation of cell count, cell death, and cell size induced by lysates and rapamycin (RM) administration (**A**) Absolute count calculated after 72 h from lysate administration in total cells. Each value is expressed as an absolute number ± SD/mL (results from $n \geq 3$ independent experiments). (**B**) Trends of percentage of AnxV-PI positive cells calculated from T0 to 72 h from lysate administration, with (RM+) or without RM (RM-). Each value is expressed as a percentage ± SD (results from $n \geq 3$ independent experiments). Asterisks denote a statistically significant difference (***= $p < 0.001$) between strains. (**C**) Trends of forward light scatter (FSC) values for each treatment during the time course from the starting time point (T0) to 72 h. Each value is expressed as a mean ± SD (results from $n \geq 3$ independent experiments). Asterisks denote a statistically significant difference (* = $p < 0.05$) between strains. (**D**) Dot plots of scatter characteristics (FSC vs. side scatter (SSC)) of U937 control cells (CTRL) and *C. jejuni* ATCC 33291 U937 treated cells with (ATCC 33291 RM+) or without (ATCC 33291) rapamycin at 72 h. Cellular distension (events in blue) is well appreciable for *C. jejuni* ATCC 33291 U937 treated cells; rapamycin, on the other hand, reduces the amount of distended cells. The gates are drawn around roughly the same areas of Figure 1.

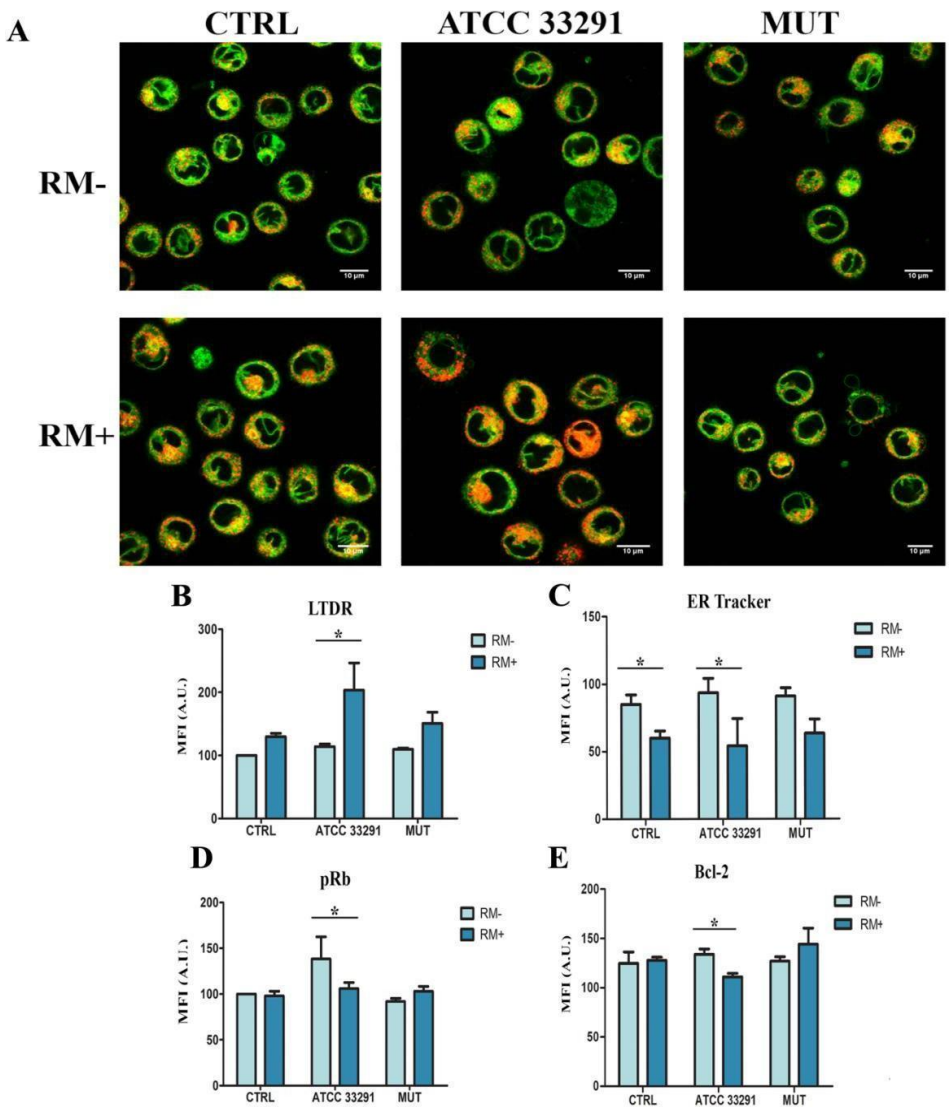


**Figure 4.** Concomitant evaluation of ER tracker and LysoTracker Deep Red (LTDR) fluorescence by qualitative analysis (confo) (**A**) Single confocal optical sections of ER Tracker (in green) and LTDR (in red) of untreated U937 cells (CTRL) and U937 cells preincubated with lysates after 72 h of treatment with and without RM. Where present, co-localization is shown in yellow-orange. Lower pictures show U937 cells pre-treated with RM for 2 h before lysate administration. Bars: 10 μM. Contemporaneous evaluation of ER tracker and LTDR fluorescence by quantitative analysis (flow cytometry). (**B,C**) For investigated parameters, ER (by ER Tracker staining) and lysosomes (by LTDR staining), a comparison between RM- and RM+ values was carried out for each experimental condition at 72 h. The pRb and bcl-2 expression modulated by lysates (light blue) and lysates + RM (dark blue). (**D**) Statistical histograms of MFI of pRb were calculated after 72 h from lysate administration in distended cells with and without RM. Each value was converted to arbitrary units (A.U.), setting the control as 100. (**E**) Statistical histograms of MFI of bcl-2 was calculated after 72 h from lysate administration in distended cells with and without RM. Each value is expressed as a mean ± SD (results from

$n \geq 3$ independent experiments). Asterisks denote a statistically significant difference (* = $p < 0.05$) between strains.

### *2.4. Rapamycin Stimulates ER-Remodelling, Increases Lysosome Number, Modifies Their Distribution, Decreasing Prb and Bcl-2 Content*

Once established the main parameters and cellular pathways in which we expected to highlight a marked role of RM, we evaluated the activation of autophagy by mTOR inhibition, investigating the effects of RM in U937 cells, uninfected or infected with the respective lysates. As shown in Figure 4, significant differences were reported between uninfected and infected cells (by lysates) and untreated and treated cells (by RM). ER stress was significantly demonstrated for the wild-type strain, although mutant treated cells also showed a certain increase of ER tracker MFI and CHOP increase (Figure 2A–C). The additional enlargement that we observed for ER tubules and sheets, in ATCC 33291 lysate-treated cells, may be due to the CDT-dependant rearrangement of the cell size [61] (Figure 4A). Although ER stress and autophagy can function independently, mounting evidence indicates that autophagy is interrelated to the ER at many levels. Cytometric data (Figure 4B) demonstrated that RM, in ATCC 33291 treated cells, significantly and deeply increase lysosomal compartment (traced by Lysotracker Deep Red-LTDR, a fluorescent dye for labelling and tracking acidic organelles in live cells): this event is certainly due to the combination of CDT plus RM, as the inhibitor of mTOR does not increase as much as lysosomes, neither in the control or in the mutant treated cells. Contemporary RM administration decreases ER-tracker fluorescence (Figure 4C), particularly and significantly in ATCC33291-treated cells.

This behaviour is accompanied by a decrease in both pRb and bcl2 (Figure 4 D,E). In fact, RM pre-treatment reduces pRb intracellular content in ATCC 33291 lysate-treated cells: this finding is consistent with the limitation of some effects exploited by CDTs, i.e., cell cycle blocking, enlargement of cell size and autophagosome/autophagolysosome induction. In fact, Rb protein is upregulated by wild-type lysate and subsequently reduced by RM pre-treatment. A decrease of the anti-apoptotic protein, Bcl-2, is usually associated with amplified apoptosis; however, as demonstrated in the previous paragraph, RM reduces PI+ events, induced by CDT. Coupling these findings, we identified that in U937 cells, the induction of cell death by CDT is, at least in part, bcl-2-independant and that RM leaves the cells still prone to apoptotic triggers.

Confocal analyses were applied not only to confirm the flow cytometric quantification of ER and lysosomal network, but also to underline a possible co-localization of the two compartments,

suggested by the flow cytometric data. ER-remodelling behaviour is focused by the orange merged-area and quantitated by Pearson's coefficient. (Figure 5A,B). RM induces a concomitant increase of LTDR MFI and the decrease of ER-tracker MFI was quantitatively calculated by FCM coupled to Pearson's coefficient evaluated by CM (Figure 5B). Furthermore, by means of TMRE (a potentiometric probe that can be used for direct measurement of the mitochondrial membrane potential $\Delta\Psi m$) [45], we evaluated the RM preservation of $\Delta\Psi m$ (Figure 5D,E) and concomitant increase in TMRE–ER-tracker co-localization (Figure 5D,F). This increase in ER–mitochondria proximity [62] and in TMRE fluorescence suggests that RM can modulate both mitochondrial bioenergetics and ER–mitochondria contacts. We want to highlight how the quantitative cytometric data help to interpret the co-localization frameworks: in fact, the increase of co-localization for lysosomes and ER happens in parallel to a significant and relevant decrease of ER-tracker fluorescence (Figure 4C) (attesting a decrease in ER *cisternae* and tubules), and a strong increase in lysosome–LTDR fluorescence (for ATCC 33291 lysate-treated cells only).

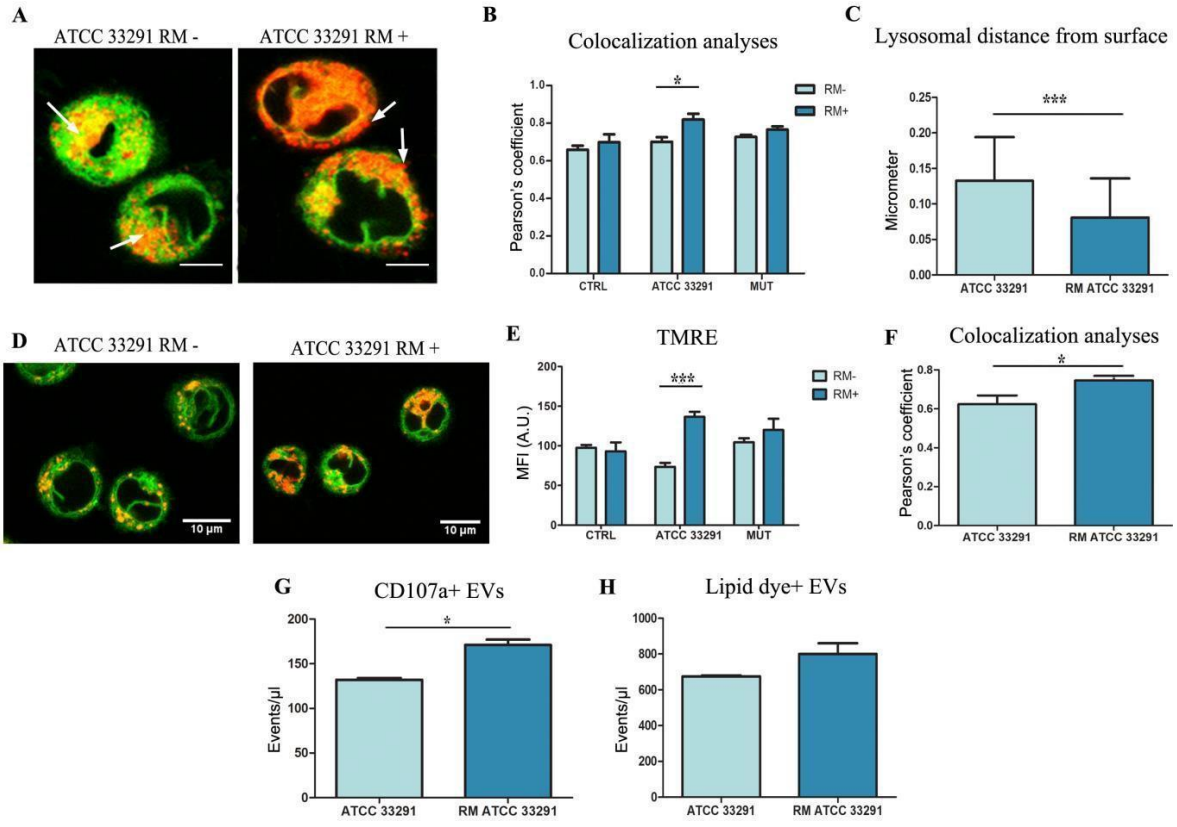


**Figure 5.** Confocal analyses: ER morhology and extension and its relationship with lysosomes.Single confocal optical sections of ER Tracker (in green) and LTDR (in red) of ATCC33291 lysate treated U937 cells and U937 cells preincubated with lysate and treated by RM, after 72 h. Co-localization is shown in yellow-orange and white arrows indicate the positioning of lysosomes, from a perinuclear area (ATCC 33291 RM-) to a peripheral

distribution (ATCC 33291 RM+). Bars: 10 μM. In (**B**), Pearson's coefficient, able to quantitate co-localization, specifically induced by RM in ATCC 33291 lysate treated cells. Asterisks denote a statistically significant difference (* = $p < 0.05$) between strains. (**C**) Lysosome distance from surface calculated by ImageJ. Calculation performed on 30 cells for each experiment ($n = 3$). Only lysosomes with a puncta and definite morphology were counted, from a minimum of 10/cell to a maximum of 30/cell. Mitochondria membrane potential and ER–mitochondria interactions. Asterisks denote a statistically significant difference (*** = $p < 0.001$) between strains. (**D**) Single confocal optical sections of ER Tracker (in green) and TMRE (in red) of ATCC33291 lysate treated U937 cells and U937 cells preincubated with lysate and treated by RM, after 72 h. Red fluorescence from mitochondria and their puncta are clearly increased in RM+ cells. Bars: 10 μM. (**E**) TMRE MFI values of RM- and RM+ lysate-treated U937 cells. Asterisks denote a statistically significant difference (*** = $p < 0.001$) between strains. (**F**) Pearson's coefficient, able to quantitate TMRE/ER-tracker co-localization, specifically induced by RM in ATCC 33291 lysate treated cells. Total extracellular vesicles (EVs) and EVs from lysosome exocytosis. Asterisks denote a statistically significant difference (* = $p < 0.05$) between strains. (**G**) Flow cytometric quantitation of CD107a + EVs with (RM ATCC 33291) or without (ATCC 33291). Asterisks denote a statistically significant difference (* = $p < 0.05$) between strains. (**H**) Flow cytometric quantitation of lipid dye + EVs with (RM ATCC 33291) or without (ATCC 33291).

In Figure 5A, we can observe a diverse positioning of lysosomes, moving from a perinuclear area to a peripheral distribution (arrows). This is an intriguing effect because lysosomal positioning influences mTOR activity, autophagosome biogenesis and autophagosome–lysosome fusion [63]. The availability of lysosomes at the perinuclear region could control the rate of autophagosomal degradation. The observed peripheral lysosome distribution (Figure 5C), induced by RM, is optimal for budding and release via lysosomal exocytosis, as previously demonstrated [45]. Autophagic flux and exosome release are two connected processes that cause loss of cellular membrane and protein content. Figure 5G,H highlights extracellular vesicle count in ATCC33291 lysate-treated cells and RM-treated counterparts. We can observe a moderate and non-significant increase (15%) in lipid dye positive vesicles of RM ATCC samples in respect of ATCC samples, whereas this increase becomes more evident (25%) and significant for $CD107a^+$ vesicles, in agreement with the peripheral dispersion of lysosomes. These data underline that RM interferes specifically in lysosomal exocytosis and not mainly on multivesicular body (MVB) formation, budding, and release.

*2.5. Evaluation of Membrane Microdomains*

CD317/tetherin is an organizer of membrane microdomains [64]. CD317/tetherin is an antigen localized within lipid rafts on the cell surface, in the TGN, and/or within recycling endosomes [17]. The different positioning of lysosomes and the extracellular vesicle release, together with its involvement during infections, prompted us to investigate the expression and the distribution of CD317 in our experimental model. As showed in Figure 6C,D, in infected U937, we found an important increase in CD317 expression after 48 h of treatment, whereas RM significantly prevented this effect. Confocal analyses confirm the cytometric data highlighting also a redistribution of CD317 on the cell surface. We observed the formation of a large number of CD317 clusters, in particular in ATCC 33291 treated samples (Figure 6C), whereas in the control condition, this surface antigen appeared to spread on the cell membrane. A similar phenomenon was also observed by other researchers that demonstrated that HIV-1 viral proteins bring to the reorganization of plasma membrane microdomains inducing the coalescence of lipid rafts and tetraspanin-enriched microdomains [65]. As evident in Figure 6C, RM pre-treatment avoided CD317 clusterization and coalescence, appearing similar to the control condition, also in the presence of lysates. It is clear that RM, by modifying the levels and distribution of CD317, plays a role in the organization of lipids in the plasma membrane and in the distribution of proteins that are confined to lipid rafts [66].

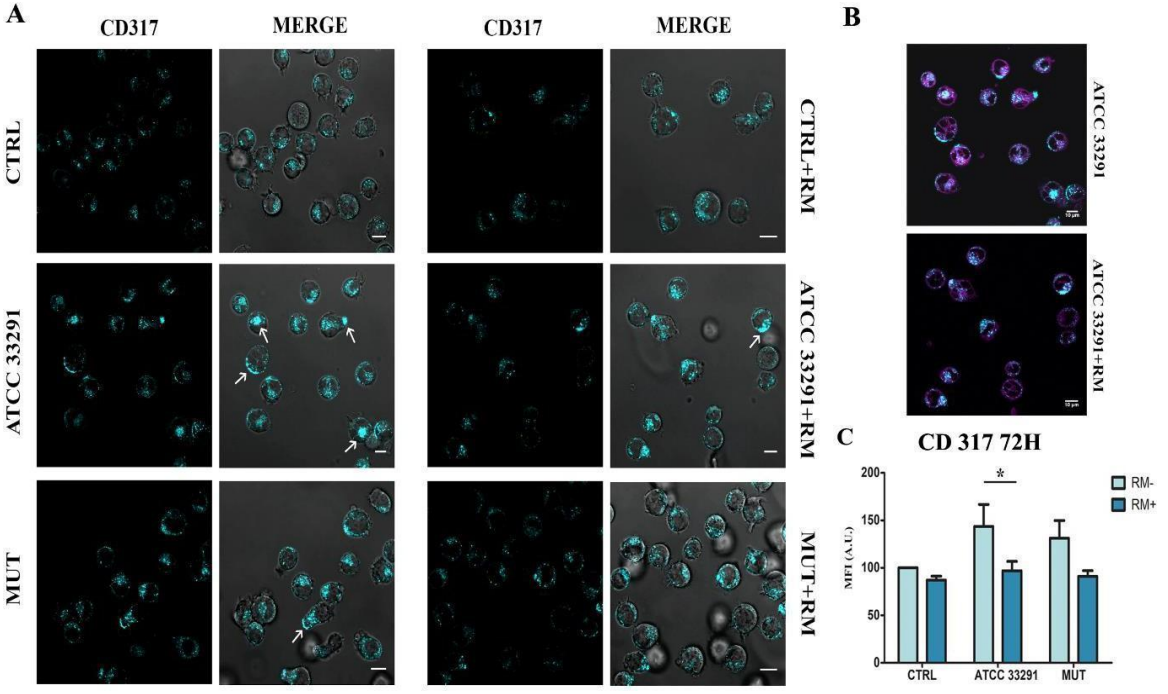


**Figure 6.** Expression of CD317/tetherin: localization and quantitation by confocal and cytometric analyses, respectively. (**A**) Single confocal optical sections of CD317 of untreated U937 cells (CTRL) and U937 cells after

72 h of treatment by lysates, with and without RM. Bars: 10 μM. (**B**) A comparison between RM- and RM+ ATCC33291 lysate (CDT active)-treated cells: magenta stain represents ER-tracker fluorescence, added to better visualize CD317 distribution and to resemble the ER decrease induced by RM. Bars: 10 μM (**C**) Statistical histograms of CD317 MFI were calculated after 72 h from lysate administration in cells with and without RM. Each value was converted to arbitrary units (A.U.), setting the control as 100. Each value is expressed as a mean ± SD (results from $n \geq 3$ independent experiments). Asterisks denote a statistically significant difference (* = $p < 0.05$) between strains.

## 3. Discussion

In this paper, we studied the effects of RM in *C. jejuni* CDT containing lysate-treated U937 cells. As it was already demonstrated [45,54], *C. jejuni* lysates were able to induce morphologic changes, cell cycle arrest, therefore a reduction in cell number, and apoptosis in different cell models. Here, we demonstrate, for the first time, the powerful action of RM on *C. jejuni* lysate-treated U937 cells, particularly on the mechanisms of CDT activity.

Adopting U937 as a cellular model [47–49], we firstly tested CDT activity on U937 cells, examining apoptosis, cell cycle blocking, ER stress, and pRb expression. Indeed, lysosome network involvement and ER-remodelling induction were found as two subcellular processes triggered by RM in saving cells from the action of CDT and, more generally, from the effects of lysates.

At the center of the regulation of mTORC1 signalling is the lysosome, and lysosome distribution influences mTORC1 activity. Intriguingly, the bulk of lysosomes, early and late endosomes, locates quiescently in the perinuclear region of the cell [67–72], poised toward the cell's periphery, as it is shown. Our data display a moderate rise in the lysosome network, primed by lysates, and significantly peaked by the addition of RM. This behaviour is particularly evident in cells preincubated with the *C. jejuni* ATCC 332921 lysate, with an active CDT. These findings demonstrate that RM specifically counteracts CDT activity. Contemporarily, after 72 h of treatment, U937 cells respond to stimuli by activating the expansion of the acidic compartment, increasing ER–lysosome contacts and decreasing the ER volume: a scenario strongly suggesting ER-phagy. Late endosomes and lysosomes also make extensive contact with the ER, and numerous studies implicate ER-endolysosomal crosstalk in organelle reshaping and migration [73]. The ER-remodelling and ER-phagy events are selectively activated and they possess the potential to rebalance the ER network and, in our data, might also impact the function of other organelles. It is known that, under basal conditions, ER-phagy occurs constantly at a low level to maintain ER homeostasis [74] and also plays

a prominent role in the innate defence against viral and bacterial infections [75,76]. In fact, after the lysate administration, we observed ER stress and ER expansion in cells, and RM, clearly triggering a lysosome increase, strengthening of acidic vacuoles, and ER-remodelling (with features of ER-phagy), represents a powerful treatment to minimize the pathogen attack [77], and it is able to re-establish the pre-stress ER volume, content, and activity [78]. The ER is the only intracellular organelle covering every corner of the cytosol, it has been shown to participate in various functional contacts with other membranous compartments, mediating exchange of metabolites and controlling transport and fusion processes [68,79].

Our findings demonstrate that ER-remodelling (with a key role in the maintenance of ER homeostasis) participates in the cell survival and functional recovery induced by RM. Bravo-Sagua and co-workers [63] showed that ER stress, during its early stage, increases the ER–mitochondria contacts, thus leading to an adaptive increase in mitochondrial energetics. This appears to be a generic response to acute stress, as we similarly observed such changes upon inhibition of the nutrient-sensing kinase mammalian target of rapamycin complex 1 (mTORC1) [80]. In fact, RM enables lysate treated cells to maintain a high mitochondrial membrane potential, accordingly to the decrease of the apoptotic process. Furthermore, RM seems to increase the ER–mitochondria proximity and higher mitochondrial membrane potential, as it appears from FCM and CM analyses of TMRE/ER-tracker labelled samples. We detected an increase in the pRb intracellular content, significantly induced by the wild-type strain and partly reverted by RM administration. We found for the first time that this drug is able to partially avoid or delay specific sub-lethal effects, most of these linked to CDT action, able to infer in U937 cells autophagic and ER stress. The pRb decrease (as well as bcl-2 drop) characterizes a cellular status prone to apoptosis. Such effect, together with the downregulation of CD317/tetherin, picked by lysates in the cell surface, represents part of the mechanistic aspects of the results shown in Figure 3. pRb has been reported to cause growth arrest and inhibit apoptosis [81]. Upregulation of pRb by the *C. jejuni* wild-type strain might represent a helpful expedient that this bacterium might activate to persist in host cells and to contrast with the programmed cell death. Noteworthy RM addition decreases nuclear pRb content. Interestingly, the recent literature on pRb indicates that loss of pRb function enhances the efficacy of several types of anticancer agents, including tamoxifen, microtubule-interfering agents, and DNA-damaging agents [82]. It has been reported that pRb and lysosomes are interconnected during senescence [83]. The lysosome also extensively communicates with other cellular structures by exchanging content and information and by establishing membrane contact sites. It is now clear that lysosome positioning is

a dynamically regulated process and a crucial determinant of lysosomal function. Our results show that RM strongly induces a redirection of lysosomes, from a juxta-nuclear position towards the periphery. Lysosomal positioning is intimately associated with mTORC1 activity and nutrient levels. For example, mTORC1 activation under nutrient-rich conditions causes scattering of lysosomes to the periphery [84,85]. Furthermore, we showed that the RM-induced lysosome redistribution is in connection with vesicle release. The directionality of vesicle transport is regulated also by ER-lysosome contact sites. Currently, contact sites between the ER and endolysosomes are emerging as potent regulatory hubs for vesicle transport [86,87], fusion [88], and fission [89] events. The process of vesicle release in our research is limited to $CD107a^{+}$ extracellular vesicles (EVs), resembling lysosomal exocytosis and clearly increased by RM.

CD317/tetherin (i.e., BST2 or HM1.24 antigen) is an interferon inducible membrane protein present in regions of the lipid bilayer enriched in sphingolipids and cholesterol (often termed lipid rafts). It has been implicated in an eclectic mix of cellular processes including, most notably, the retention of fully formed viral particles at the surface of cells infected with HIV and other enveloped viruses [90]. Edgar and co-workers [20] demonstrated that reduction of tetherin strongly reduces the number of exosomes associated with the plasma membrane with a concomitant increase in exosomes released into the medium. In agreement with these findings, we found an increase of extracellular vesicles in the medium of RM+ ATCC 33291-treated cells, together with a decreased amount of CD317 in the plasma membrane.

In fact, in our model, rapamycin pre-treatment avoids CD317 clusterization and coalescence, previously induced by lysates, particularly by CDT. RM not only decreases CD317 expression but impacts on its distribution: this molecule displays antiviral (and antibacterial) functions, and it is involved in disease manifestation [91]. Therefore, modulating CD317 expression and/or activity has the potential to influence the course of disease.

In summary, *C. jejuni* cytolethal distending toxin impairs apoptosis and lysosomal routes with evidence of ER stress; RM modifies this cellular response to CDT exposition, increasing and redirecting lysosomes, in order to unlock the later stages of lysosomal exocytosis, increasing the release of extracellular vesicles, and the clear reduction and re-assembly of CD317/tetherin.

This research, although with the known limitations of the cellular "*in vitro*" model, opens up the possibility to use RM as a drug to minimize the risk of the onset of sequelae such as the Guillain–Barré syndrome, in case of massive and important infections by *C. jejuni*. Further aspects are under

investigation, to deeply monitor the pathways identified here in the RM control of U937 *C jejuni* lysate intoxication.

A deeper understanding of the modulations and interconnection between these physiological processes, especially under pathological conditions, will be of great importance and may shed light on developing new strategies in treating *C. jejuni* infections.

## 4. Materials and Methods

### *4.1 Cell Culture*

U937 (human myelomonocytic cell line) cells (Sigma-Aldrich, St Louis, MO, USA) were grown in RPMI 1640 supplemented with 10% heat-inactivated fetal bovine serum (FBS), 2 mM glutamine, and 1% antibiotics, and was maintained at 37 °C in humidified air with 5% $CO_2$.

### *4.2 Growth Conditions of Bacterial Strains and Cell Lysate Preparation*

*C. jejuni* ATCC 33291 and *C. jejuni* 11168H *cdtA* mutants were grown at 37b °C in a microaerobic chamber (Don Whitley Scientific, Shipley, United Kingdom) containing 85% N2, 10% CO2, and 5% O2, either on blood agar (BA) plates containing Columbia agar base (Oxoid, Basingstoke, United Kingdom) supplemented with 7% (*v*/*v*) horse blood (TCS Microbiology, United Kingdom) and *Campylobacter* Selective Supplement (Oxoid), or in Brucella broth (Oxoid) with shaking at 75 rpm. *C. jejuni* strains were grown on BA plates for 24 h prior to use in all assays, unless otherwise stated.

*C. jejuni* strains were grown in 50 mL Brucella broth (Oxoid) at 37 °C in a shaking incubator under microaerophilic condition for 48 h. The bacterial suspensions were centrifuged at 4000 rpm for 10 min and the pellets were resuspended in 20 mL of Dulbecco's modified eagle medium (D-MEM) (Sigma-Aldrich, St Louis, MO, USA). Then, bacterial suspensions were adjusted spectrophotometrically to approximately $10^8$ bacteria/mL and lysed by sonication (2 × 30 s bursts with 30 s intervals between each burst) by using a sonicator (Sonifier 450, Branson, Danbury, CT, USA). Cell debris and un-lysed bacterial cells were then removed by centrifugation at 4000 rpm for 10 min. Aliquots of each lysate were sterilized by a 0.22-μm membrane filter (Millipore, Milano, Italy) and stored at −20 °C before use [68].

### 4.3 *Pre-Treatment of U937 Cells with Rapamycin*

RM is an efficient pharmacological inhibitor of mTOR (mammalian target of rapamycin), which is able to induce autophagy in mammal cells [9]; mTOR is a complex composed of two entities, mTORC1 (mTOR complex 1) and mTORC2 (mTOR complex 2); mTORC1 is a downstream target of PI3K (phosphoinositide 3-kinase) and is sensitive to the RM [92]; mTOR plays an important role in cell growth and proliferation [93] and its activation was recently associated to intestinal inflammation induced by *C. jejuni* [94]. U937 cells were pre-treated with RM 100 nM for 2 h before the treatment with lysates.

### 4.4 *Pre-Treatment of U937 Cells With C. jejuni Lysates*

U937 cells were incubated for 6, 12, 24, 48, and 72 h with 2 mL of media enriched with *C. jejuni* cell lysates (1:100 dilution) from ATCC 33291 and 11168H *cdtA* mutant strains previously prepared. Treated cells were analyzed by means of flow cytometry and confocal microscopy to evaluate different cellular parameters. For the negative control, cells were incubated with media only.

### 4.5 *Detection of Cytotoxin Activity in C. jejuni Lysates*

U937 cells were seeded into 24-well tissue culture plates at a density of $2.6 \times 10^5$ cells per well for 2 h prior to the addition of the lysates diluted at 1:5, 1:10, 1:50, 1:100, and 1:500, respectively. The cultures were incubated at 37 °C in 5% $CO_2$ atmosphere and examined microscopically at 24-hour intervals for 4 days to evaluate morphological changes. The best acting dilution was the 1:100 which was chosen for all subsequent evaluations. All strains were tested in at least three independent experiments.

### 4.6 *Morphological Feature Evaluation*

To evaluate changes in cell morphology and size, both cytometry and confocal microscopy were used. In flow cytometry, populations that differed in size and morphology were distinguished by using their physical characteristics: forward scatter (FSC, cell size) and side scatter (SSC, cell granularity). Although a quantitative analysis was carried out by flow cytometry, a parallel microscopic evaluation of cell dimension was performed.

### *4.7 Flow Cytometry (FCM) and Confocal Microscopy (CM) Stainings*

#### 4.7.1. Flow Cytometric Detection of Cell Death and Flow Cytometric Absolute Count

Cell death features were evaluated using supravital propidium iodide (PI) (Sigma-Aldrich) that is capable of binding and labeling DNA. No permeabilized cells were incubated 30 min in the dark with 50 μg/mL PI. Cells were washed with PBS and then analyzed by flow cytometry. Apoptotic and necrotic cells were detected as $PI_{dim}$ and $PI_{bright}$ clusters, respectively.

To investigate programmed cell death features (early and late apoptotic, as well as necrotic cells), we also used a double staining FITC-conjugated Annexin V-PI (AnxV-PI). AnxV allows to detect phosphatidylserines exposed on the outer cell membrane following caspase activation. AnxV-PI staining was carried out according to the manufacturer's instructions (Immunostep, Spain). Absolute cell counting was performed by using Dako CytoCount™ beads (Thermo Fisher Scientific, Waltham, MA, USA). 200 μL of sample was carefully dispensed at the bottom of the tube and 50-μL beads were added. Samples were acquired by using a FACSCanto II cytometer ((BD, Franklin Lakes, NJ, USA)) within 60 min. Approximately 20,000 cell events were collected. Setup and calibration procedures were optimized for the absolute counting protocols [95].

#### 4.7.2. Evaluation of Cellular Division by CFSE Staining

Carboxyfluoresceinsuccinimidyl ester (CFSE) is a fluorescent dye that can measure cell proliferation using flow cytometry. CFSE was transported into the cell during incubation with mononuclear cells binding covalently to cytoplasmic proteins, without adversely affecting cellular function. Analysis of cell division can be determined through measuring CFSE intensity by flow cytometry: with each cell division, the fluorescent intensity per cell division is reduced by 50 %, thus providing a readout of the mitotic activity within a specific population of cells. U937 cells were stained with 3 μM CFSE at day 0 and then analyzed at 24, 48, and 72 h [54]. At these times, U937 treated and untreated samples were harvested and acquired by flow cytometry.

#### 4.7.3. Assessment of Lysosomal Involvement

To label and trace lysosomes in U937 cells, the acidotropic dye LysoTracker Deep Red (LTDR) (Thermo Fisher Scientific, Waltham, MA, USA) was used. LysoTracker probes are fluorescent acidotropic probes for labeling and tracking acidic organelles in live cells: it means that the amount of fluorescence obtained from staining with LysoTracker is directly related to the volume of lysosome-related organelles in a cell [96]. Cells were cultured at 37 °C and resuspended in pre-

warmed (37 °C) medium containing 100 nM of LysoTracker (diluted in RPMI). After 45 min of incubation, red lysosomal fluorescence was detected by flow cytometry and confocal microscopy [97].

#### 4.7.4. Determination of Mitochondria and Mitochondrial Membrane Potential (ΔΨm)

Mitochondrial features were investigated by Tetramethylrhodamine ethyl ester perchlorate (TMRE) (Sigma-Aldrich, St. Louis, MO, USA) is a ΔΨm-specific stain able to selectively enter the mitochondria depending on ΔΨm, producing red fluorescence. TMRE 40 nM was added to the samples 15 min before the acquisition time. The samples were analyzed by confocal microscopy and flow cytometry using the appropriate fluorescence channel [45,98].

#### 4.7.5. ER Stress Evaluation

ER-Tracker Green (Thermo Fisher Scientific, Waltham, MA, USA) is a live-cell stain highly selective for the ER. This stain consists of the green-fluorescent BODIPY® FL dye and glibenclamide that bind to the sulfonylurea receptors of ATP-sensitive $K^+$ channels which are prominent on the ER and have a critical role in the ER luminal homeostasis. Indeed, ER $K^+$ channels are involved in functions such as protein folding, apoptosis, and $Ca^{2+}$ homeostasis [99,100].

U937 were incubated with 100 nM ER-Tracker Green for 30 min at 37 °C and subjected to flow cytometry and confocal analyses.

#### 4.7.6. CD317 Expression Evaluation

To evaluate CD317 expression, fluorochrome-conjugated monoclonal antibodies were added to 50 µL of cell pellet. Mouse monoclonal anti-human antibodies Alexa Fluor® 647 anti-CD317 (129C1) (BioLegend, San Diego, CA, USA) was added at dilutions according to the manufacturer's instructions. After 15 min of incubation at RT, samples were acquired by flow cytometry and/or confocal microscopy.

#### 4.7.7. Intracellular Detection of Prb and Bcl-2 Antigens

U937 were washed in PBS for 10 min at RT, resuspended in 300 µL formaldehyde 3.7% and incubated at 4 °C for 15 min; 2 mL perm/washing buffer was added and cells were centrifuged at 1200 rpm for 10 min. Pellets were resuspended in 300 µL Cytoperm reagent [101]. Monoclonal anti-human antibodies Anti-pRb PE conjugated (clone G3-245) (BD) and anti bcl-2 FITC (clone 124) (Dako, Milan, Italy) were added to samples at concentrations according to the manufacturer's

instructions. Cells were incubated at 4 °C for 30 min before being processed by flow cytometry and/or confocal microscopy.

#### 4.7.8. Extracellular Vesicle Detection

In order to detect microparticles in the extracellular environment, without any preparation step of ultracentrifugation, we resuspended each sample (20 μL) in 0.22-filtered PBS 1X. We performed the test by using a BD custom product, i.e., a kit based on an APC emitting lipophilic cationic dye that diffuses through the plasma membranes [102]. After an incubation of 60 min to ensure the binding of the monoclonal antibody (CD107a mAb, clone H4A3) (BioLegend, London, UK) to the specific epitope, we proceeded with FC analyses. The flow cytometry approach consisted of acquiring samples mixed with beads of defined size (Ø 0.5 μm, 1 μm, 5.2 μm) to obtain a size calibration of small particles detected outside the scatter area of intact cells. Furthermore, it is important to specify that the FCS of the complete medium was ultracentrifuged to minimize contamination by serum microvesicles. Samples were acquired by a FACSCanto flow cytometer and a FACSDiva™ software was used to analyze all data.

#### 4.7.9. Cytometric Investigations

Cytometric experiments were carried out with a FACSCanto II flow cytometer (BD, Franklin, Lakes, NJ, USA) equipped with an argon laser (Blue, Excitation 488 nm), a helium-neon laser (Red, Excitation 633 nm), and a solid-state diode laser (Violet, Ex 405 nm). Analyses were performed with the FACSDiva™ software (BD); approximately 10,000 cell events were acquired for each sample.

#### 4.7.10. Confocal Microscopy Analyses

Confocal microscopy analyses were applied by a Leica TCS SP5 II confocal microscope (Leica Microsystem, Germany) with 488, 543, and 633 nm illuminations and oil-immersed objectives. For confocal live imaging, cells were grown on MatTek glass bottom chambers (MatTek Corporation, Bratislava, Slovak Republic). The images were further processed and analyzed in ImageJ software (NIH, Bethesda, MD, USA).

### *4.8. RNA Isolation and cDNA Synthesis*

Cells were directly lysed with 700 µL of QIAzol® Lysis Reagent (Qiagen, Hilden, Germany). Total RNA extraction was performed with the miRNeasy Mini Kit (Qiagen, Hilden, Germany) following the manufacturer's instructions. The extracted RNA was quantified using a NanoVue Plus™ spectrophotometer (GE Healthcare Life Sciences, Piscataway, NJ, USA). The cDNA synthesis was performed from 500 ng of total RNA using PrimeScript™ RT Master Mix (Perfect Real Time) (Takara Bio Inc. Shiga, Japan) according to the manufacturer's instructions.

### *4.9. Quantitative Real-Time PCR*

The expression of CHOP was monitored by qPCR using RT² SYBR Green ROX FAST Mastermix (Qiagen, Hilden, Germany) in a RotorGene 6000 instrument (Corbett life science, Sydney, Australia), as described previously [103]. A non-template control was included in duplicate for each primer pair reaction, as a negative control. To exclude the presence of non-specific products or primer dimers, a melting curve analysis from 65 °C to 95 °C was performed at the end of each run. GUSB (Beta-D-Glucuronidase) gene was used as reference. Relative mRNA expression was calculated using the comparative quantitation analysis of the RotorGene 6000 software.

### *4.10. Statistical Analyses*

Data are shown as mean (or percentage, as indicated) ± standard deviation (SD) of at least three independent experiments. Analyses of variance (ANOVA) approaches were used to compare values among more than two different experimental groups for data that met the normality assumption. One-way ANOVA or two-way ANOVA were followed by a Bonferroni post-hoc test. The means of two groups were compared by using a t test. The $p$ values less than 0.05 were considered statistically significant. All statistical analyses were performed using GraphPad Prism 5.0 (GraphPad software, San Diego, CA, USA).

**Supplementary Materials:**

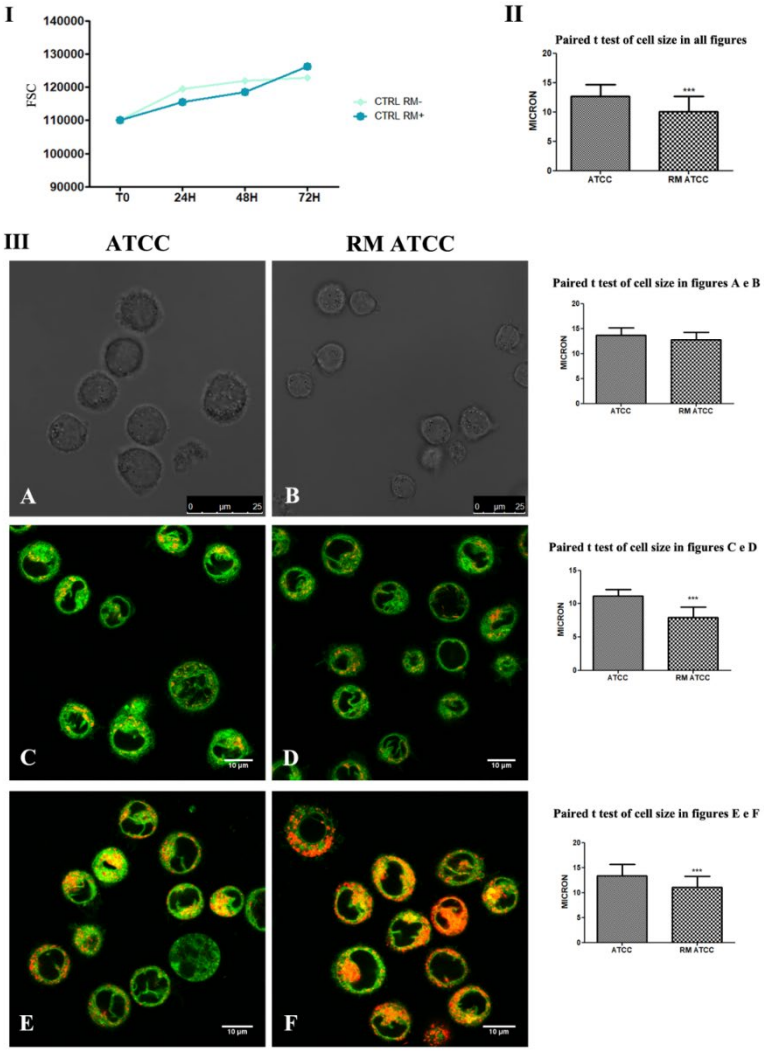


**Figure S1 Evaluation of cell size induced by lysates and RM administration I** Trends of forward light scatter (FSC) values for control cells with (RM+) or without (RM-) Rapamycin, during the time course from the starting point (T0) to 72h. Each value is expressed as a mean ± SD (Results from n ≥ 3 independent experiments). **II** Statistical histograms on cell size evaluated by microscopic measurements, comparing ATCC33291 lysate treated U937 cells (ATCC) and the same cells pre-treated with Rapamycin (RM ATCC).. Paired t test (two-tailed P value) revealed: ***P<0.0001 ATCC 33291vs RM ATCC 33291. **III** Single confocal optical sections of ATCC33291 lysate treated U937 cells (ATCC) and the same cells pre-treated with Rapamycin (RM ATCC), from different analyses: **A-B**: Brightfield, **C-D**: ER Tracker/TMRE; **E-F**: ER tracker/LTDR utilized for cell size measurements.

**Author Contributions:** Conceptualization, B.C.; methodology, B.C., G.D.S., and E.C.; validation, B.C., E.C., and M.M.; formal analysis, B.C., E.C., L.G., and M.M.; investigation, B.C., G.D.S., E.C., R.C., and A.D.; resources, W.B., S.P., O.G., and F.S.; data curation, B.C., E.C., M.M., and L.G.; writing—original draft preparation, B.C.; visualization, B.C., E.C., M.M., R.C., and F.L.; supervision, B.C.; project administration, B.C. and G.D.S.; funding acquisition, W.B., A.G., and S.P. All authors have read and agreed to the published version of the manuscript.

**Funding:** This research received no external funding.

**Conflicts of Interest:** The authors declare no conflict of interest.

## Abbreviations

| | |
|---|---|
| *C. jejuni* | *Campylobacter jejuni* |
| AnxV | Annexin V |
| Atg | Autophagy-Related Proteins |
| CDT | Cytolethal Distending Toxin |
| CFSE | Carboxyfluoresceinsuccinimidyl ester |
| ER | Endoplasmic Reticulum |
| EVs | Extracellular vesicles |
| GBS | Guillain-Barré syndrome |
| LTDR | LysoTracker Deep Red |
| MFI | Mean Fluorescence Intensity |
| MVB | Multivesicular body |
| pRb | Retinoblastoma Protein |
| ReA | reactive arthritis |
| RM | Rapamycin |
| TGN | Trans-Golgi Network |
| TMRE | Tetramethylrhodamine ethyl ester perchlorate |
| UPR | Unfolded protein response |

## References


1. Shen, H.M.; Mizushima, N. At the end of the autophagic road: An emerging understanding of lysosomal functions in autophagy. *Trends Biochem. Sci.* **2014**, *39*, 61–71. [CrossRef] [PubMed]

2. Py, B.F.; Lipinski, M.M.; Yuan, J. Autophagy limits Listeria monocytogenes intracellular growth in the early phase of primary infection. *Autophagy* **2007**, *3*, 117–125. [CrossRef] [PubMed]

3. Galluzzi, L.; Green, D.R. Autophagy-Independent Functions of the Autophagy Machinery. *Cell* **2019**, *177*, 1682–1699. [CrossRef] [PubMed]

4. Lum, J.J.; Bauer, D.E.; Kong, M.; Harris, M.H.; Li, C.; Lindsten, T.; Thompson, C.B. Growth Factor Regulation of Autophagy and Cell Survival in the Absence of Apoptosis. *Cell* **2005**, *120*, 237–248. [CrossRef] [PubMed]

5. Shimizu, S.; Kanaseki, T.; Mizushima, N.; Mizuta, T.; Arakawa-Kobayashi, S.; Thompson, C.B.; Tsujimoto, Y. Role of Bcl-2 family proteins in a non-apoptotic programmed cell death dependent on autophagy genes. *Nat. Cell Biol.* **2004**, *6*, 1221–1228. [CrossRef]

6. Booth, L.A.; Roberts, J.L.; Dent, P. The role of cell signaling in the crosstalk between autophagy and apoptosis in the regulation of tumor cell survival in response to sorafenib and neratinib. *Semin. Cancer Biol.* **2019**. [CrossRef]

7. Nikoletopoulou, V.; Markaki, M.; Palikaras, K.; Tavernarakis, N. Crosstalk between apoptosis, necrosis and autophagy. *Biochim. Biophys. Acta - Mol. Cell Res.* **2013**, *1833*, 3448–3459. [CrossRef]

8. Maiuri, M.C.; Zalckvar, E.; Kimchi, A.; Kroemer, G. Self-eating and self-killing: Crosstalk between autophagy and apoptosis. *Nat. Rev. Mol. Cell Biol.* **2007**, *8*, 741–752. [CrossRef]

9. Sehgal, S.N. Sirolimus: Its discovery, biological properties, and mechanism of action. *Transplant. Proc.* **2003**, *35*, 7S–14S. [CrossRef]

10. Babcock, J.T.; Nguyen, H.B.; He, Y.; Hendricks, J.W.; Wek, R.C.; Quilliam, L.A. Mammalian Target of Rapamycin Complex 1 (mTORC1) enhances bortezomib-induced death in Tuberous Sclerosis Complex (TSC)-null cells by a c-MYC-dependent induction of the unfolded protein response. *J. Biol. Chem.* **2013**, *288*, 15687–15698. [CrossRef]

11. Kato, H.; Nakajima, S.; Saito, Y.; Takahashi, S.; Katoh, R.; Kitamura, M. MTORC1 serves ER stress-triggered apoptosis via selective activation of the IRE1-JNK pathway. *Cell Death Differ.* **2012**, *19*, 310–320. [CrossRef] [PubMed]

12. Ji, Y.; Luo, X.; Yang, Y.; Dai, Z.; Wu, G.; Wu, Z. Endoplasmic reticulum stress-induced apoptosis in intestinal epithelial cells: A feed-back regulation by mechanistic target of rapamycin complex 1 (mTORC1). *J. Anim. Sci. Biotechnol.* **2018**, *9*. [CrossRef] [PubMed]

13. Boesze-Battaglia, K.; Alexander, D.; Dlakic´, M.; Shenker, B.J. A Journey of Cytolethal Distending Toxins through Cell Membranes. *Front. Cell. Infect. Microbiol.* **2016**, *6*, 81. [CrossRef] [PubMed]

14. Berry, K.N.; Kober, D.L.; Su, A.; Brett, T.J. Limiting Respiratory Viral Infection by Targeting Antiviral and Immunological Functions of BST-2/Tetherin: Knowledge and Gaps. *BioEssays* **2018**, *40*, 1800086. [CrossRef] [PubMed]

15. Kupzig, S.; Korolchuk, V.; Rollason, R.; Sugden, A.; Wilde, A.; Banting, G. Bst-2/HM1.24 is a raft-associated apical membrane protein with an unusual topology. *Traffic* **2003**, *4*, 694–709. [CrossRef]

16. Masuyama, N.; Kuronita, T.; Tanaka, R.; Muto, T.; Hirota, Y.; Takigawa, A.; Fujita, H.; Aso, Y.; Amano, J.; Tanaka, Y. HM1.24 Is Internalized from Lipid Rafts by Clathrin-mediated Endocytosis through Interaction with α-Adaptin. *J. Biol. Chem.* **2009**, *284*, 15927–15941. [CrossRef]

17. Zhang, G.; Li, X.; Liu, L.; Li, J.; Chen, Q.; Huang, S.; Li, Y.; Wan, X. Vaccination with a DNA vaccine encoding CD317-targeting HBs antigen elicits enhanced immunity in mice. *Biochem. Biophys. Res. Commun.* **2018**, *504*, 865–870. [CrossRef]

18. Yi, E.; Oh, J.; Kang, H.R.; Song, M.J.; Park, S.H. BST2 inhibits infection of influenza A virus by promoting apoptosis of infected cells. *Biochem. Biophys. Res. Commun.* **2019**. [CrossRef]

19. Neil, S.J.D.; Zang, T.; Bieniasz, P.D. Tetherin inhibits retrovirus release and is antagonized by HIV-1 Vpu. *Nature* **2008**, *451*, 425–430. [CrossRef]

20. Edgar, J.R.; Manna, P.T.; Nishimura, S.; Banting, G.; Robinson, M.S. Tetherin is an exosomal tether. *Elife* **2016**, *5*. [CrossRef]

21. Mead, P.S.; Slutsker, L.; Dietz, V.; McCaig, L.F.; Bresee, J.S.; Shapiro, C.; Griffin, P.M.; Tauxe, R. V Food-related illness and death in the United States. *Emerg. Infect. Dis.* **1999**, *5*, 607–625. [CrossRef] [PubMed]

22. Corry, J.E.L.; Atabay, H.I. Poultry as a source of Campylobacter and related organisms. *J. Appl. Microbiol.* **2001**, *90*, 96S–114S. [CrossRef] [PubMed]

23. Johnson, W.M.; Lior, H. A new heat-labile cytolethal distending toxin (CLDT) produced by Campylobacter spp. *Microb. Pathog.* **1988**, *4*, 115–126. [CrossRef]

24. Lin, C.-D.; Lai, C.-K.; Lin, Y.-H.; Hsieh, J.-T.; Sing, Y.-T.; Chang, Y.-C.; Chen, K.-C.; Wang, W.-C.; Su, H.-L.; Lai, C.-H. Cholesterol Depletion Reduces Entry of Campylobacter jejuni Cytolethal Distending Toxin and Attenuates Intoxication of Host Cells. *Infect. Immun.* **2011**, *79*, 3563–3575. [CrossRef] [PubMed]

25. Ohara, M.; Oswald, E.; Sugai, M. Cytolethal Distending Toxin: A Bacterial Bullet Targeted to Nucleus. *J. Biochem.* **2004**, *136*, 409–413. [CrossRef] [PubMed]

26. Cope, L.D.; Lumbley, S.; Latimer, J.L.; Klesney-Tait, J.; Stevens, M.K.; Johnson, L.S.; Purven, M.; Munson, R.S.; Lagergard, T.; Radolf, J.D.; et al. A diffusible cytotoxin of Haemophilus ducreyi. *Proc. Natl. Acad. Sci. USA* **1997**, *94*, 4056–4061. [CrossRef]

27. Young, V.B.; Chien, C.; Knox, K.A.; Taylor, N.S.; Schauer, D.B.; Fox, J.G. Cytolethal Distending Toxin in Avian and Human Isolates of *Helicobacter pullorum*. *J. Infect. Dis.* **2000**, *182*, 620–623. [CrossRef]

28. Okuda, J.; Kurazono, H.; Takeda, Y. Distribution of the cytolethal distending toxin A gene (*cdtA*) among species of Shigella and Vibrio, and cloning and sequencing of the cdt gene from Shigella dysenteriae. *Microb. Pathog.* **1995**, *18*, 167–172. [CrossRef]

29. Zhang, B.; He, Y.; Xu, C.; Xu, L.; Feng, S.; Liao, M.; Ren, T. Cytolethal distending toxin (CDT) of the Haemophilus parasuis SC096 strain contributes to serum resistance and adherence to and invasion of PK-15 and PUVEC cells. *Vet. Microbiol.* **2012**, *157*, 237–242. [CrossRef]

30. Whitehouse, C.A.; Balbo, P.B.; Pesci, E.C.; Cottle, D.L.; Mirabito, P.M.; Pickett, C.L. Campylobacter jejuni Cytolethal Distending Toxin Causes a G 2 -Phase Cell Cycle Block. *Infect. Immun.* **1998**, *66*, 1934–1940. [CrossRef]

31. Nesic, D.; Stebbins, C.E. Mechanisms of Assembly and Cellular Interactions for the Bacterial Genotoxin CDT. *PLoS Pathog.* **2005**, *1*, e28. [CrossRef] [PubMed]

32. Lindmark, B.; Rompikuntal, P.; Vaitkevicius, K.; Song, T.; Mizunoe, Y.; Uhlin, B.; Guerry, P.; Wai, S. Outer membrane vesicle-mediated release of cytolethal distending toxin (CDT) from Campylobacter jejuni. *BMC Microbiol.* **2009**, *9*, 220. [CrossRef]

33. Bezine, E.; Vignard, J.; Mirey, G.; Bezine, E.; Vignard, J.; Mirey, G. The Cytolethal Distending Toxin Effects on

Mammalian Cells: A DNA Damage Perspective. *Cells* **2014**, *3*, 592–615. [CrossRef] [PubMed]

34. Boesze-Battaglia, K.; Besack, D.; McKay, T.; Zekavat, A.; Otis, L.; Jordan-Sciutto, K.; Shenker, B.J. Cholesterol-rich membrane microdomains mediate cell cycle arrest induced by Actinobacillus actinomycetemcomitans cytolethal-distending toxin. *Cell. Microbiol.* **2006**, *8*, 823–836. [CrossRef] [PubMed]

35. Boesze-Battaglia, K. Isolation of membrane rafts and signaling complexes. *Methods Mol. Biol.* **2006**, *332*, 169–179. [PubMed]

36. Damek-Poprawa, M.; Jang, J.Y.; Volgina, A.; Korostoff, J.; DiRienzo, J.M. Localization of Aggregatibacter

actinomycetemcomitans Cytolethal Distending Toxin Subunits during Intoxication of Live Cells. *Infect. Immun.* **2012**, *80*, 2761–2770. [CrossRef] [PubMed]

37. He, Z.; Gharaibeh, R.Z.; Newsome, R.C.; Pope, J.L.; Dougherty, M.W.; Tomkovich, S.; Pons, B.; Mirey, G.; Vignard, J.; Hendrixson, D.R.; et al. Campylobacter jejuni promotes colorectal tumorigenesis through the action of cytolethal distending toxin. *Gut* **2019**, *68*, 289–300. [CrossRef]

38. Haghjoo, E.; Galán, J.E. Salmonella typhi encodes a functional cytolethal distending toxin that is delivered into host cells by a bacterial-internalization pathway. *Proc. Natl. Acad. Sci. USA* **2004**, *101*, 4614–4619. [CrossRef]

39. Nath, G.; Gulati, A.K.; Shukla, V.K. Role of bacteria in carcinogenesis, with special reference to carcinoma of the gallbladder. *World J. Gastroenterol.* **2010**. [CrossRef]

40. Shenker, B.J.; McKay, T.; Datar, S.; Miller, M.; Chowhan, R.; Demuth, D. Actinobacillus actinomycetemcomitans immunosuppressive protein is a member of the family of cytolethal distending toxins capable of causing a G2 arrest in human T cells. *J. Immunol.* **1999**, *162*, 4773–4780.

41. Sandra Trott; Reinhard Bauer; Hans-Joachim Knackmuss; Andreas Stolz Campylobacter upsaliensis exerts a cytolethal distending toxin effect on HeLa cells and T lymphocytes. *Microbiology* **2001**, 1815–1824.

42. Kostia, S.; Veijalainen, P.; Hirvi, U.; Hänninen, M.L. Cytolethal distending toxin B gene (cdtB) homologues in taxa 2, 3 and 8 and in six canine isolates of Helicobacter sp. flexispira. *J. Med. Microbiol.* **2003**, *52*, 103–108. [CrossRef] [PubMed]

43. Nougayrède, J.P.; Taieb, F.; De Rycke, J.; Oswald, E. Cyclomodulins: Bacterial effectors that modulate the

eukaryotic cell cycle. *Trends Microbiol.* **2005**, *13*, 103–110. [CrossRef] [PubMed]

44. Biasoli, D.; Kahn, S.A.; Cornélio, T.A.; Furtado, M.; Campanati, L.; Chneiweiss, H.; Moura-Neto, V.; Borges, H.L. Retinoblastoma protein regulates the crosstalk between autophagy and apoptosis, and favors glioblastoma resistance to etoposide. *Cell Death Dis.* **2013**, *4*. [CrossRef]

45. Canonico, B.; di Sario, G.; Cesarini, E.; Campana, R.; Luchetti, F.; Zamai, L.; Ortolani, C.; Nasoni, M.G.; Baffone, W.; Papa, S. Monocyte response to different Campylobacter jejuni lysates involves endoplasmic reticulum stress and the lysosomal–mitochondrial axis: When cell death is better than cell survival. *Toxins (Basel)* **2018**, *10*. [CrossRef]

46. Wrigley, B.J.; Lip, G.Y.H.; Shantsila, E. The role of monocytes and inflammation in the pathophysiology of heart failure. *Eur. J. Heart Fail.* **2011**, *13*, 1161–1171. [CrossRef]

47. Guerra, L.; Guidi, R.; Frisan, T. Do bacterial genotoxins contribute to chronic inflammation, genomic instability and tumor progression? *FEBS J.* **2011**, *278*, 4577–4588. [CrossRef]

48. Eshraghi, A.; Maldonado-Arocho, F.J.; Gargi, A.; Cardwell, M.M.; Prouty, M.G.; Blanke, S.R.; Bradley, K.A. Cytolethal distending toxin family members are differentially affected by alterations in host glycans and membrane cholesterol. *J. Biol. Chem.* **2010**, *285*, 18199–18207. [CrossRef]

49. Rabin, S.D.P.; Flitton, J.G.; Demuth, D.R. Aggregatibacter actinomycetemcomitans cytolethal distending toxin induces apoptosis in nonproliferating macrophages by a phosphatase-independent mechanism. *Infect. Immun.* **2009**, *77*, 3161–3169. [CrossRef]

50. Choo, A.Y.; Yoon, S.O.; Sang, G.K.; Roux, P.P.; Blenis, J. Rapamycin differentially inhibits S6Ks and 4E-BP1 to mediate cell-type-specific repression of mRNA translation. *Proc. Natl. Acad. Sci. USA* **2008**. [CrossRef]

51. Komiya, T.; Memmott, R.M.; Blumenthal, G.M.; Bernstein, W.; Ballas, M.S.; De Chowdhury, R.; Chun, G.; Peer, C.J.; Figg, W.D.; Liewehr, D.J.; et al. A phase I/II study of pemetrexed with sirolimus in advanced, previously treated non-small cell lung cancer. *Transl. Lung Cancer Res.* **2019**. [CrossRef] [PubMed]

52. Eriksson, P.; Wallin, P.; Sjöwall, C. Clinical experience of sirolimus regarding efficacy and safety in systemic lupus erythematosus. *Front. Pharmacol.* **2019**. [CrossRef] [PubMed]

53. Mohankumar, V.; Ramalingam, S.; Chidambaranathan, G.P.; Prajna, L. Autophagy induced by type III secretion system toxins enhances clearance of Pseudomonas aeruginosa from human corneal epithelial cells. *Biochem. Biophys. Res. Commun.* **2018**. [CrossRef] [PubMed]

54. Canonico, B.; Campana, R.; Luchetti, F.; Arcangeletti, M.; Betti, M.; Cesarini, E.; Ciacci, C.; Vittoria, E.; Galli, L.; Papa, S.; et al. Campylobacter jejuni cell lysates differently target mitochondria and lysosomes on HeLa cells. *Apoptosis* **2014**, *19*, 1225–1242. [CrossRef] [PubMed]

55. Jia, W.; Pua, H.H.; Li, Q.-J.; He, Y.-W. Autophagy Regulates Endoplasmic Reticulum Homeostasis and Calcium Mobilization in T Lymphocytes. *J. Immunol.* **2011**, *186*, 1564–1574. [CrossRef] [PubMed]

56. Tentaku, A.; Shimohata, T.; Hatayama, S.; Kido, J.; Nguyen, A.Q.; Kanda, Y.; Fukushima, S.; Uebanso, T.; Iwata, T.; Mawatari, K.; et al. Host cellular unfolded protein response signaling regulates Campylobacter jejuni invasion. *PLoS ONE* **2018**, *13*, e0205865. [CrossRef] [PubMed]

57. Nicolay, B.N.; Dyson, N.J. The multiple connections between pRB and cell metabolism. *Curr. Opin. Cell Biol.* **2013**, *25*, 735–740. [CrossRef]

58. D'Angelo, B.; Astarita, C.; Boffo, S.; Massaro-Giordano, M.; Antonella Ianuzzi, C.; Caporaso, A.; Macaluso, M.; Giordano, A. LPS-induced inflammatory response triggers cell cycle reactivation in murine neuronal cells through retinoblastoma proteins induction. *Cell Cycle* **2017**, *16*, 2330–2336. [CrossRef]

59. Flatt, P.M.; Tang, L.J.; Scatena, C.D.; Szak, S.T.; Pietenpol, J.A. p53 regulation of G(2) checkpoint is retinoblastoma protein dependent. *Mol. Cell. Biol.* **2000**, *20*, 4210–4223. [CrossRef]

60. Fingar, D.C.; Blenis, J. Target of rapamycin (TOR): An integrator of nutrient and growth factor signals and coordinator of cell growth and cell cycle progression. *Oncogene* **2004**, *23*, 3151–3171. [CrossRef]

61. Zhang, C.; Syed, T.W.; Liu, R.; Yu, J. Role of Endoplasmic Reticulum Stress, Autophagy, and Inflammation in Cardiovascular Disease. *Front. Cardiovasc. Med.* **2017**, *4*, 29. [CrossRef] [PubMed]

62. Bravo-Sagua, R.; Parra, V.; Ortiz-Sandoval, C.; Navarro-Marquez, M.; Rodríguez, A.E.; Diaz-Valdivia, N.; Sanhueza, C.; Lopez-Crisosto, C.; Tahbaz, N.; Rothermel, B.A.; et al. Caveolin-1 impairs PKA-DRP1-mediated remodelling of ER–mitochondria communication during the early phase of ER stress. *Cell Death Differ.* **2019**, *26*, 1195–1212. [CrossRef] [PubMed]

63. Korolchuk, V.I.; Rubinsztein, D.C. Regulation of autophagy by lysosomal positioning. *Autophagy* **2011**, *7*, 927–928. [CrossRef] [PubMed]

64. Billcliff, P.G.; Rollason, R.; Prior, I.; Owen, D.M.; Gaus, K.; Banting, G. CD317/tetherin is an organiser of membrane microdomains. *J. Cell Sci.* **2013**, *126*, 1553–1564. [CrossRef]

65. Hogue, I.B.; Grover, J.R.; Soheilian, F.; Nagashima, K.; Ono, A. Gag induces the coalescence of clustered lipid rafts and tetraspanin-enriched microdomains at HIV-1 assembly sites on the plasma membrane. *J. Virol.* **2011**, *85*, 9749–9766. [CrossRef]

66. Mahauad-Fernandez, W.D.; Okeoma, C.M. The role of BST-2/Tetherin in host protection and disease manifestation. *Immun. Inflamm. Dis.* **2016**, *4*, 4–23. [CrossRef]

67. Anikeeva, N.; Sykulev, Y. Mechanisms controlling granule-mediated cytolytic activity of cytotoxic T lymphocytes. *Immunol. Res.* **2011**, *51*, 183–194. [CrossRef]

68. Jongsma, M.L.L.M.; Berlin, I.; Wijdeven, R.H.H.M.; Janssen, L.; Janssen, G.M.M.C.; Garstka, M.A.A.; Janssen, H.; Mensink, M.; van Veelen, P.A.A.; Spaapen, R.M.M.; et al. An ER-Associated Pathway Defines Endosomal Architecture for Controlled Cargo Transport. *Cell* **2016**, *166*, 152–166. [CrossRef]

69. Reed, S.E.; Hodgson, L.R.; Song, S.; May, M.T.; Kelly, E.E.; McCaffrey, M.W.; Mastick, C.C.; Verkade, P.; Tavare, J.M. A role for Rab14 in the endocytic trafficking of GLUT4 in 3T3-L1 adipocytes. *J. Cell Sci.* **2013**, *126*, 1931–1941. [CrossRef]

70. Rojo Pulido, I.; Nightingale, T.D.; Darchen, F.; Seabra, M.C.; Cutler, D.F.; Gerke, V. Myosin Va acts in concert with Rab27a and MyRIP to regulate acute von-Willebrand factor release from endothelial cells. *Traffic* **2011**, *12*, 1371–1382. [CrossRef]

71. Sadacca, L.A.; Bruno, J.; Wen, J.; Xiong, W.; Mcgraw, T.E. Specialized sorting of GLUT4 and its recruitment to the cell surface are independently regulated by distinct Rabs. *Mol. Biol. Cell* **2013**, *24*, 2544–2557. [CrossRef] [PubMed]

72. Wasmeier, C.; Hume, A.N.; Bolasco, G.; Seabra, M.C. Melanosomes at a glance. *J. Cell Sci.* **2008**, *121*, 3995–3999. [CrossRef] [PubMed]

73. Henne, W.M. Organelle remodeling at membrane contact sites. *J. Struct. Biol.* **2016**. [CrossRef] [PubMed]

74. Dikic, I. Open questions: Why should we care about ER-phagy and ER remodelling? *BMC Biol.* **2018**, *16*, 131. [CrossRef] [PubMed]

75. Chiramel, A.I.; Dougherty, J.D.; Nair, V.; Robertson, S.J.; Best, S.M. FAM134B, the Selective Autophagy Receptor for Endoplasmic Reticulum Turnover, Inhibits Replication of Ebola Virus Strains Makona and Mayinga. *J. Infect. Dis.* **2016**, *214*, S319–S325. [CrossRef]

76. Lennemann, N.J.; Rhein, B.A.; Ndungo, E.; Chandran, K.; Qiu, X.; Maury, W. Comprehensive functional analysis of N-linked glycans on ebola virus GP1. *MBio* **2014**, *5*. [CrossRef]

77. Moretti, J.; Roy, S.; Bozec, D.; Martinez, J.; Chapman, J.R.; Ueberheide, B.; Lamming, D.W.; Chen, Z.J.; Horng, T.; Yeretssian, G.; et al. STING Senses Microbial Viability to Orchestrate Stress-Mediated Autophagy of the Endoplasmic Reticulum. *Cell* **2017**, *171*, 809–823.e13. [CrossRef]

78. Loi, M.; Fregno, I.; Guerra, C.; Molinari, M. Eat it right: Er-phagy and recover-phagy. *Biochem. Soc. Trans.* **2018**, *46*, 699–706. [CrossRef]

79. Helle, S.C.J.; Kanfer, G.; Kolar, K.; Lang, A.; Michel, A.H.; Kornmann, B. Organization and function of membrane contact sites. *Biochim. Biophys. Acta - Mol. Cell Res.* **2013**. [CrossRef]

80. Bravo-Sagua, R.; López-Crisosto, C.; Parra, V.; Rodriguez-Peña, M.; Rothermel, B.A.; Quest, A.F.G.; Lavandero, S. MTORC1 inhibitor rapamycin and ER stressor tunicamycin induce differential patterns of ER-mitochondria coupling. *Sci. Rep.* **2016**, *6*, 1–12. [CrossRef]

81. Haupt, Y.; Rowan, S.; Oren, M. p53-mediated apoptosis in HeLa cells can be overcome by excess pRB. *Oncogene* **1995**, *10*, 1563–1571. [PubMed]

82. Popowski, M.; Ferguson, H.A.; Sion, A.M.; Koller, E.; Knudsen, E.; Van Den Berg, C.L. Stress and IGF-I differentially control cell fate through mammalian target of rapamycin (mTOR) and retinoblastoma protein (pRB). *J. Biol. Chem.* **2008**. [CrossRef] [PubMed]

83. Martínez-Zamudio, R.I.; Robinson, L.; Roux, P.F.; Bischof, O. SnapShot: Cellular Senescence Pathways. *Cell* **2017**, *170*, 816–816.e1. [CrossRef] [PubMed]

84. Cabukusta, B.; Neefjes, J. Mechanisms of lysosomal positioning and movement. *Traffic* **2018**, *19*, 761–769. [CrossRef]

85. Korolchuk, V.I.; Saiki, S.; Lichtenberg, M.; Siddiqi, F.H.; Roberts, E.A.; Imarisio, S.; Jahreiss, L.; Sarkar, S.; Futter, M.; Menzies, F.M.; et al. Lysosomal positioning coordinates cellular nutrient responses. *Nat. Cell Biol.* **2011**, *13*, 453–462. [CrossRef]

86. Raiborg, C.; Wenzel, E.M.; Pedersen, N.M.; Olsvik, H.; Schink, K.O.; Schultz, S.W.; Vietri, M.; Nisi, V.; Bucci, C.; Brech, A.; et al. Repeated ER-endosome contacts promote endosome translocation and neurite outgrowth. *Nature* **2015**. [CrossRef]

87. Rocha, N.; Kuijl, C.; Van Der Kant, R.; Janssen, L.; Houben, D.; Janssen, H.; Zwart, W.; Neefjes, J. Cholesterol sensor ORP1L organizes late endosomal contacts with the ER protein VAP that controls Rab7-RILP-p150 Glued and late endosomal positioning. *J. Cell Biol.* **2009**. [CrossRef]

88. Van Der Kant, R.; Neefjes, J. Small regulators, major consequences-Ca2+ and cholesterol at the endosome-ER interface. *J. Cell Sci.* **2014**. [CrossRef]

89. Rowland, A.A.; Chitwood, P.J.; Phillips, M.J.; Voeltz, G.K. ER contact sites define the position and timing of endosome fission. *Cell* **2014**. [CrossRef]

90. Rollason, R.; Dunstan, K.; Billcliff, P.G.; Bishop, P.; Gleeson, P.; Wise, H.; Digard, P.; Banting, G. Expression of HIV-1 Vpu Leads to Loss of the Viral Restriction Factor CD317/Tetherin from Lipid Rafts and Its Enhanced Lysosomal Degradation. *PLoS ONE* **2013**, *8*. [CrossRef]

91. Mahauad-Fernandez, W.D.; Okeoma, C.M. BST-2: At the crossroads of viral pathogenesis and oncogenesis. *Future Virol.* **2016**, *11*, 127–140. [CrossRef]

92. Inoki, K.; Li, Y.; Zhu, T.; Wu, J.; Guan, K.-L. TSC2 is phosphorylated and inhibited by Akt and suppresses mTOR signalling. *Nat. Cell Biol.* **2002**, *4*, 648–657. [CrossRef] [PubMed]

93. Wullschleger, S.; Loewith, R.; Hall, M.N. TOR Signaling in Growth and Metabolism. *Cell* **2006**, *124*, 471–484. [CrossRef] [PubMed]

94. Sun, X.; Threadgill, D.; Jobin, C. Campylobacter jejuni Induces Colitis Through Activation of Mammalian Target of Rapamycin Signaling. *Gastroenterology* **2012**, *142*, 86–95.e5. [CrossRef]

95. Brando, B.; Barnett, D.; Janossy, G.; Mandy, F.; Autran, B.; Rothe, G.; Scarpati, B.; D'Avanzo, G.; D'Hautcourt, J.-L.; Lenkei, R.; et al. Cytofluorometric methods for assessing absolute numbers of cell subsets in blood. *Cytometry* **2000**, *42*, 327–346. [CrossRef]

96. Chazotte, B. Labeling lysosomes in live cells with LysoTracker. *Cold Spring Harb. Protoc.* **2011**, *2011*, pdb.prot5571. [CrossRef]

97. Canonico, B.; Cesarini, E.; Salucci, S.; Luchetti, F.; Falcieri, E.; Sario, G.D.; Palma, F.; Papa, S. Defective autophagy, mitochondrial clearance and lipophagy in niemann-pick type B lymphocytes. *PLoS ONE* **2016**. [CrossRef]

98. Luchetti, F.; Canonico, B.; Arcangeletti, M.; Guescini, M.; Cesarini, E.; Stocchi, V.; Degli Esposti, M.; Papa, S. Fas Signalling Promotes Intercellular Communication in T Cells. *PLoS ONE* **2012**, *7*, e35766. [CrossRef]

99. Hogg, R.C.; Adams, D.J. An ATP-sensitive K(+) conductance in dissociated neurones from adult rat intracardiac ganglia. *J. Physiol.* **2001**, *534*, 713–720. [CrossRef]

100. Ghasemi, M.; Khodaei, N.; Salari, S.; Eliassi, A.; Saghiri, R. Gating behavior of endoplasmic reticulum potassium channels of rat hepatocytes in diabetes. *Iran. Biomed. J.* **2014**.

101. Li, H.; Mao, G.; Carlson, J.; Leng, S.X. A novel flow cytometry-based tool for determining the efficiency of human cytomegalovirus infection in THP-1 derived macrophages. *J. Virol. Methods* **2015**. [CrossRef] [PubMed]

102. Brocco, D.; Lanuti, P.; Simeone, P.; Bologna, G.; Pieragostino, D.; Cufaro, M.C.; Graziano, V.; Peri, M.; Di Marino, P.; De Tursi, M.; et al. Circulating Cancer Stem Cell-Derived Extracellular Vesicles as a Novel Biomarker for Clinical Outcome Evaluation. *J. Oncol.* **2019**. [CrossRef] [PubMed]

103. Galluzzi, L.; Diotallevi, A.; De Santi, M.; Ceccarelli, M.; Vitale, F.; Brandi, G.; Magnani, M. Leishmania infantum Induces Mild Unfolded Protein Response in Infected Macrophages. *PLoS ONE* **2016**, *11*, e0168339. [CrossRef] [PubMed]



**CHAPTER TWO**

# *Deeply investigating the multiple ways of damage to the target cells and the routes that bring the "intoxication" to persist and spread*

## *U937 behaviour during intoxication by lysates: a summary to be compared to Caco-2 behaviour*

The investigation of the CDT effects of C. jejuni wild-type and mutant strains in U937 cells, were conducted in the previous chapter. Other alterations induced by the wild-type lysate will also be considered in this paragraph, with the aim to deeply characterise damages to target cells and to compare not only the sources of infection, but also the source of the target cell type.

Lysosomal involvement was monitored by staining U937 cells with LysoTracker Deep Red (LTDR). As shown in Figure 1A-B, C. jejuni lysates from ATCC wild-type strain induced a bit but also a significant increase in the amount of LTDR-accumulating lysosomes after 24, 48 and 72 hours.

TMRE results reported interesting mitochondrial membrane potential perturbations after treatments (Figure 1 C), yet reported (Canonico et al., 2020). Significant changes in TMRE MFI occurred after 24 hours in cells preincubated with the wild-type strain and revealed an increase in mitochondrial membrane potential in U937 cells until 48 h. At 72 h ATCC -treated cells show a significant decrease of MMP compared to Ctrl and Mutant treated cells. Normally, cells maintain stable levels of intracellular ATP and $\Delta\Psi m$, and this stability is thought to be a requisite for normal cell functioning (Zamzami et al., 1995; Yaniv et al., 2010; Zorov, Juhaszova and Sollott, 2014), therefore, according to recent findings (Zorova et al., 2018), $\Delta\Psi m$ can be used not only for ATP synthesis but it is also a factor determining viability of mitochondria (involved in a process of elimination of disabled mitochondria). Such instabilities of $\Delta\Psi m$ have been described (Hüser, Rechenmacher and Blatter, 1998; Krippeit-Drews, Düfer and Drews, 2000; Zorov et al., 2000; Slodzinski, Aon and O'Rourke, 2008), and occasionally they are attributed to the oscillations of the mitochondrial permeability transition (MPT) (Zorov, Juhaszova and Sollott, 2014) that, in significant portion of cases are associated with ROS increase and oxidative stress, as detected in the previous published manuscript by Canonico et al. (Canonico et al., 2018).

Monodansylcadaverine (MDC) staining, a marker for autophagolysosome and autophagic-like vacuoles, was used to investigate the involvement of the autophagic machinery in C. jejuni infected

U937 cells. Particularly after 48 hours of treatment MDC MFI significantly increased in U937 cells infected with C. jejuni ATCC 33291 lysate (Figure 1 D). These results are consistent with LTDR data at 72 hours that show a significant lysosomal destabilisation in cells preincubated with this same lysate.

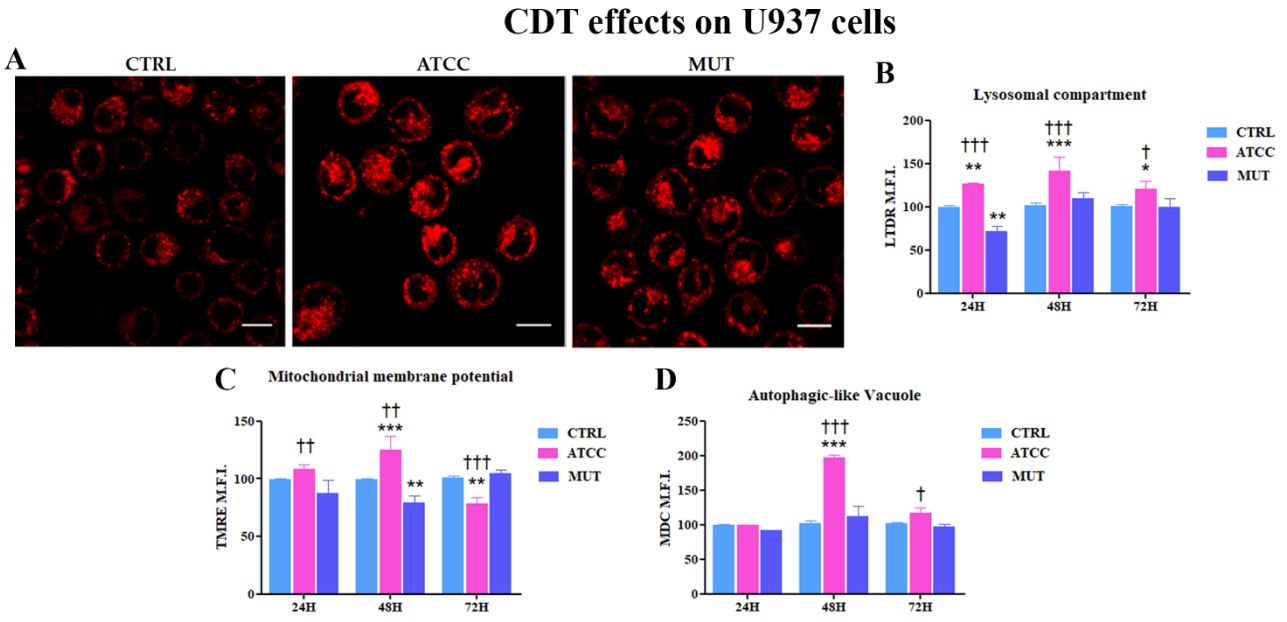


**Figure 1.** (**A**) Single confocal optical sections of LTDR of CTRL, ATTC and MUT treated U937 at 72 hours. Bars: 10 μm. (**B**) Statistical histograms of LTDR MFI from 24 h to 72 h from lysate administration in total cells. Each value was converted to arbitrary units (A.U.) setting control as 100. Each value was expressed as a mean ± SD (Results from n ≥ 3 independent experiments). Two-way ANOVA with Bonferroni's multiple comparison test revealed * = $p < 0.05$, ** = $p < 0.01$, *** = $p < 0.001$ vs. control and † = $p < 0.05$, †† = $p < 0.01$, ††† = $p < 0.001$ vs. mut. (**C**) Statistical histograms of TMRE MFI calculated after 24, 48 and 72 h from lysate administration. Each value was converted to arbitrary units (A.U.) setting control as 100. Each value was expressed as a mean ± SD (Results from n ≥ 3 independent experiments). Two-way ANOVA with Bonferroni's multiple comparison test revealed * = $p < 0.05$, ** = $p < 0.01$, *** = $p < 0.001$ vs. control and † = $p < 0.05$, †† = $p < 0.01$, ††† = $p < 0.001$ vs. mut. (**D**) Statistical histograms of MDC MFI after 24, 48 and 72 h from lysate administration. Each value was converted to arbitrary units (A.U.) setting control as 100. Each value was expressed as a mean ± SD (Results from n ≥ 3 independent experiments). Two-way ANOVA with Bonferroni's multiple comparison test revealed * = $p < 0.05$, ** = $p < 0.01$, *** = $p < 0.001$ vs. control and † = $p < 0.05$, †† = $p < 0.01$, ††† = $p < 0.001$ vs. mut.

CDT intoxication was characterised by progressive cell distension and cytotoxicity in cultured eukaryotic cells. Host response to CDT intoxication differs depending on the target cells (as appears

by other following data on Caco-2 cells). Indeed, apoptosis was reported in T-cell and B-cell lines, while other cells preferentially arrest in the G1 and/or G2 phases of the host cell cycle (Cortes-Bratti *et al.*, 2001; Ohara, Oswald and Sugai, 2004; Taieb *et al.*, 2016).

U937 data showed that *C. jejuni* CDT inhibits the proliferation (**Figure 2 A/B**) and the expression of NF-kB in U937 cells (**Figure 2 C**). These findings, together with the induction of autophagy and cell cycle arrest are in agreement with authors reporting the anticancer effects of several molecules (Zhang, Li and Ji, 2018).

In fact, NF-kB signal transduction pathway is considered an important pathway that regulates the proliferation and tumorigenesis of several types of cancers (Zhang *et al.*, 2019): the in depth analyses of CDT effects on U937 cells are conclude with a focus on cell cycle arrest at the G1/S and/or G2/M transitions, allowing DNA-repairing machinery to correct DNA damaging insults (Cortes-Bratti *et al.*, 2001; Alaoui-El-Azher *et al.*, 2010; Fahrer *et al.*, 2014; Tremblay *et al.*, 2021) and by modulating the expression of NF-kB (Babaei *et al.*, 2018).

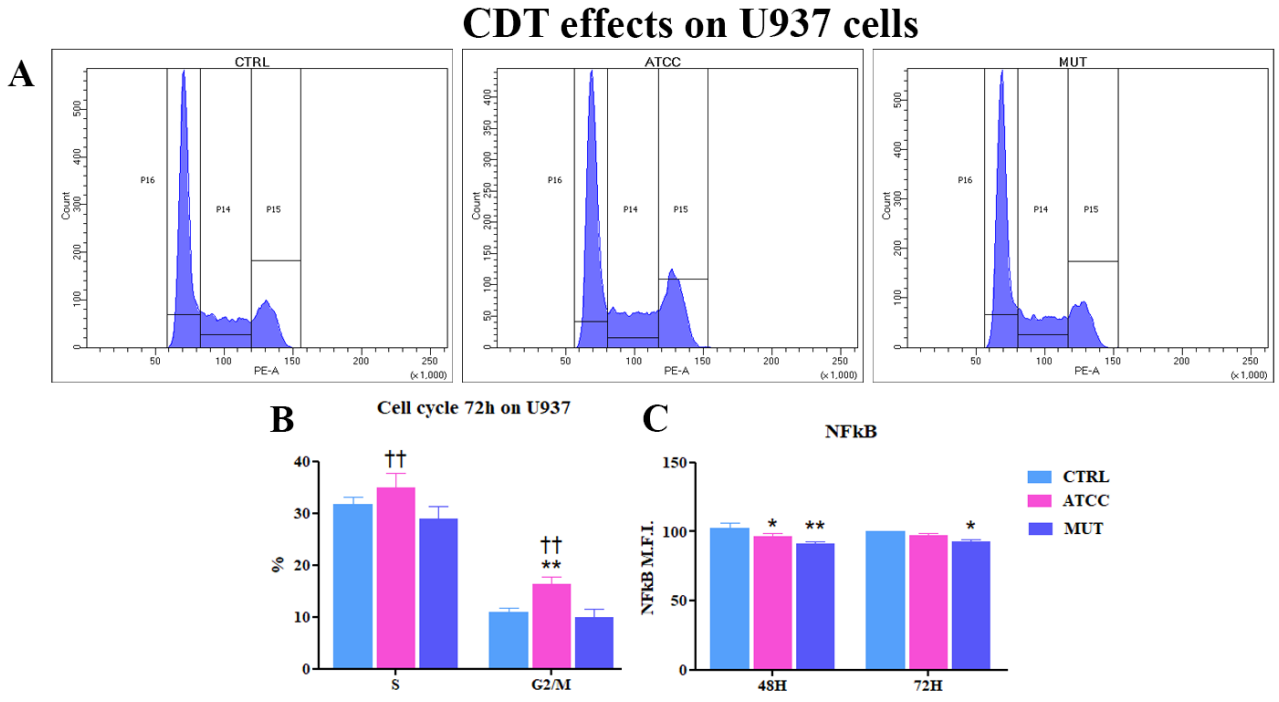


**Figure 2.** (**A**) Flow cytometry histograms representing U937 cells population in G0/G1 (P16), S (P14), and G2/M (P15) phases of cell cycle after 72 h of lysates administration (**B**) Statistical histogram of S and G2/M phases of cell cycle calculated in cytometry via PI staining at 72 h. Each value was expressed as a percentage ± SD (Results from n ≥ 3 independent experiments). Two-way ANOVA with Bonferroni's multiple comparison test revealed * = $p < 0.05$, ** = $p < 0.01$, *** = $p < 0.001$ vs. control and † = $p < 0.05$, †† = $p < 0.01$, ††† = $p < 0.001$ vs. mut. (**C**) Statistical histograms of NF-kB MFI cells at 48 and 72 h. Each value was converted to arbitrary units

(A.U.) setting control as 100. Each value was expressed as a mean ± SD (Results from n ≥ 3 independent experiments). Two-way ANOVA with Bonferroni's multiple comparison test revealed * = $p < 0.05$, ** = $p < 0.01$, *** = $p < 0.001$ vs. control.

### *CDT-effects on Caco-2 cells: Morphological Features, Absolute Count, Cell Death, and evaluation of cell cycle blocking*

It has been widely shown how CDT intoxication induces cellular distension and enlargement in target cells (Tremblay 2021, Pérés et al., 1997; Sugai et al., 1998; Blazkova et al., 2010).

As previously observed in U937 cells, morphologic appearance was studied by microscopic and cytometric investigations. Also, in Caco-2 cells, *C. jejuni* wild-type lysate caused the typical CDT-dependent cellular distension, compared with untreated control cells and cells treated with the CdtA mutant strain lysate. Different sub-populations are visible based on cellular scatter characteristics: we can distinguish normo-sized cells (red events) and distended/enlarged cells (green events) (**Figure 3 A**). We compared the FSC values of untreated control cells and cells treated with mutant strain with the FSC values of cells that were treated with *C. jejuni* lysate. ATCC treatment induced a significant increase in the FSC values and cell enlargement after 48 h (**Figure 3 B**).

The 7'AAD results demonstrated that the wild-type lysate caused a significant increase in 7'AAD - positive cells (apoptotic cells) (**Figure 3 C**). From 24 h, the lysate from the mutant strain seems to induce a slight increase of dead cells with respect to the untreated control. Instead, the wild-type strain acted as death-inducers from 48 h to 72 h. To deeply monitor the phenomenon of cell death, we performed an absolute cell counting by flow cytometry. In fact, cell number decreases due to two separate processes: by G2/M blocking mechanism and cell death. The reduction in cell number was particularly evident in Caco-2 preincubated with the *C. jejuni* ATCC lysate at 72 h (**Figure 3 D**).

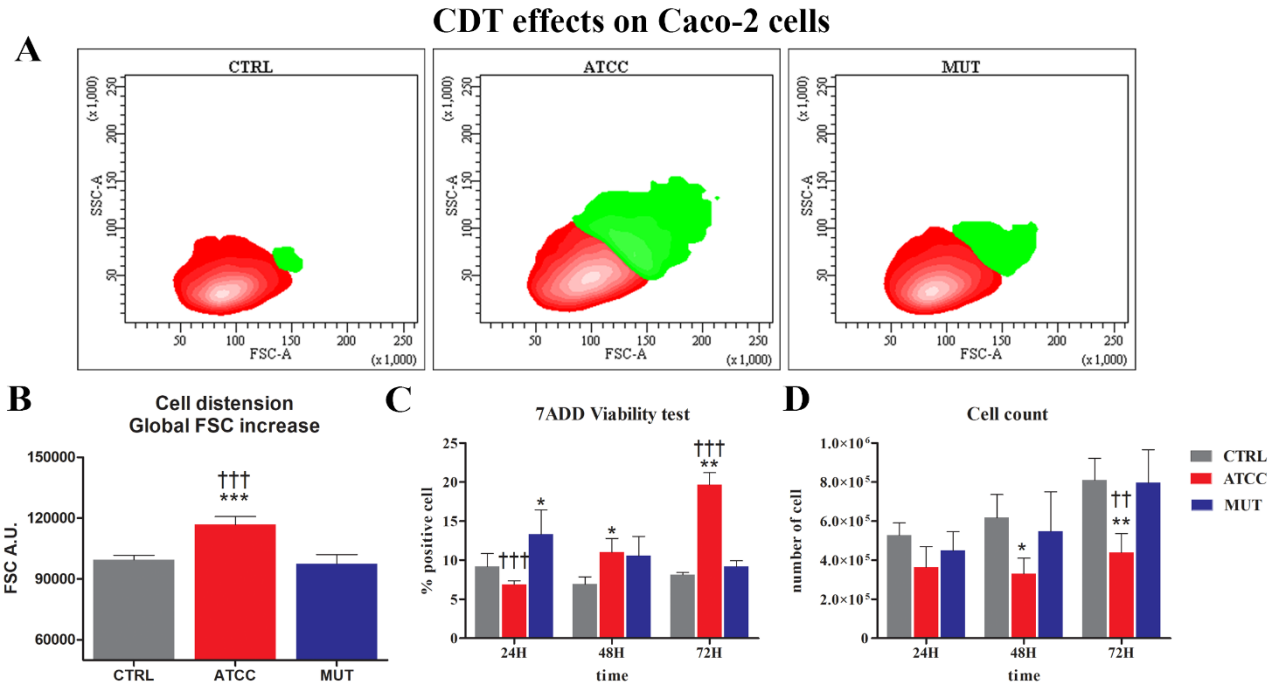


**Figure 3.** Evaluation of the efficiency of the toxin and induction of cell death (**A**) Caco-2 were split into different sub-populations depending on the morphologic parameter, green gate shows distended cells, and red gate shows normo-size cells. Cellular distension (events in green) is well appreciable for *C. jejuni* ATCC 33291 Caco-2 treated cells. Total cells were the summary of red and green gates. Dot plots in the picture show control (CTRL) untreated cells, cells treated with the *C. jejuni* ATCC 33291 lysate and cells treated with the CdtA mutant strain lysate for 48 h. (**B**) Statistical histograms of mean FSC value after 48 h from lysate administration in total cells. Each value is expressed as a mean _ SD (results from n _ 3 independent experiments). Two-way ANOVA with Bonferroni's multiple comparison test revealed * = $p < 0.05$, ** = $p < 0.01$, *** = $p < 0.001$ vs. control and † = $p < 0.05$, †† = $p < 0.01$, ††† = $p < 0.001$ vs. mut (**C**) Statistical histograms of the percentage of 7'AAD positive cells from 24 h to 72 h. Each value is expressed as a percentage _ SD (results from n _ 3 independent experiments). (**D**) Statistical histogram of absolute counts of viable cells from 24 h after lysates administration to 72 h. Each value is expressed as absolute count _ SD (results from n _ 3 independent experiments). Two-way ANOVA with Bonferroni's multiple comparison test revealed * = $p < 0.05$, ** = $p < 0.01$, *** = $p < 0.001$ vs. control.

The efficacy of bacterial lysates was tested by analysis of cell cycle arrest (typical of CDT). Briefly, cells were ethanol-fixed and then stained with propidium iodide (PI) at 48 h. As shown in **Figure 4 A/B** the wild-type lysate induces a cell cycle block in G2/M phase whereas this does not take place in mutant-treated cells.

Furthermore, cells treated by *C. jejuni* lysates show an increased presence of proliferating cell nuclear antigen (PCNA) in G2/M cells (**Figure 4 C**) reported by He at al. 2019 (He *et al.*, 2019) and Benzine

and co-workers describe a process in which cells, preceding the G2/M arrest, suffer a slight replicative slow-down, underscored by the accumulation of chromatin bound PCNA-positive cells (Bezine, Vignard and Mirey, 2014).

As performed during investigations of CDT effects and the involved pathways for U937 cells, also Caco-2 intestinal cells were tested for pRb expression. **Figure 4 D** showed an overexpression of pRb in cells preincubated with the wild-type lysates after 72h, compared to the control and the CdtA mutant strain-treated cells.

As cited, the retinoblastoma protein (pRb) pathway has a key role in the regulation of several cellular processes, and this protein as well as its regulators—cyclins, cyclin-dependent kinases (Cdks) and Cdk inhibitors—are frequently deregulated in human cancer (Malumbres and Barbacid, 2001; Quereda *et al.*, 2016). In quiescent cells, pRb represses the transcription of genes required for DNA replication or mitosis: this role is appropriate for cells in replicative stress, such as wild-type ATCC CDT intoxicated Caco-2 cells. Indeed, pRb is implicated in cellular senescence, together with p53, a protein involved in both senescence induction and maintenance (Johmura and Nakanishi, 2016). Of note, both cell lines adopted in the study do not involve p53 pathways, since U937 are p53-mutant cells and Caco-2 are p53-null cells.

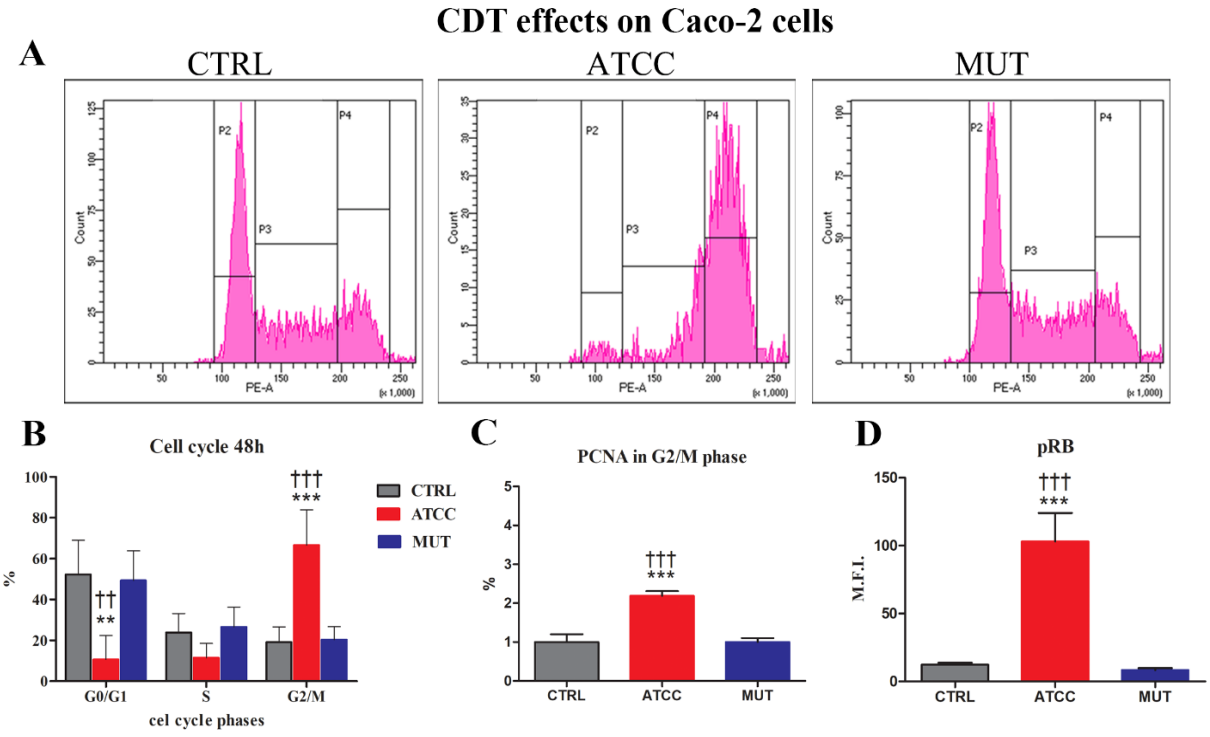


**Figure 4.** Evaluation of the efficiency of the toxin and induction of the cell cycle block. (**A**) Flow cytometry histograms representing Caco-2 cells population in G0/G1 (P2), S (P3), and G2/M (P4) phases of cell cycle after

48 h of lysates administration (**B**) Statistical histogram of cell cycle phases calculated in cytometry via PI staining at 48 h. Each value is expressed as a percentage _ SD (results from n _ 3 independent experiments). Two-way ANOVA with Bonferroni's multiple comparison test revealed * = $p < 0.05$, ** = $p < 0.01$, *** = $p < 0.001$ vs. control and † = $p < 0.05$, †† = $p < 0.01$, ††† = $p < 0.001$ vs. mut. (**C**) Statistical histograms of percentage of PCNA positive cells at G2/M phase cells at 72 h. Each value was expressed as a mean ± SD (Results from n ≥ 3 independent experiments). One-way ANOVA with Bonferroni's multiple comparison test revealed * = $p < 0.05$, ** = $p < 0.01$, *** = $p < 0.001$ vs. control and † = $p < 0.05$, †† = $p < 0.01$, ††† = $p < 0.001$ vs. mut. (**D**) Statistical histograms of intracellular pRB MFI cells at 72 h. Each value was expressed as a mean ± SD (Results from n ≥ 3 independent experiments). One-way ANOVA with Bonferroni's multiple comparison test revealed * = $p < 0.05$, ** = $p < 0.01$, *** = $p < 0.001$ vs. control and † = $p < 0.05$, †† = $p < 0.01$, ††† = $p < 0.001$ vs. mut.

### *Flow cytometric analysis of mitochondria status: transmembrane potential and ROS generation*

Therefore, we next checked perturbations of mitochondrial transmembrane potential after preincubation with the lysates. Mitochondrial function was evaluated with the mitochondrial membrane potential indicating dye, TMRE. Caco-2 treated with wild-type strain show elevated TMRE intensities at different time-points (from 24 h to 72 h) with respect to untreated and the CdtA mutant strain treated cells. These results indicated that ATCC induces mitochondrial hyperpolarization (**Figure 5 A/B**). Excessive ROS are often generated by damaged mitochondria (Choi *et al.*, 2009).

Thus, we further assessed whether mitochondrial ROS were increased by ATCC treatment. Mitochondrial ROS was evaluated by a specific mitochondrial ROS indicator, MitoSOX Red. We found that ATCC increased MitoSOX Red positive cells at 48 h and 72 h (**Figure 5 C**).

In addition, we investigated intracellular ROS levels, obtained by the 5-(and-6)-chloromethyl-20 ,70 -dichlorodihydrofluorescein diacetate acetyl ester probe (CM-H2DCFDA) (**Figure 5 D**), increased in ATCC treated cells to control at 48 h and 72 h, and, to a lesser extent, in CdtA mutant-treated cells at the same investigated time points. Data illustrated in **Figure 5**, clearly show that active CDT specifically targets mitochondria, inducing ROS generation, whereas intracellular ROS (i.e. hydrogen peroxide) are however partly stimulated also by the mutant lysate, containing the inactive toxin.

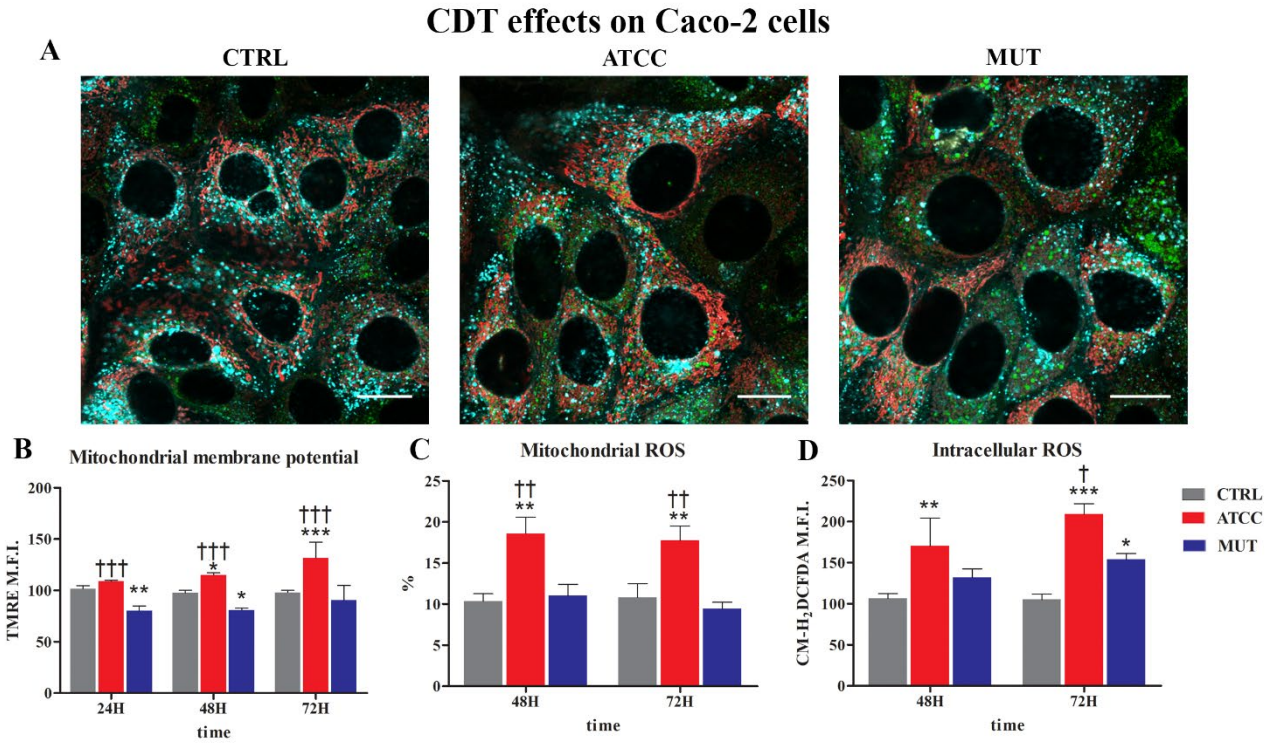


**Figure 5.** Evaluation of mitochondrial dysfunction and ROS production (**A**) Single confocal optical sections is showing overlay of TMRE (red) for mitochondria, LTDR (cyan) for lysosome, and LipidTox (green) for lipid labelling at 48h. Bars: 20 μm (**B**) Statistical histograms of TMRE MFI value from 24 h to 72 h lysate administration in Caco-2 cells. Each value is expressed as a mean ± SD (results from n ≥ 3 independent experiments). Two-way ANOVA with Bonferroni's multiple comparison test revealed * = $p < 0.05$, ** = $p < 0.01$, *** = $p < 0.001$ vs. control and † = $p < 0.05$, †† = $p < 0.01$, ††† = $p < 0.001$ vs. mut. (**C**) Statistical histograms of the percentage of MitoSox positive cells at 48 h and 72 h after lysates administration. Each value is expressed as a percentage ± SD (results from n ≥ 3 independent experiments). Two-way ANOVA with Bonferroni's multiple comparison test revealed * = $p < 0.05$, ** = $p < 0.01$, *** = $p < 0.001$ vs. control and † = $p < 0.05$, †† = $p < 0.01$, ††† = $p < 0.001$ vs. mut. (**D**) Statistical histogram of CM-H2DCFDA MFI at 48 h and 72 h after lysate administration. Each value is expressed as a MFI ± SD (results from n ≥ 3 independent experiments). Two-way ANOVA with Bonferroni's multiple comparison test revealed * = $p < 0.05$, ** = $p < 0.01$, *** = $p < 0.001$ vs. control and † = $p < 0.05$, †† = $p < 0.01$, ††† = $p < 0.001$ vs. mut.

### *Lysosomal and autophagic-like vacuoles involvement and aberrant endocytic activity detection*

To deeply characterise the cells death pathway, we extended our investigation by employing the lysosomal, autophagic and differentiation of endo-lysosomal vacuole markers LysoTracker Deep Red (LTDR), Monodansylcadaverine (MDC), Acridine Orange (AO) and LAMP-1 surface expression.

The LTDR data show a slightly progressive increase of lysosomes from 24 h to 48 h (**Figure 6 B**) for the cell treated with wild-type toxin. Confocal analyses detail (**Figure 6 A**) the expansion of the lysosomal compartment and their massive positioning in the periphery.

Cytometric analyses (**Figure 6 D**) from monodansylcadaverine labelling focused on autophagic-like vacuole accumulation in untreated and treated cells. Autophagic-like vacuole accumulation increases in ATCC treated cells (**Figure 6 C**). However, monodansylcadaverine indicates increased degradative activity, but it cannot entirely describe macroautophagy because it also marks autophagic compartments after their fusion to acidic endo/lysosomes.

Furthermore, we assessed the rate of acidic vesicular organelle accumulation using Acridine Orange (AO). This metachromatic probe is able to evaluate both more acidic (FL3) and less acidic (FL1) vacuoles, that usually are referred as early endosomes, since they are still not mature and are acidified to pH 6.2 by V-ATPase (Canonico et al., 2018; Marshansky and Futai, 2008). The ratio FL3/FL1 takes into account these probe's capabilities.

Data from this acidotropic dye (**Figure 6 E**) not only confirmed the results obtained by LTDR but also traced the changes in autophagic-like vacuoles and endosomes/lysosomes, suggesting the modulation of the conventional and unconventional secretion. These data were definitely supported by quantification of surface expression of LAMP-1/CD107a (**Figure 6 F**), a major integral membrane glycoprotein of late endosomes and lysosomes.

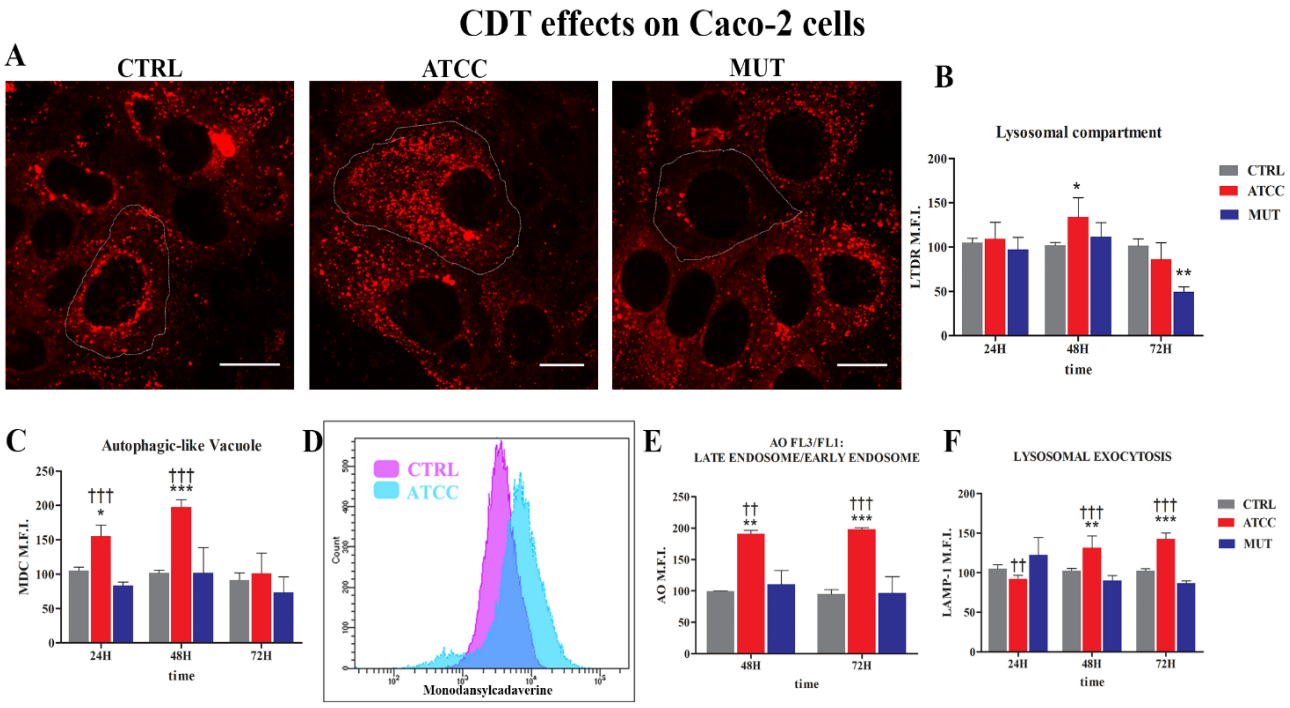


**Figure 6.** Evaluation of endo-lysosomal and autophagic-like involvement (**A**) Single confocal optical sections is showing LTDR (red) for lysosome tracking at 48 h. Bars: 20 μm (**B**) Statistical histograms of LTDR MFI value from 24 h to 72 h lysate administration in Caco-2 cells. Each value is expressed as a mean _ SD (results from n _ 3 independent experiments). Two-way ANOVA with Bonferroni's multiple comparison test revealed * = p < 0.05, ** = p < 0.01, *** = p < 0.001 vs. control and † = p < 0.05, †† = p < 0.01, ††† = p < 0.001 vs. mut. (**C**) Statistical histogram of MDC MFI from 24 h to 72 h. Each value is expressed as a percentage _ SD (results from n _ 3 independent experiments). Two-way ANOVA with Bonferroni's multiple comparison test revealed * = p < 0.05, ** = p < 0.01, *** = p < 0.001 vs. control and † = p < 0.05, †† = p < 0.01, ††† = p < 0.001 vs. mut. (**D**) Representative cytometric histogram of MDC channel for CTRL in violet and ATCC in cyan (**E**) Statistical histograms of ratio FL3/FL1 AO value at 48 h and 72 h after lysate administration. Each value is expressed as a ratio _ SD (results from n _ 3 independent experiments). Two-way ANOVA with Bonferroni's multiple comparison test revealed * = p < 0.05, ** = p < 0.01, *** = p < 0.001 vs. control and † = p < 0.05, †† = p < 0.01, ††† = p < 0.001 vs. mut. (**F**) Statistical histograms of LAMP-1 MFI value at 24h, 48 h and 72 h after lysate administration. Each value is expressed as a mean _ SD (results from n _ 3 independent experiments). Two-way ANOVA with Bonferroni's multiple comparison test revealed * = p < 0.05, ** = p < 0.01, *** = p < 0.001 vs. control and † = p < 0.05, †† = p < 0.01, ††† = p < 0.001 vs. mut.

The autophagic machinery, in particular those vesicular components here investigated, seems involved in unconventional protein secretion and autophagy-dependent secretion, which are fundamental mechanisms for toxic protein disposal, immune signalling and pathogen surveillance:

in our study we speculate the involvement of lysosomal exocytosis and the secretory autophagy in toxin clearance. However, these mechanisms are not degradative: cellular entities and various molecules are not degraded into lysosomes and therefore the mechanism could be not properly defined as autophagic (Galluzzi *et al.*, 2017). This evidence and our data (decrease of lysosome amount and acidity, modulation of autophagic-like vacuole, increase of lysosomal exocytosis) strongly suggest the extracellular release of toxin and bacterial molecules, previously internalised. However, although lysosomal exocytosis enhancement (besides lysosomal degradation) can represent a very appealing strategy of the cell for surviving, the effect on neighbouring cells of a large amount of toxic materials released in the extracellular space should be investigated.

### *Lysosomal Exocytosis and EV Release and Secretory Autophagy: The Autophagic- and Endo-Lysosomal Systems Go Extracellular*

Recent evidence (Eitan *et al.*, 2016) underlined that lysosomal activity plays a role in the secretion of EVs and sorting of their cargo. The release of EVs often serves as an alternative disposal pathway to the lysosome, as previously cited.

The extracellular vesicles produced by intestinal Caco-2 cells treated with *C. jejuni* lysates were evaluated by flow cytometry. The density plots show extracellular vesicles as positive events for the LCD probe (cationic lipophilic dye), whereas, by means of anti CD63 antibody, it is possible to specifically detect exosomes, as CD63 + vesicles (**Figure 7 A**).

Counting beads allowed the absolute counting of EVs, highlighting an increase in LCD+ events (EVs) and CD63+ events (exosomes), in the medium of cells treated by ATCC (**Figure 7 B/C**).

Furthermore, as other researchers (Harting *et al.*, 2018) during the study of EVs, we performed the detection of CD107a (LAMP-1), to be compared to the data on lysosomal exocytosis. Regarding this marker, CD107a (LAMP-1) different reports are collected in the literature: in fact some authors (Fedele *et al.*, 2018) describe the presence of this molecule only in the cells (in the endo-lysosomal compartment), others (Wäster *et al.*, 2020) confirms also a possible lysosomal origin of the vesicles. However, we reason that the vesicles expressing CD107a are not exosomes, even though exosomes derived from multivesicular bodies also contain LAMP-1. In fact, these EVs show a larger dimension in respect to classic exosomes: for this reason, we enumerated these EVs independently to CD63 tetraspanin expression. Our data focused on a relevant and significant increase of LAMP-1 positive

EVs in the medium from ATCC treated Caco-2 cells (**Figure 7 D**). EVs from the medium of CdtA mutant treated Caco-2 cells show a moderate increase, although statistically significant. Our interpretation of this EV scenario implies an involvement of lysosomal pathway and autophagy secretion, induced by both lysates (wild type and mutant) although to a different extent. On the contrary, the targeting of the endosomal pool and of the mechanisms of extracellular release, are mainly primed and hijacked by the active CDT.

To enlighten the presence of inflammatory signals inside EVs we investigated the expression of selected inflammation-related miRNAs (miR-16 and miR-146a) (**Figure 7 E/F**). These short RNAs are considered as important regulators of cytokine gene expression acting either as posttranscriptional regulators or as repressors of mRNA-translation.

Specifically, earlier observations on immune cells, from Bhaumik et co-workers (Bhaumik *et al.*, 2009), demonstrate that miR-146a/b negatively regulates NF-kB activity and the inflammatory pathway, in breast cancer cells (Taganov *et al.*, 2006; Bhaumik *et al.*, 2008).

Levels of miR-146a in Caco-2-secreted EVs are moderately and decreased in response to the active CDT exposure (**Figure 7 E**). Similar pattern of miR-146a expression was also observed by other researchers (Caggiu *et al.*, 2018; Du *et al.*, 2021).

Regarding miR-16 (**Figure 6 F**), previous studies have demonstrated that it plays a crucial role in anti-inflammation in some diseases, such as atherosclerosis (Liang *et al.*, 2016), multiple myeloma (Khalife *et al.*, 2019), and osteoarthritis (Xu and Xu, 2017). Moreover, several studies have revealed that miR-16 could inhibit LPS-induced inflammation (Wang & Zhang, 2021). Indeed, You and co-workers report findings supporting the role of miR-16 as a tumour suppressor in Colorectal Cancer Cells (CRCs), by targeting KRAS (You *et al.*, 2016). MiRNA-16 was greatly upregulated in ATCC-intoxicated Caco-2-derived microvesicles and not in the mutant-intoxicated cells, demonstrating that the active toxin is a key-factor priming this miRNA loading into EVs. To this regard, it is important to take into account both microvesicles (LCD+ events) and exosomes (CD63+ events), as performed.

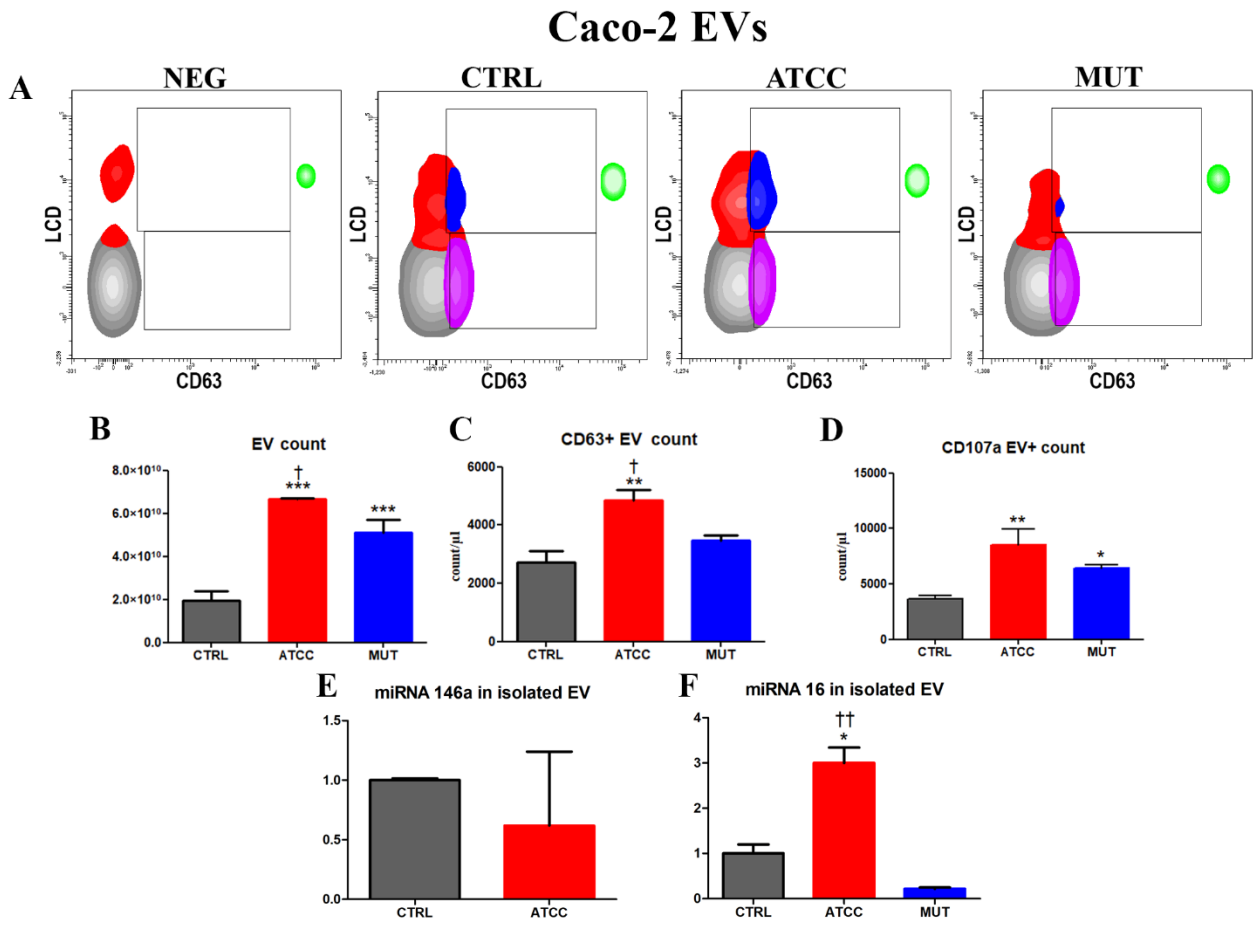


**Figure 7: (A)** Density plot of EVs from Caco-2 cells of NEG, CTRL, ATCC, MUT at 72 hours. **(B)** Histogram of EV count Histogram of EV. **(C)** Histogram of CD63 positive EV at 72 hours. **(D)** Histogram of CD107a positive EV at 72 hours. **(E)** Histogram of EV-miRNA-146a content. **(F)** Histogram of EV-miRNA-16 content. One-way ANOVA with Bonferroni's multiple comparison test revealed * = $p < 0.05$, ** = $p < 0.01$, *** = $p < 0.001$ vs. control and † = $p < 0.05$, †† = $p < 0.01$, ††† = $p < 0.001$ vs. mut.

In fact, exosome biogenesis includes either the recruitment of the endosomal sorting complex required for transport system (ESCRT-dependent) or the synthesis of ceramide (ESCRT-independent) (van Niel, D'Angelo and Raposo, 2018); miRNA loading is more likely to be involved in the ESCRT-independent pathway (Cohen *et al.*, 2018) (**Figure 8**).

These data suggest the presence of stimulus specific regulatory mechanisms, which influence miRNA packaging and secretion in EVs, and may support a possible role in anticancer strategies for *C jejuni* Cytolethal distending toxin and EVs (or OMVs, directly).

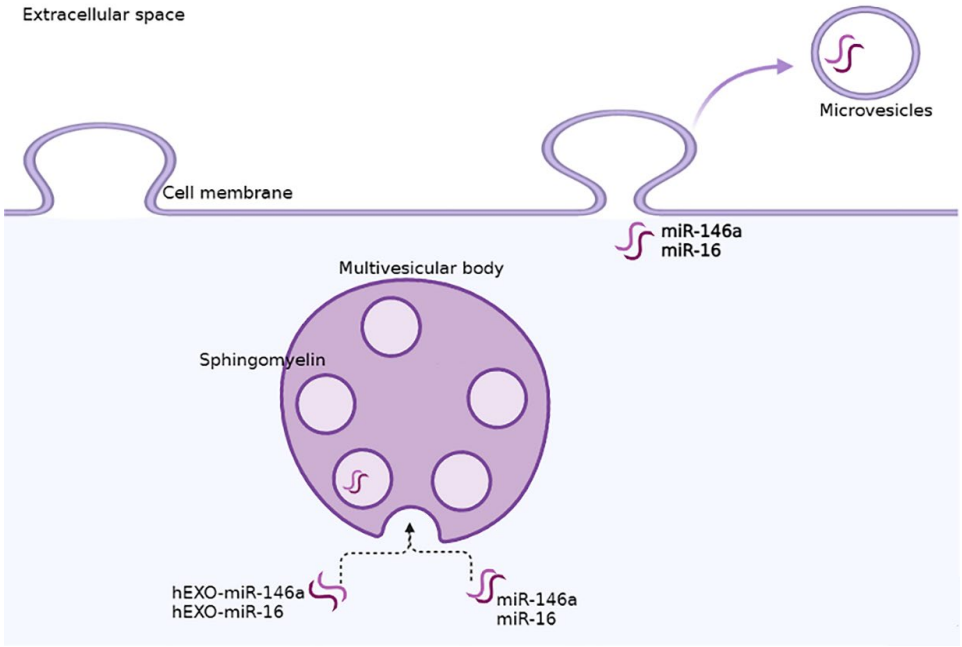


**Figure 8. Incorporation of miRNAs into EVs**. Different mechanisms govern the transfer of miRNAs from the cytosol into EVs. Created in Biorender.com (modified (Vu et al., 2020)**).**

The involvement of Lysosomal Exocytosis, Secretory Autophagy and EV Release, induced and modulated by *C jejuni* CDT are illustrated in **Figure 9**.

These cellular processes underline the crosstalk between the autophagic and the endosomal system and indicate an intersection between degradative and secretory functions, particularly triggered by active CDT.

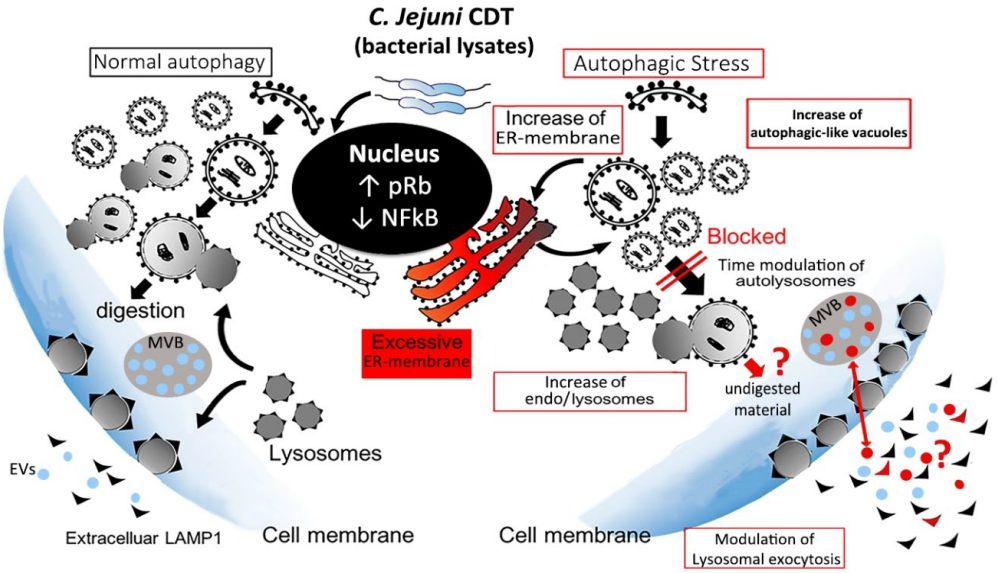


**Figure 9**. Scheme of *C. jejuni* CDT alteration induces on U937/Caco-2 cells.

### *Co-culture results: mimicking the "in vivo" interactions between epithelial intestinal cells and myeloid cells*

The second aim of this work was to evaluate the crosstalk between Caco-2 and U937 in an *in vitro* model.

Co cultivation of more than one type of cell, for example, epithelial and immune cells, gives more valuable information as to understanding basic biology than mono cultivation of cells, such as cell cell contact and extra-communication.

Caco-2 cells were seeded in the apical *trans-well insert membrane* at a concentration of ~ (2.5)× $10^5$ cell/mL and placed in the cell culture incubator. Caco-2 cells were maintained for 15 day to reach a fully confluent monolayer (Kämpfer *et al.*, 2017; Elsheikh *et al.*, 2018), every two days the medium was replaced. On day 9, the Caco-2 were treated with lysates (wild-type CDT and CdtA mutant CDT, for control fresh medium). U937 were added to day 10 ($10^6$/ml). A graphic description of co-culture set-up is given in **Figure 10**.

Caco-2 adherent cells on *trans-well insert membrane* were washed with PBS and harvested using trypsin-EDTA solution and analysed by FCM and confocal microscopy. In addition, the U937 populations in the basal compartment of the 24-wells were characterized by FCM and confocal microscopy.

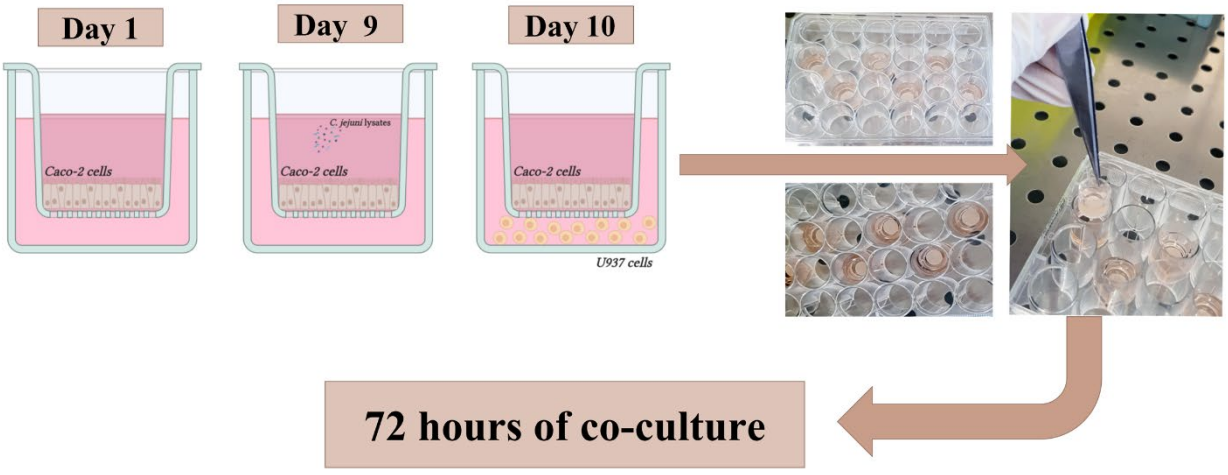


**Figure 10:** Schematic description of the co-culture set-up. The schematic diagram for the intestinal epithelial-myeloid cell co-culture**.** Created in Biorender.com

### *Subcellular response of the co-cultured cell lines*

We firstly investigated the effects of co-culture treatment on Caco-2 cells. Cells, pre-incubated 24h with ATCC lysate show an increase in lysosomal compartment (**Figure 11 A/B**), as we found in Caco-2 monolayers treated cells, whereas mutant-treated Caco-2 cells show a lysosomal compartment similar to control cells.

Differently from the study conducted on Caco-2 monolayers treated cells, a significant decrease in mitochondrial ROS (by using the MitoSOX staining, **Figure 10 A/C**), was detected in ATCC samples. This is due to the time of investigations and to the interactions with U937 cells. Besides the onset of classical apoptotic-necrotic pathway in mutant–treated cells (detectable also in SEM images, **Figure 12 A**), we observed in ATCC –treated cells a decrease in mitochondrial ROS level, an event often analysed in Cancer Stem cells (CSCs). It was demonstrated, in fact, that Caco-2 cells are representative of metastatic colorectal carcinoma, and that they might have some properties of CSCs (Maimaitiyiming *et al.*, 2019). Numerous cancers, including colon cancer, rely on the redox system for survival (Kang, Lee and Lee, 2018; Song *et al.*, 2021). It was very recently confirmed that ROS levels were higher in colon CSCs than in non-CSCs (Song *et al.*, 2021). Therefore, low ROS levels should be reached to eliminate (or limit) the stemness of colon CSCs.

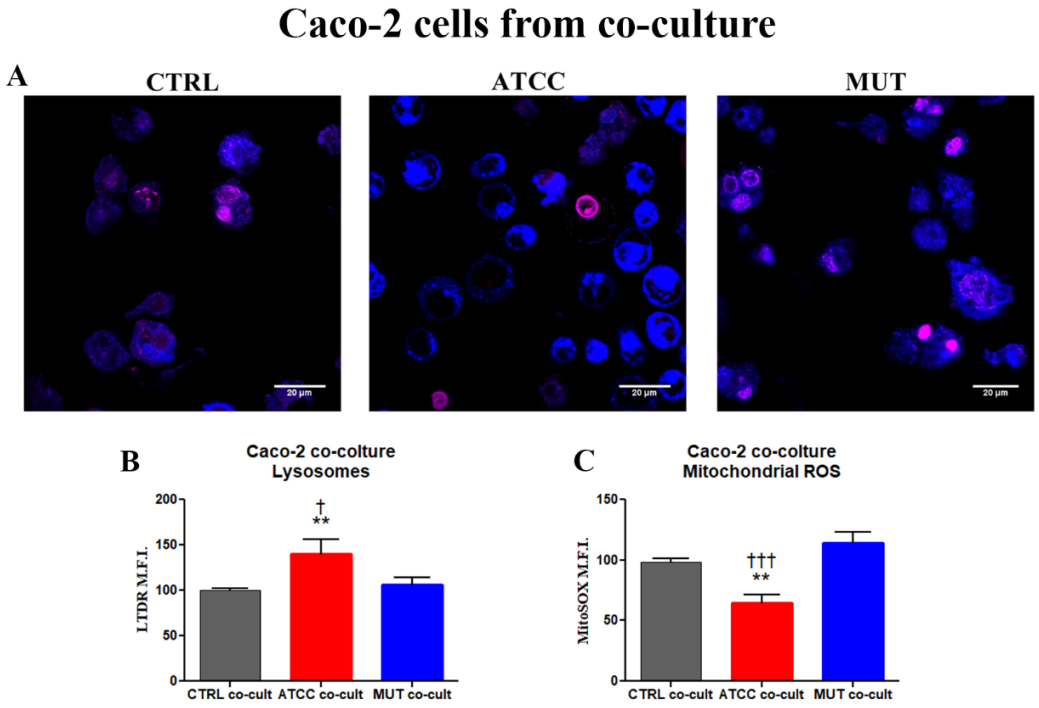


**Figure 11:** (**A**) Single confocal optical sections showing mitochondrial ROS (MitoSOX magenta) and lysosome (LTDR blue) on detached Caco-2 cell at 72 h of co-culture. Bar 20µm. (**B**) Statistical histograms of LTDR MFI

value after 72 h of co-culture on Caco-2 cells. Each value is expressed as a mean _ SD. Two-way ANOVA with Bonferroni's multiple comparison test revealed * = $p < 0.05$, ** = $p < 0.01$, *** = $p < 0.001$ vs. control and † = $p < 0.05$, †† = $p < 0.01$, ††† = $p < 0.001$ vs. mut. (**B**) Statistical histograms of MitoSOX MFI value after 72 h of co-culture on Caco-2 cells. Each value is expressed as a mean _ SD. Two-way ANOVA with Bonferroni's multiple comparison test revealed * = $p < 0.05$, ** = $p < 0.01$, *** = $p < 0.001$ vs. control and † = $p < 0.05$, †† = $p < 0.01$, ††† = $p < 0.001$ vs. mut.

The surface morphology of the Caco-2 cells on *trans-well insert membrane* has been investigated by conventional Scanning Electron Microscopy (SEM). Results from SEM observations of polarised Caco-2 cells showed a massive enlargement of cell size (a typical CDT –effect) and a dense network of long apical microvilli on the surface of ATCC-treated cells (**Figure 12 A**).

CD133 (prominin-1) is predominantly located on plasma membrane processes and microvilli, which indicates possible involvement of this molecule in membrane structure organisation (Corbeil *et al.*, 2001). CD133 is directly associated with cholesterol-containing lipid rafts and therefore can be involved in various signalling pathways (Röper, Corbeil and Huttner, 2000; Gisina *et al.*, 2019).

Accumulating evidence has shown that CD133 might be responsible for various roles: it is reported to be highly expressed in Caco-2 cells, indicating that Caco-2 cells may have stemness like that of CSCs (Dubreuil *et al.*, 2007; Ferrandina *et al.*, 2009; Ren, Sheng and Du, 2013). It is involved in the organisation of plasma-membrane protrusions, maintenance of the apical-basal polarity of epithelial cells, biogenesis of the photoreceptive disc and mechanism of multidrug resistance, and the capacity for self-renewal and tumour formation (Corbeil et al., 2001, 2010; Jászai et al., 2011; Barzegar Behrooz, Syahir and Ahmad, 2019).

Data depicted in **Figure 12**, clearly show a decrease in the amount of surface CD133 in Caco-2 cells, treated by wild-type CDT (**Figure 12 C**). Indeed, confocal images of the detached Caco-2 cells, highlight CD133 distribution on cell surface and on membrane protrusions, as detectable in the white box (white arrow) (**Figure 12 B**).

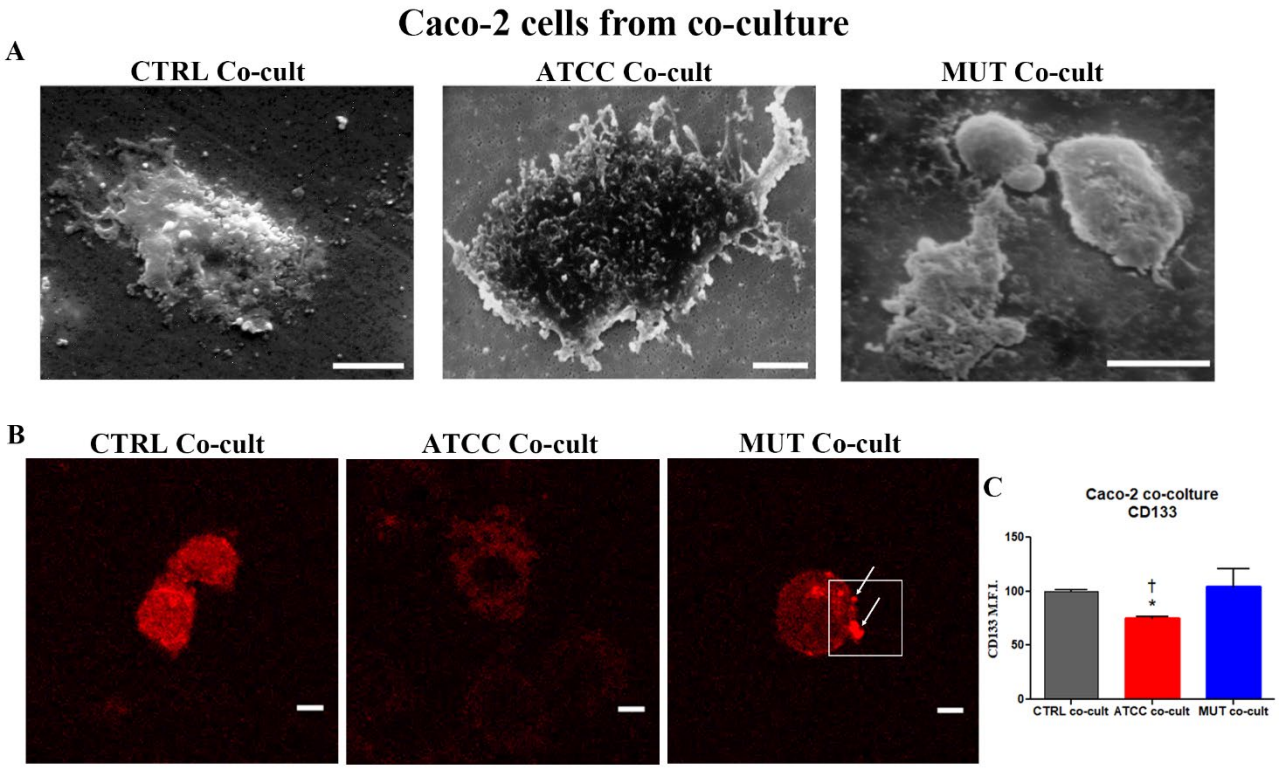


**Figure 12:** (**A**) SEM micrographs of Caco-2 co-culture for CTRL co-cult, ATCC co-cult and MUT co-cult. Bar 10 μm. (**B**) Single confocal optical sections of CD133 localization on detached Caco-2 cell at 72 h of co-culture. Bar 20μm (**C**) Statistical histograms of CD133 MFI value after 72 h of co-culture on Caco-2 cells. Each value is expressed as a mean _ SD. One-way ANOVA with Bonferroni's multiple comparison test revealed * = $p < 0.05$, ** = $p < 0.01$, *** = $p < 0.001$ vs. control and † = $p < 0.05$, †† = $p < 0.01$, ††† = $p < 0.001$ vs. mut.

### *Cell response of U937 to stimulation through Caco-2-treated cells*

U937 cells from co-culture conditions were tested for cytotoxicity, mitochondria alterations (TMRE) and oxidative stress (DCF) (**Figure 13** A). The 7'AAD positive events (dead cells) increase in both ATCC and MUT Caco-2 co-culture samples (**Figure 13 B**). Moreover, ROS levels and mitochondria membrane potential appear modulated (**Figure 13 C/D**), in respect to the status of U937 cells harvested from the co-culture with Caco-2 uninfected cells.

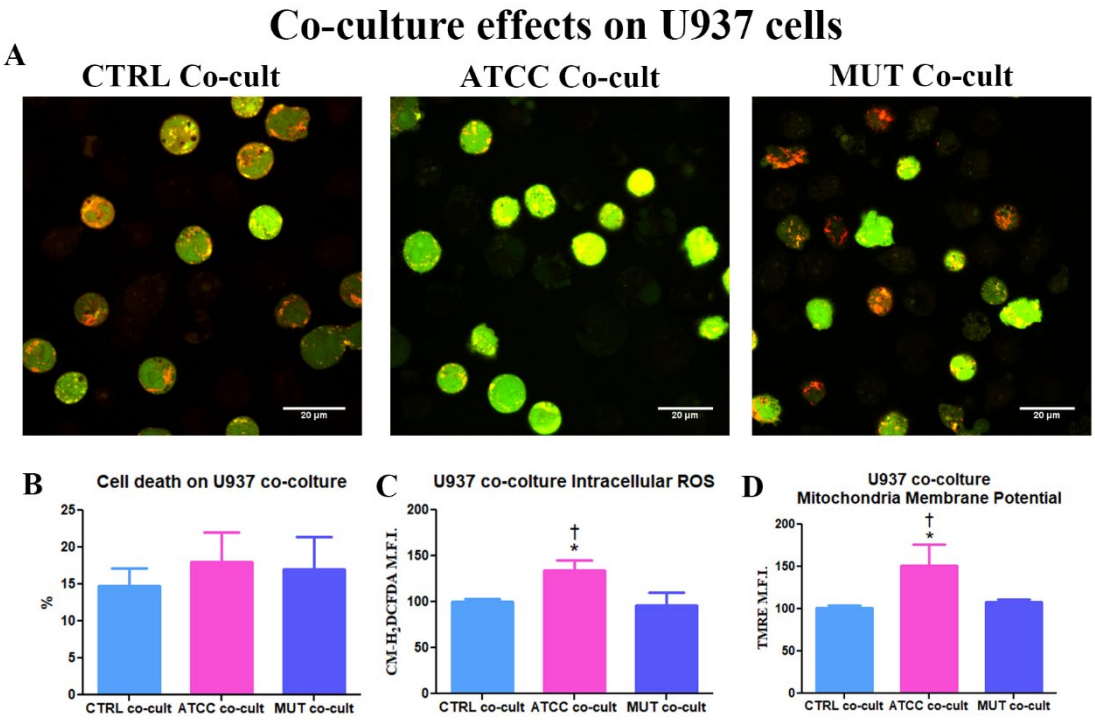


**Figure 13:** (**A**) Single confocal optical sections of CM-H2DCFDA (green) and TMRE (red) on U37 cell at 72 h of co-culture. Scale bar 20µm (**B**) Statistical histograms of the percentage of 7'AAD positive cells after 72 h of co-culture on U937 cells. Each value is expressed as a mean _ SD (results from n _ 3 independent experiments). Two-way ANOVA with Bonferroni's multiple comparison test revealed * = $p < 0.05$, ** = $p < 0.01$, *** = $p < 0.001$ vs. control and † = $p < 0.05$, †† = $p < 0.01$, ††† = $p < 0.001$ vs. mut. (**C**) Statistical histogram of CM-H2DCFDA MFI value after 72 h of co-culture on Caco-2 cells. Each value is expressed as a mean _ SD (results from n _ 3 independent experiments). Two-way ANOVA with Bonferroni's multiple comparison test revealed * = $p < 0.05$, ** = $p < 0.01$, *** = $p < 0.001$ vs. control and † = $p < 0.05$, †† = $p < 0.01$, ††† = $p < 0.001$ vs. mut. (**D**) Statistical histograms of TMRE MFI value after 72 h of co-culture on Caco-2 cells. Each value is expressed as a mean _ SD (results from n _ 3 independent experiments). Two-way ANOVA with Bonferroni's multiple comparison test revealed * = $p < 0.05$, ** = $p < 0.01$, *** = $p < 0.001$ vs. control and † = $p < 0.05$, †† = $p < 0.01$, ††† = $p < 0.001$ vs. mut.

These evaluations correlate with those performed on directly-lysate-treated U937 cells, specifically modulated by the active (ATCC) and inactive (CdtA Mut) toxin. Such findings propelled us to detect DNA content and cell cycle phases to undoubtedly trace the effect of CDT, transferred from intestinal to myeloid cells, pointing out a possible transfer of the disease.

CDT causes DNA damage that leads to 2 types of cell cycle arrest: G1 arrest and G2/M arrest. In ATCC-Caco-2 co-culture system-U937, S and G2/M phases (**Figure 14**) (El-Aouar Filho *et al.*, 2017) significantly increase, revealing a proliferation block, normally referred to DNA injury with Cytolethal distending toxins (Fahrer *et al.*, 2014). As an appropriate control for the specific CDT effects, Mut co-culture U937 samples display a cell cycle similar to that from U937 cells co-cultured with Caco-2 uninfected cells.

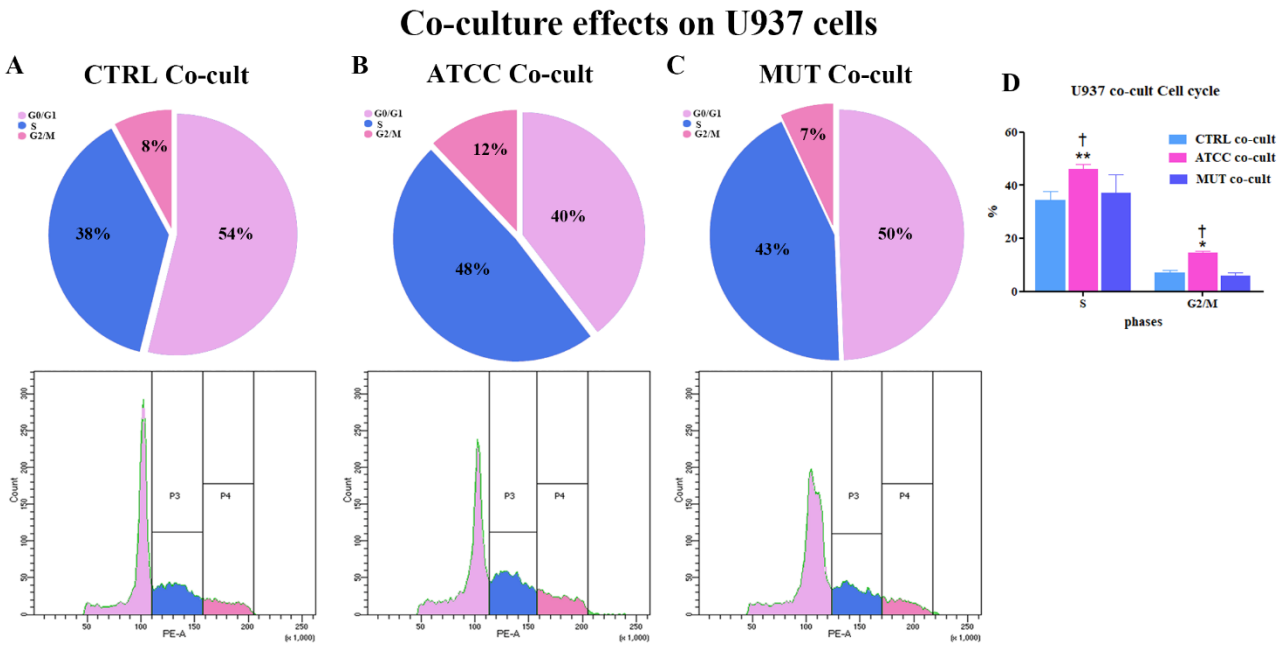


**Figure 14:** Pie chart (above) and cytometric histograms (below) for cell cycle distribution of U937 CTRL-co-culture (**A**), ATCC-co-culture (**B**), MUT-co-culture(**C**). (**D**) Statistical histogram of S and G2/M phases of cell cycle calculated in cytometry via PI staining at 72 h. Each value was expressed as a percentage ± SD (Results from n ≥ 3 independent experiments). Two-way ANOVA with Bonferroni's multiple comparison test revealed * = $p < 0.05$, ** = $p < 0.01$, *** = $p < 0.001$ vs. control and † = $p < 0.05$, †† = $p < 0.01$, ††† = $p < 0.001$ vs. mut.

Obviously, the different extracellular environments are the source of the different pathways induced in myeloid cells and, although several soluble factors can be released by the infected Caco-2 cells, we focused our attention on EVs, taking into account their role in the Autophagic- and Endo-Lysosomal Systems.

We investigate the extracellular environment; in particular the presence of EVs (**Figure 15 A**), detecting, by FCM, the total amount of EVs in the co-culture media.

**Figure 15 B** illustrates that the presence of toxin increases EV release. However, the first statistic histogram shows the total amount of EVs in the medium of the co-culture: these data are relative to the EVs released by both Caco-2 cells (initially infected in the starting monoculture) and U937 myeloid cells (uninfected and added to Caco-2 monolayer after 10 days).

Therefore, we choose the stem cell marker CD133 (prominin-1) to specifically evaluate exosomes released by Caco-2 cells, since we also detected CD133 relevant modulation (induced by lysate administration) on the surface of the membrane.

As cited, this molecule is associated with plasma membrane protrusions (e.g., microvilli and cilia) and regulates their organisation and function (Marzesco *et al.*, 2009; Taïeb *et al.*, 2009; Corbeil *et al.*, 2020). In epithelial cells, CD133+ EVs bud as microvesicles/exosomes from primary cilium and/or microvilli present at the apical (**Figure 15 C**).

Kang and co-workers demonstrated that the membrane glycoprotein CD133 acts as a novel regulator of EV release (by regulating the activities of the small GTPases RhoA and Rac1) (Kang, Kim and Ko, 2019). In agreement with this study, our above findings (**Figure 15D**) suggest this novel function of CD133 in the regulation of loading cargo proteins. They found that, although $CD133^+$ EVs did not affect proliferation of nontumorigenic cells, incubation of $CD133^+$ EVs with Caco-2 cells (which express wild-type KRAS), activates KRAS downstream signalling.

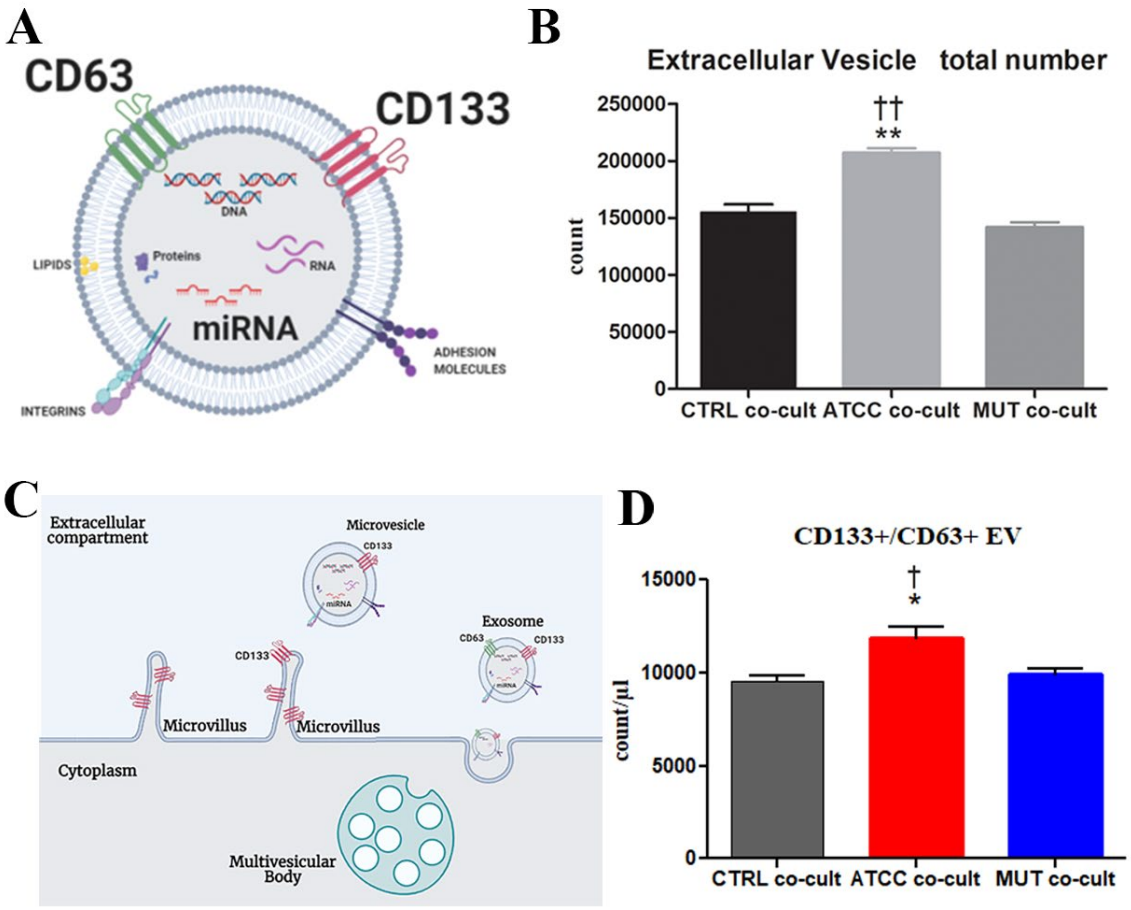


**Figure 15: (A)** Scheme of extracellular vesicles are cell secreted vesicles packed with a variety of cellular components including mRNAs, miRNAs, proteins, enzymes, lipids. The EV surface is decorated with various membrane proteins responsible for different pathophysiological functions. Created in Biorender.com **(B)** Statistical histogram of EV-count of CTRL-co-culture, ATCC-co-culture, MUT-co-culture at 72 hours. **(C)** Statistical histogram of exosome-count of CTRL-co-culture, ATCC-co-culture, MUT-co-culture at 72 hours. **(D)** Statistical histogram of Caco-2 EV count of CTRL-co-culture, ATCC-co-culture, MUT-co-culture at 72 hours.

**CHAPTER THREE**

# *EVs from C. jejuni CDT intoxicated-Caco-2 cells differently inhibit proliferation in tumour intestinal epithelial and myeloid cells: potential utility for antitumor strategies*

## *Extracellular vesicles from Caco-2 treated-cells on Caco-2 and U937 cells*

EVs play roles in cell-cell communication via the presence of specific proteins and nucleic acids, which may also serve as biomarkers of disease (Jutley *et al.*, 1987). Moreover, EVs released by infected host cells contribute significantly to promoting an inflammatory response and therefore, to promoting the development of disease (González *et al.*, 2021). The anthrax toxin produced by Bacillus anthracis can be released inside EVs from an infected epithelial cell line (Abrami *et al.*, 2013). In this chapter, we evaluate toxin effects mediated by EVs released from infected Caco-2 and transferred to uninfected homologous Caco-2 and heterologous U937 cells, taking into account EV contribution (**Figure 16**).

EVs from the medium of Caco-2 treated cells were isolated by ultracentrifugation and were characterised using Nanoparticle Tracking Analysis (NTA) (**Figure 17**) together with flow cytometric approach (**Figure 18**). In fact, since the EVs were labelled by PKH67, we analysed them by flow cytometry before their interaction with Caco-2 and U937 cells respectively.

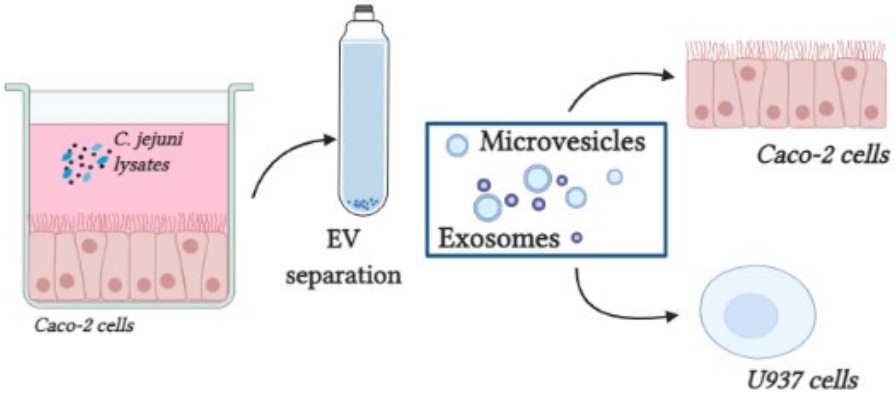


**Figure 16:** Scheme of EV separation by ultracentrifugation and EV administration to uninfected Caco-2 and U937 cells. Created in Biorender.com

Our data demonstrated a peculiar size difference for EvA (Figure 17 D) and the good detectability by fluorescence.

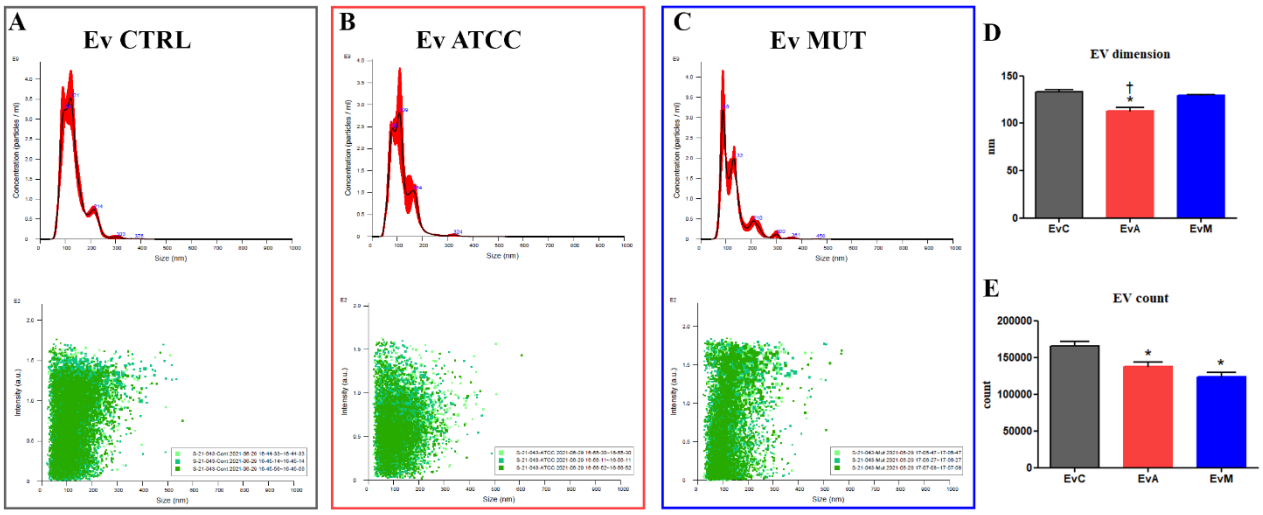


**Figure 17:** EVs were dynamically observed by nanoparticle tracking analysis. Particle size distribution is expressed as the average and standard error of the mean of nanoparticle concentration (n=3) for EvC (**A above)**, EvA **(B above)**, EvM **(C above)**. Different colours and sizes of markers represent measures of particle size and scattered light intensity of single particles from the 3 exp for EvC **(A below)**, EvA **(B below)**, EvM **(C below)**. **(D)** Statistical histogram for size distribution for EvC, EvA and EvM. One-way ANOVA with Bonferroni's multiple comparison test revealed * = $p < 0.05$, ** = $p < 0.01$, *** = $p < 0.001$ vs. EvC. **(E)** Statistical histogram for particle concentration for EvC, EvA and EvM. One-way ANOVA with Bonferroni's multiple comparison test revealed * = $p < 0.05$, ** = $p < 0.01$, *** = $p < 0.001$ vs. EvC.

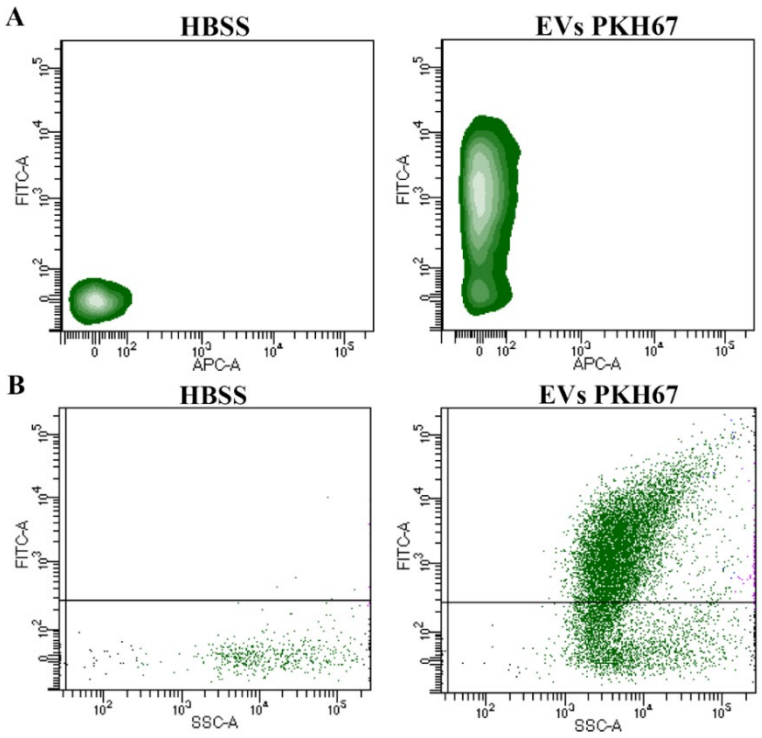


**Figure 18: (A)** Density plot of HBSS and PKH67-labelled EVs. **(B)** Dot plot of HBSS and PKH67-labelled EVs

### *EVS on Caco-2*

To quantitatively evaluate the cellular uptake of EVs, the Caco-2 cells were incubated with $2x10^4$ PKH67-labelled EVs/cell for 48 h, 72 h and analysed by flow cytometry and confocal microscopy (**Figure 19**).

Our data highlighted a similar EV uptake for EvC and EvA, whereas EvM appear less internalised in the cells (**Figure 19 A/B**), as confirmed also by confocal microscopy (**Figure 19 E**). Of note, (after 48h), data on absolute cell counting show a significant reduction of cell number in the EvA samples, whereas EvM cells are in the same (or more) numerous than EvC cells (**Figure 19 C**). Indeed, morphologic analyses underline an apparent dissimilar intracellular distribution (punctate and scattered in EvC samples, perinuclear and "grouped" in EvA samples) and an almost complete internalisation, excluding a considerable contribution from EV membrane/plasma membrane fusion processes (**Figure 19 D**).

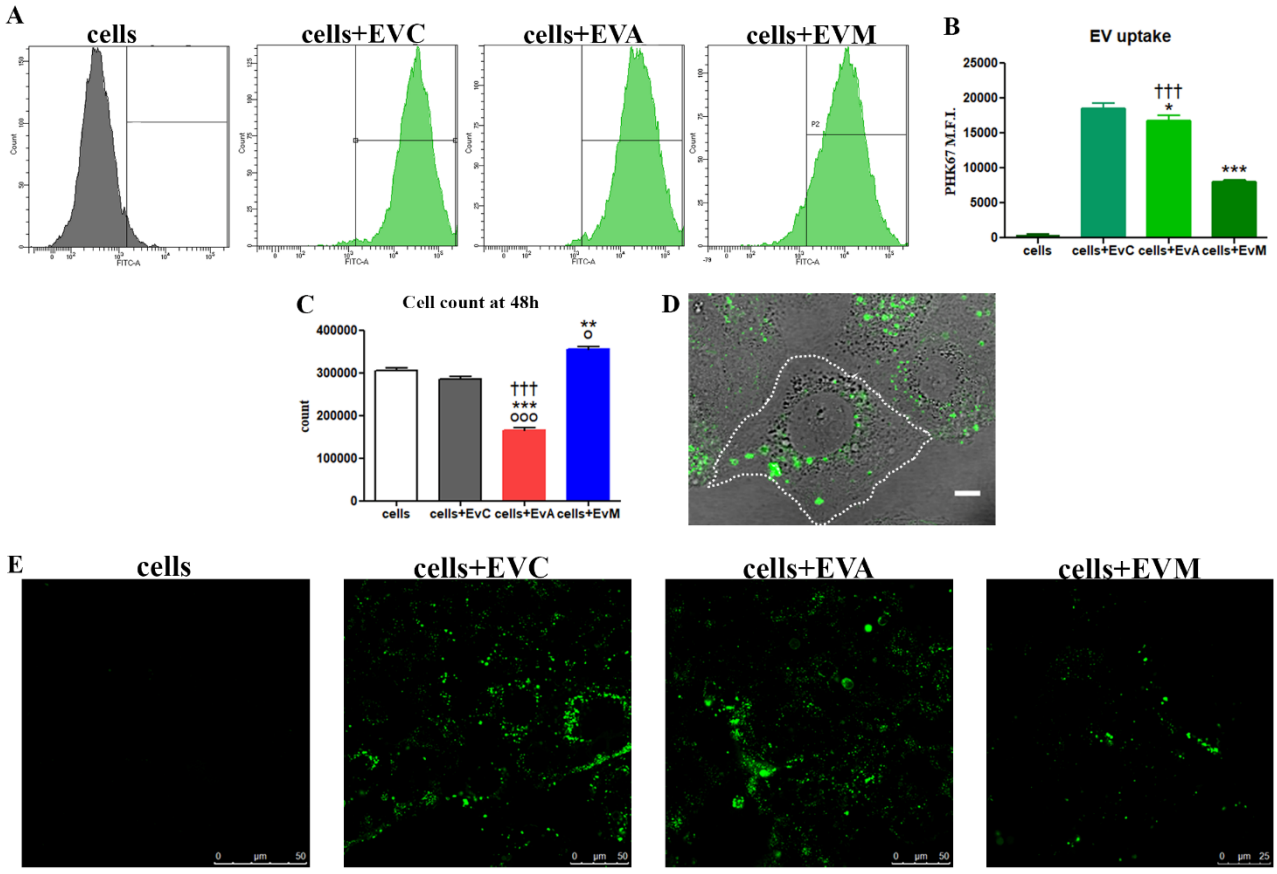


**Figure 19:** *In vitro* cellular uptake of PKH67-labelled EVs. **(A)** FCM Histogram of uptake of PKH67-labelled EV for Caco-2 cells treated EvC, EvA and EvM at 48 h. **(B)** Statistical histogram of uptake of PKH67-labelled EV for Caco-2 cells treated EvC, EvA and EvM at 48 h. Each value was expressed as MFI ± SD (Results from n ≥ 3 independent experiments). One-way ANOVA with Bonferroni's multiple comparison test revealed * = $p < 0.05$, ** = $p < 0.01$, *** = $p < 0.001$ vs. cells. **(C)** Statistical histogram of cell count at 48 h. Each value was expressed as absolute count ± SD (Results from n ≥ 3 independent experiments). One-way ANOVA with Bonferroni's multiple comparison test revealed ° = $p < 0.05$, °° = $p < 0.01$, °°° = $p < 0.001$ vs. cells and * = $p < 0.05$, ** = $p < 0.01$, *** = $p < 0.001$ vs. cells+EvC and and † = $p < 0.05$, †† = $p < 0.01$, ††† = $p < 0.001$ vs. cells+EvM. **(D)** Representative micrograph of EV-labelled PKH-67 (green) internalisation on Caco-2 cells. Bar: 20µm **(E)** Single confocal optical sections of the Caco-2 cells treated with PKH67-labeled EvC, EvA and EvM at 48 h. Bar: 20µm.

To deeply investigate these evidences we perform co-staining by PKH67 +EVs, LTDR and TMRE: the merging images of **Figure 20 A** confirmed not only a different subcellular distribution but also the typical CDT cell distension, starting at 48 h. Briefly, almost all functional parameters (mitochondrial membrane potential, lysosomal compartment and Autophagic-like vacuole) (**Figure 20 C/D/E/F**) are in agreement with those collected from directly lysates intoxicated Caco-2 cells, with

the exception of mitochondrial ROS that decrease in respect of both cells+EvC and EvM. Such discrepancy could derive from the analyses and interpretation of colocalization data (**Figure 21**). The exosomes were distributed throughout the cytoplasm, especially in the perinuclear region.

The localization of EVs (assessed by confocal imaging) demonstrated that the EVs distributed throughout the cytoplasm, especially in the perinuclear region for cells-EvA treated, as shown in **Figure 20 A**(Zeng, Zhang and Nyström, 2012). These results concur with results obtained by Mantel et al. (Mantel *et al.*, 2016), who observed perinuclear localization of RBC-derived EVs in bone marrow endothelial cells. Lombardo et al. (Lombardo *et al.*, 2016) also observed internalisation of endothelial-derived EVs by endothelial cells (Durak-Kozica *et al.*, 2018).

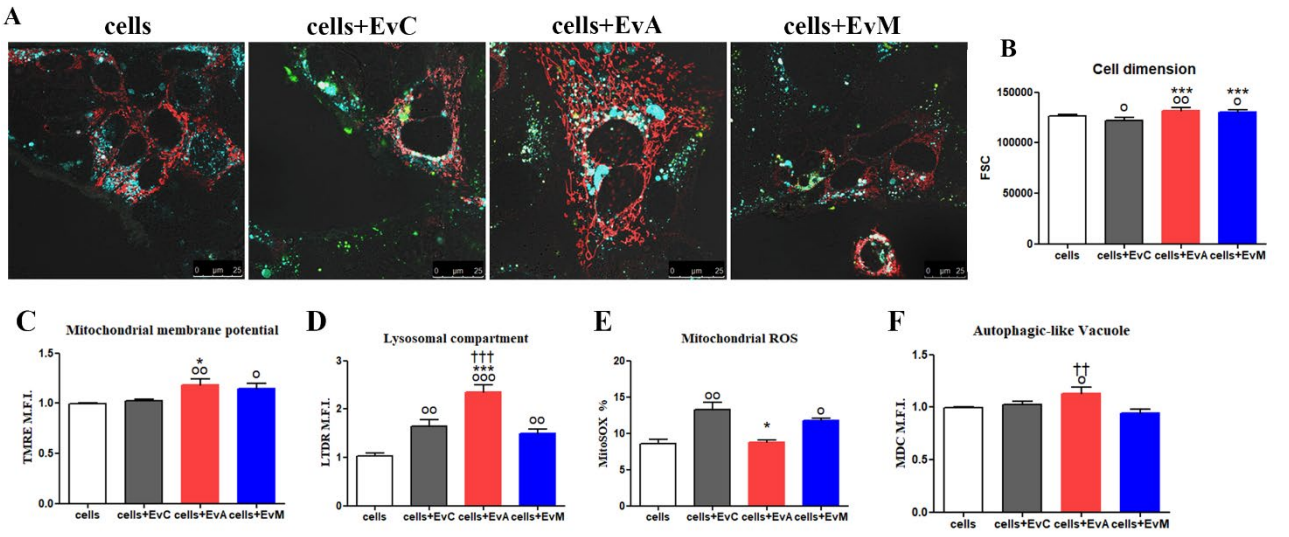


**Figure 20:** (**A**) Single confocal optical sections is showing overlay of mitochondria (TMRE red), lysosome (LTDR cyan) and EV (PKH67 green) at 48h for cells, cells+EvC, cells+EvA and cells+EvM. (**B**) Statistical histograms of alterations in forward scattering (FSC) (cell size) for cells, cells+EvC, cells+EvA and cells+EvM. Each value is expressed as a mean _ SD (results from n _ 3 independent experiments). One-way ANOVA with Bonferroni's multiple comparison test revealed ° = $p < 0.05$, °° = $p < 0.01$, °°° = $p < 0.001$ vs. cells and * = $p < 0.05$, ** = $p < 0.01$, *** = $p < 0.001$ vs. cells+EvC. (**C**) Statistical histograms of TMRE MFI value on cells, cells+EvC, cells+EvA and cells+EvM. Each value is expressed as a mean _ SD (results from n _ 3 independent experiments). One-way ANOVA with Bonferroni's multiple comparison test revealed ° = $p < 0.05$, °° = $p < 0.01$, °°° = $p < 0.001$ vs. cells and * = $p < 0.05$, ** = $p < 0.01$, *** = $p < 0.001$ vs. cells+EvC. (**D**) Statistical histograms of LTDR MFI value for cells, cells+EvC, cells+EvA and cells+EvM. Each value is expressed as a mean _ SD (results from n _ 3 independent experiments). One-way ANOVA with Bonferroni's multiple comparison test revealed ° = $p < 0.05$, °° = $p < 0.01$, °°° = $p < 0.001$ vs. cells and * = $p < 0.05$, ** = $p < 0.01$, *** = $p < 0.001$ vs. cells+EvC and and † = $p < 0.05$, †† = $p < 0.01$, ††† = $p < 0.001$ vs. cells+EvM. (**E**) Statistical histograms of the percentage of

MitoSox positive cells for cells, cells+EvC, cells+EvA and cells+EvM. Each value is expressed as a percentage _ SD (results from n _ 3 independent experiments). One-way ANOVA with Bonferroni's multiple comparison test revealed ° = p < 0.05, °° = p < 0.01, °°° = p < 0.001 vs. cells and * = p < 0.05, ** = p < 0.01, *** = p < 0.001 vs. cells+EvC, (**F**) Statistical histograms of MDC MFI for cells, cells+EvC, cells+EvA and cells+EvM after 48 h. Each value was converted to arbitrary units (A.U.) setting control as 1. Each value was expressed as a mean ± SD (Results from n ≥ 3 independent experiments). One-way ANOVA with Bonferroni's multiple comparison test revealed ° = p < 0.05, °° = p < 0.01, °°° = p < 0.001 vs. cells and * = p < 0.05, ** = p < 0.01, *** = p < 0.001 vs. cells+EvC.

EVs can colocalize with lysosomes indicating that some EV-material is subject to lysosomal degradation (Hansen *et al.*, 2020) as observable, EvA partially co-localize with lysosomes (**Figure 21 A/B**), suggesting a certain EvA degradation that might be responsible of a mitochondria targeted decreased effect. Our data are in agreement with specific studies, finding that EVs were delivered to the nucleus of recipient cells (Santos *et al.*, 2018), and to the ER before ending up in lysosomes as the final destination (Heusermann *et al.*, 2016; Hansen *et al.*, 2020).

Moreover, regarding mitochondria-EV colocalization, the data show a similar behaviour for cells+EvC, EvA and EvM (**Figure 21 C/D**), excluding the mitochondrial route from the EV intracellular journey.

This implies that EV cargo is released from late endosomes and lysosomes and/or that EV cargo is released from (early) endosomes that subsequently undergo maturation. In this step of our evaluation, the topical process is the fusion of a fraction of the internalised EVs with lysosomes, resulting in EV cargo exposure to the cell cytosol, a mechanism well described by Joshi and co-workers (Joshi *et al.*, 2020).

Different sites for EV cargo release in acceptor cells have been proposed, including

(i) the plasma membrane (Parolini *et al.*, 2009),

(ii) the endosome (Del Conde *et al.*, 2005; Yao *et al.*, 2018) and

(iii) the endoplasmic reticulum (Heusermann *et al.*, 2016).

Our experiments reveal that EVs do not fuse with the plasma membrane (**Figure 19 D**) in investigated Caco-2 cells: in fact, green fluorescence of PKH67-labelled EVs is mainly located in the perinuclear area (where the perinuclear pool of ER accumulates due to dynein activity) and scattered in the cytoplasm, partially co-localizing with LTDR, highlighting targeting of endo-lysosomal systems.

It is well known that the study of the fate of EV cargoes is tricky due to the low quantities of encapsulated cargo molecules (Chen *et al.*, 2018; Joshi *et al.*, 2020), however in line with previous data, we proceed to evaluate the typical CDT-induced effects and, among all, the most characteristic effect is the blocking of proliferation.

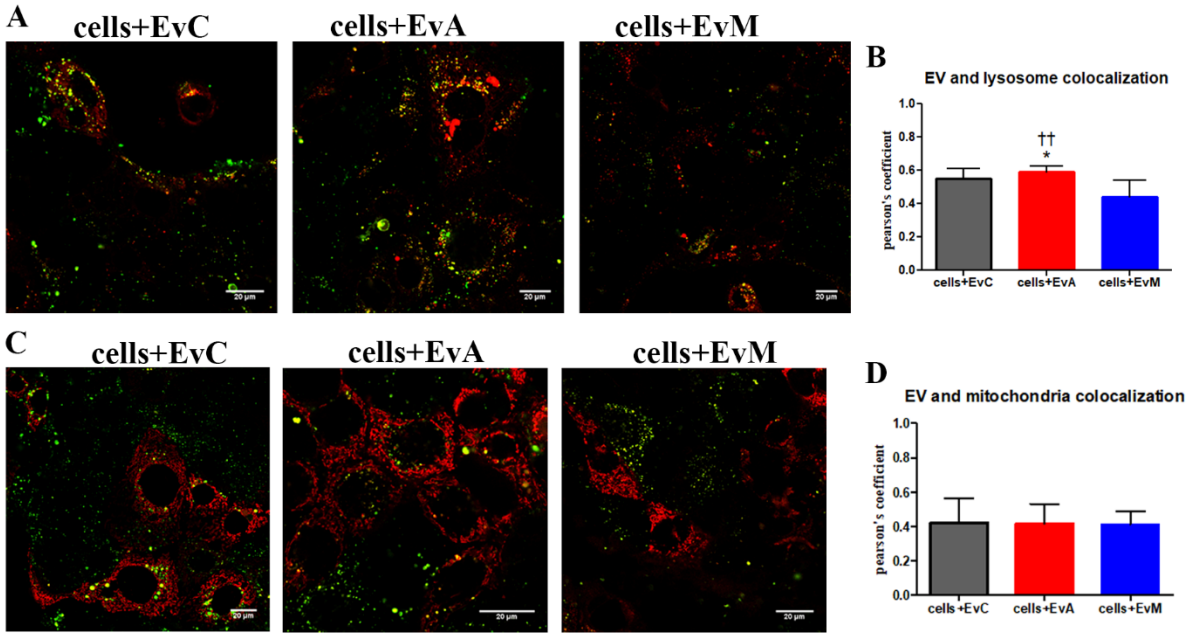


**Figure 21: (A)** Single confocal optical sections showing overlay of lysosome (LTDR red) and EV (PKH67 green) at 48h for cells+EvC, cells+EvA and cells+EvM. Colocalization of EVs (green) and lysosomes (red) is manifested in yellow. The bar: 20 μm **(B)** Pearson's coefficient, able to quantitate LTDR/EV co-localization for cells+EvC, cells+EvA and cells+EvM. Pearson's coefficients were derived from three completely independent experiments with >10 fields per experiment contributing to the cumulative result. Each value is expressed as PCC ± SD; asterisks denote a statistically significant difference. One-way ANOVA with Bonferroni's multiple comparison test revealed * = $p < 0.05$, ** = $p < 0.01$, *** = $p < 0.001$ vs. cells+EvC. The bar: 20 μm (**C**) Single confocal optical sections showing overlay of mitochondria (TMRE red) and EV (PKH67 green) at 48h for cells+EvC, cells+EvA and cells+EvM. **(D)** Pearson's coefficient, able to quantitate TMRE/EV co-localization for cells+EvC, cells+EvA and cells+EvM. Pearson's coefficients were derived from three completely independent experiments with >10 fields per experiment contributing to the cumulative result. Each value is expressed as PCC ± sd; asterisks denote a statistically significant difference. One-way ANOVA with Bonferroni's multiple comparison test revealed * = $p < 0.05$, ** = $p < 0.01$, *** = $p < 0.001$ vs. cells+EvC.

To evaluate the G2/M block, the cells were ethanol-fixed and tested for PKH26-EVs fluorescence, then were separately monitored for DNA content.

EvC (Evs from uninfected CaCo-2 cells) cells show an uptake similar to the EvA cells (EVs from ATCC infected CaCo-2 cells). EV positive cells (EV + cells) and EV negative cells (EV-) cells are depicted in **Figure 22 A**: DNA content (**Figure 22 C/E**) was analysed after 72 h. The two different subsets were analysed to discriminate cell cycle phases. To determine if EvA induced the typical cell cycle arrest, flow cytometry analysis was performed (**Figure 22 B/D**). EvA+ and EvM+ cells highlight the G2/M block. Indeed, also in the cells currently EV- a progressive accumulation in S and G2/M phases is observable.

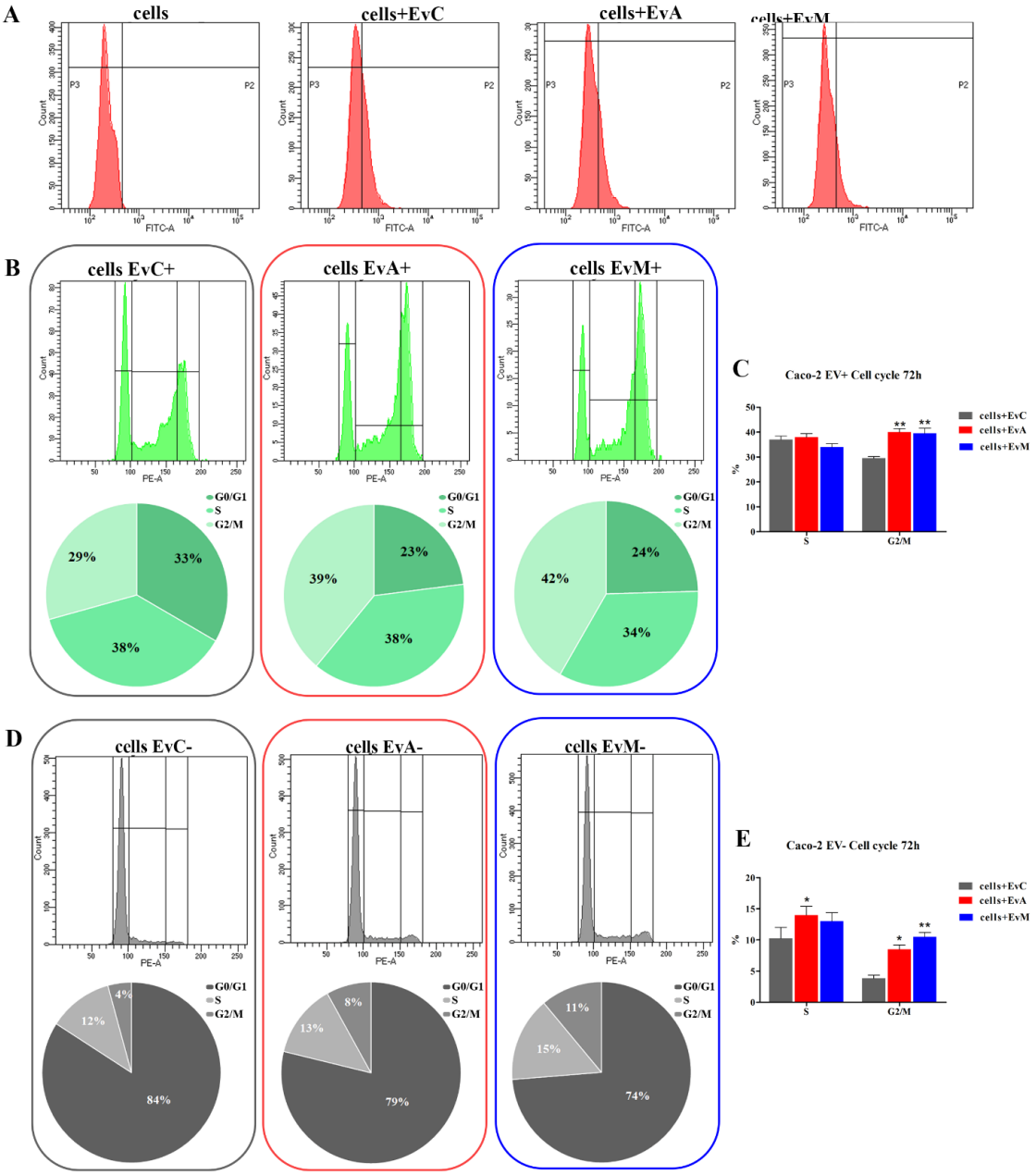


**Figure 22: (A)** Gating strategy for the detection of EV + (P2) and EV- (P3) cells, starting from negative ctrl (cell without EV). **(B)** Cytometric histograms (above) and Pie chart (below) for cell cycle distribution of Caco-2

cells+EvC, cells+EvA, cells+EvM. (**C**) Statistical histogram of S and G2/M phases of cell cycle calculated in cytometry via PI staining at 72 h. Each value was expressed as a percentage ± SD (Results from n ≥ 3 independent experiments). Two-way ANOVA with Bonferroni's multiple comparison test revealed * = $p < 0.05$, ** = $p < 0.01$, *** = $p < 0.001$ vs. cells+EvC and † = $p < 0.05$, †† = $p < 0.01$, ††† = $p < 0.001$ vs. cells+EvM. **(D)** Cytometric histograms (above) and Pie chart (below) for cell cycle distribution of Caco-2 cells-EvC, cells-EvA, cells-EvM. (**E**) Statistical histogram of S and G2/M phases of cell cycle calculated in cytometry via PI staining at 72 h. Each value was expressed as a percentage ± SD (Results from n ≥ 3 independent experiments). Two-way ANOVA with Bonferroni's multiple comparison test revealed * = $p < 0.05$, ** = $p < 0.01$, *** = $p < 0.001$ vs. cells+EvC and † = $p < 0.05$, †† = $p < 0.01$, ††† = $p < 0.001$ vs. cells+EvM.

These data, on the one hand, confirm our hypothesis on the active ATCC CDT enclosed in the cargo of EVs, on the other hand arouse perplexity with regard to the mutant CDT effects: in fact, although proliferation is clearly reduced only in EvA cells, cell cycle is altered in both EvA and EvM samples.

*EVS on U937*

We monitored EV cellular uptake in U937 myeloid cells and analysed by flow cytometry and confocal microscopy at the following incubation times: 24h, 48h and 72h.

Our data underlined a similar EV uptake for EvC and EvA whereas EvM appear less fluorescent, revealing a minor internalisation in U937 cells (**Figure S1**), by both flow cytometry and confocal microscopy, as observed in EV-treated CaCo-2 cells (**Figure 23 A/B**).

Moreover, as for Caco-2 cells, we performed the absolute cell count after 48 h: in myeloid cells EvA sample shows only a moderate reduction of cell number (**Figure 23 C**).

Data from lysosomal compartment, autophagic-like vacuole and mitochondrial membrane potential (**Figure 23 E/F/G**) are in accordance with those collected from directly intoxicated U937 cells (**Figure 1 B/C/D**).

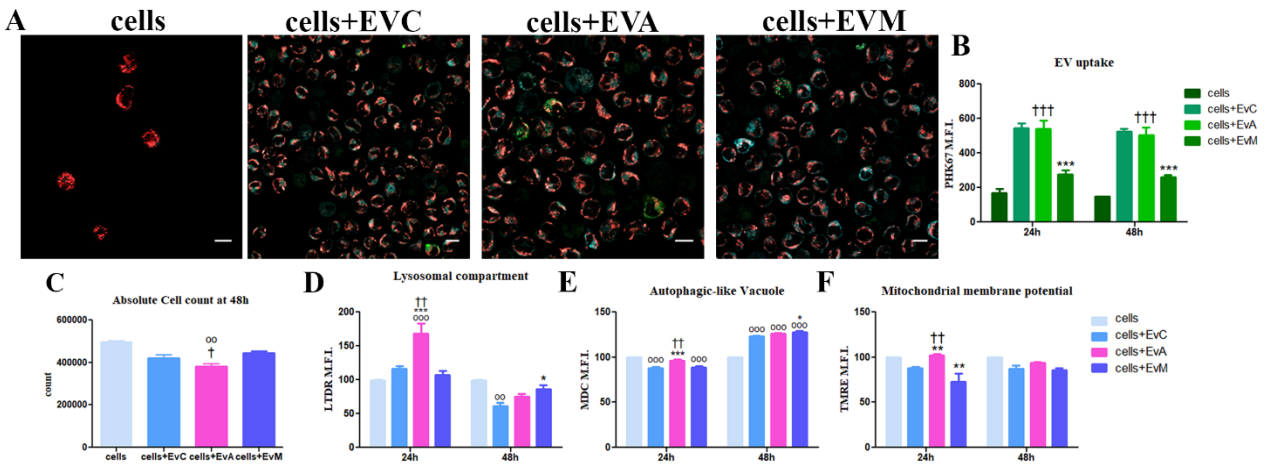


**Figure 23:** (**A**) Single confocal optical sections is showing overlay of mitochondria (TMRE red), lysosome (LTDR cyan) and EV (PKH67 green) at 48h for cells, cells+EvC, cells+EvA and cells+EvM. (**B**) Statistical histogram of PKH67-labelled EV uptake for Caco-2 cells treated by EvC, EvA and EvM at 24 and 48 h. (**C**) Statistical histogram of cell count at 48 h. Each value was expressed as absolute count ± SD (Results from n ≥ 3 independent experiments). One-way ANOVA with Bonferroni's multiple comparison test revealed ° = p < 0.05, °° = p < 0.01, °°° = p < 0.001 vs. cells and * = p < 0.05, ** = p < 0.01, *** = p < 0.001 vs. cells+EvC and and † = p < 0.05, †† = p < 0.01, ††† = p < 0.001 vs. cells+EvM. (**D**) Statistical histograms of LTDR MFI value for cells, cells+EvC, cells+EvA and cells+EvM. Each value is expressed as a mean _ SD (results from n _ 3 independent experiments). Two -way ANOVA with Bonferroni's multiple comparison test revealed ° = p < 0.05, °° = p < 0.01, °°° = p < 0.001 vs. cells and * = p < 0.05, ** = p < 0.01, *** = p < 0.001 vs. cells+EvC and and † = p < 0.05, †† = p < 0.01, ††† = p < 0.001 vs. cells+EvM. (**E**) Statistical histograms of MDC MFI for cells, cells+EvC, cells+EvA and cells+EvM at 24 h and 48 h. Each value was expressed as a mean ± SD (Results from n ≥ 3 independent

experiments). Two-way ANOVA with Bonferroni's multiple comparison test revealed ° = p < 0.05, °° = p < 0.01, °°° = p < 0.001 vs. cells and * = p < 0.05, ** = p < 0.01, *** = p < 0.001 vs. cells+EvC. (**F**) Statistical histograms of TMRE MFI value on cells, cells+EvC, cells+EvA and cells+EvM at 24 h and 48 h. Each value is expressed as a mean _ SD (results from n _ 3 independent experiments). Two -way ANOVA with Bonferroni's multiple comparison test revealed ° = p < 0.05, °° = p < 0.01, °°° = p < 0.001 vs. cells and * = p < 0.05, ** = p < 0.01, *** = p < 0.001 vs. cells+EvC.

The evaluation of the interactions between EVs and intracellular structures, including lysosomes and mitochondria, are detailed by Confocal analyses, revealing a significant co-localization of EvA with lysosomes (**Figure 24 A/B**). Mitochondria, conversely, do not appear significantly targeted by EVs (**Figure 24 C/D**).

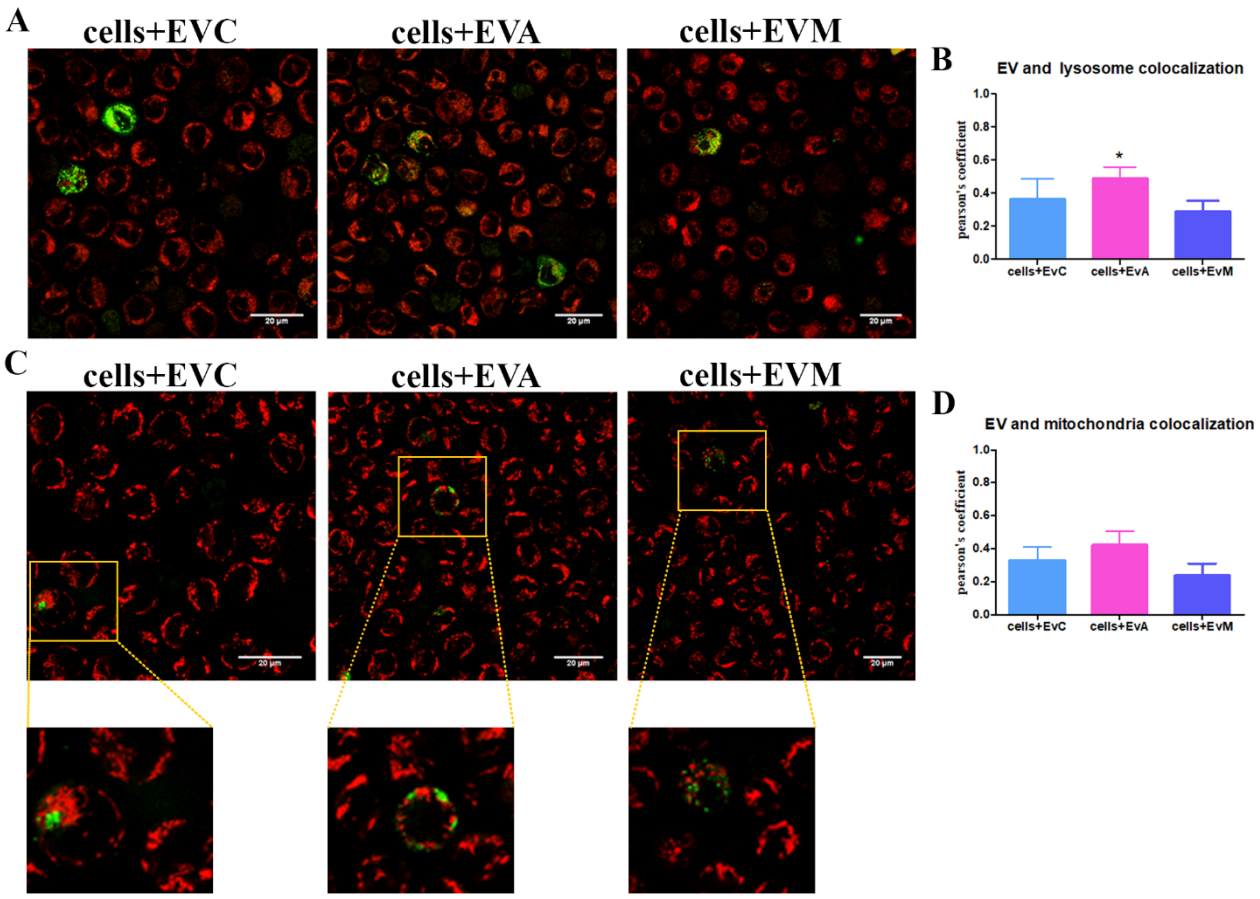


**Figure 24: (A)** Single confocal optical section showing an overlay of lysosome (LTDR red) and EV (PKH67 green) at 48h for cells+EvC, cells+EvA and cells+EvM. Colocalization of EVs (green) and lysosomes (red) is manifested in yellow. The bar: 20 μm **(B)** Pearson's coefficient, able to quantitate LTDR/EV co-localization for cells+EvC, cells+EvA and cells+EvM. Pearson's coefficients were derived from three completely independent

experiments with >10 fields per experiment contributing to the cumulative result. Each value is expressed as PCC ± sd; asterisks denote a statistically significant difference. One-way ANOVA with Bonferroni's multiple comparison test revealed * = $p < 0.05$, ** = $p < 0.01$, *** = $p < 0.001$ vs. cells+EvC. (**C**) Single confocal optical section showing an overlay of mitochondria (TMRE red) and EV (PKH67 green) at 48h for cells+EvC, cells+EvA and cells+EvM. Colocalization of EVs (green) and mitochondria (red) is manifested in yellow. The bar: 20 µm **(D)** Pearson's coefficient, able to quantitate TMRE/EV co-localization for cells+EvC, cells+EvA and cells+EvM. Pearson's coefficients were derived from three completely independent experiments with >10 fields per experiment contributing to the cumulative result. Each value is expressed as PCC ± sd; asterisks denote a statistically significant difference. One-way ANOVA with Bonferroni's multiple comparison test revealed * = $p < 0.05$, ** = $p < 0.01$, *** = $p < 0.001$ vs. cells+EvC.

As performed on intestinal epithelial cells, the DNA content was evaluated after 72 h from EV administration. As illustrated, EV+ cells and EV- cells were analysed to discriminate cell cycle phases (**Figure S1**). The EV+ cells of the EvA U937 samples, demonstrate the highest number of events in G2/M phase, (**Figure 25 A above/B**), whereas the highest percentage of G2/M events in the EV- fraction was detected in EvM samples (**Figure 25 A below/C**).

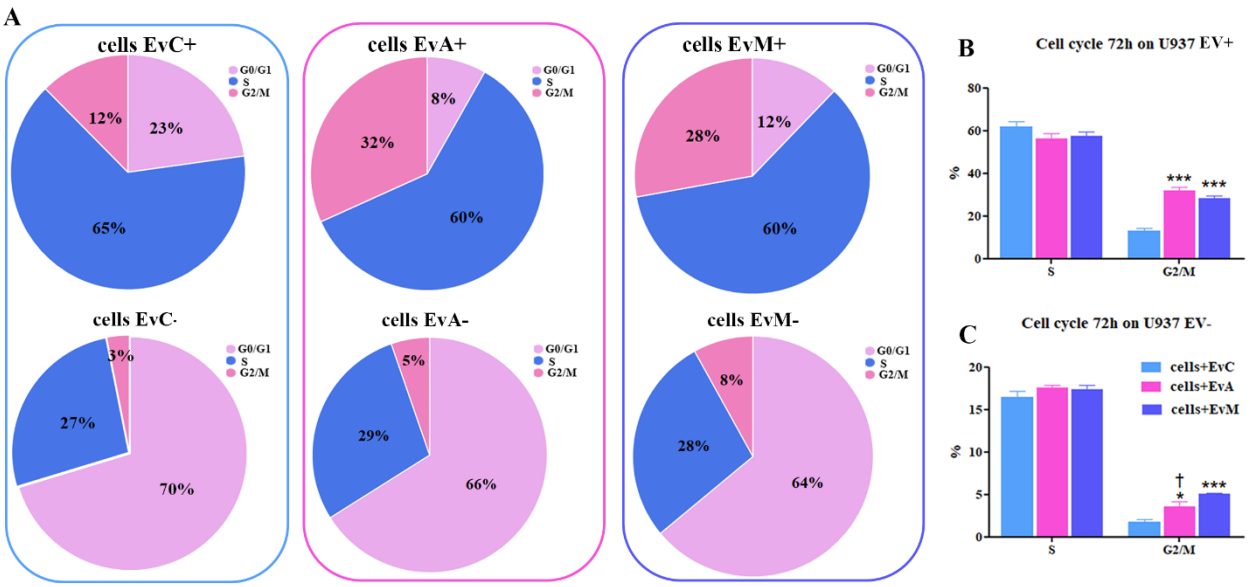


**Figure 25: (A)** Pie chart of cell EV+ cells (above) and Pie chart of cell EV- cells (below) for cell cycle distribution of U937 cells+EvC, cells+EvA, cells+EvM. **(B)** Statistical histogram of S and G2/M phases of cell cycle of cells EV+ calculated in cytometry via PI staining at 72 h. Each value was expressed as a percentage ± SD (Results from n ≥ 3 independent experiments). Two-way ANOVA with Bonferroni's multiple comparison test revealed * = $p < 0.05$, ** = $p < 0.01$, *** = $p < 0.001$ vs. cells+EvC and † = $p < 0.05$, †† = $p < 0.01$, ††† = $p < 0.001$ vs. cells+EvM.

**(C)** Statistical histogram of S and G2/M phases of cell cycle of cells EV- calculated in cytometry via PI staining at 72 h. Each value was expressed as a percentage ± SD (Results from n ≥ 3 independent experiments). Two-way ANOVA with Bonferroni's multiple comparison test revealed * = $p < 0.05$, ** = $p < 0.01$, *** = $p < 0.001$ vs. cells+EvC and † = $p < 0.05$, †† = $p < 0.01$, ††† = $p < 0.001$ vs. cells+EvM.

The pool of data from intestinal and myeloid cells highlight that EV uptake is differentiated on the basis of their source and their target. It is demonstrated that EV cargo contains the still active CDT, able to typically affect the various recipient cells, however EvM seems to induce a partially unexpected behaviour. We speculated that the mutant toxin (CdtA mutant), after the cellular administration, remains still anchored to the membrane of the donor cell and it may be, secondarily, transported as part of the membrane of the EVs, to the recipient cells (**Figure 26**).

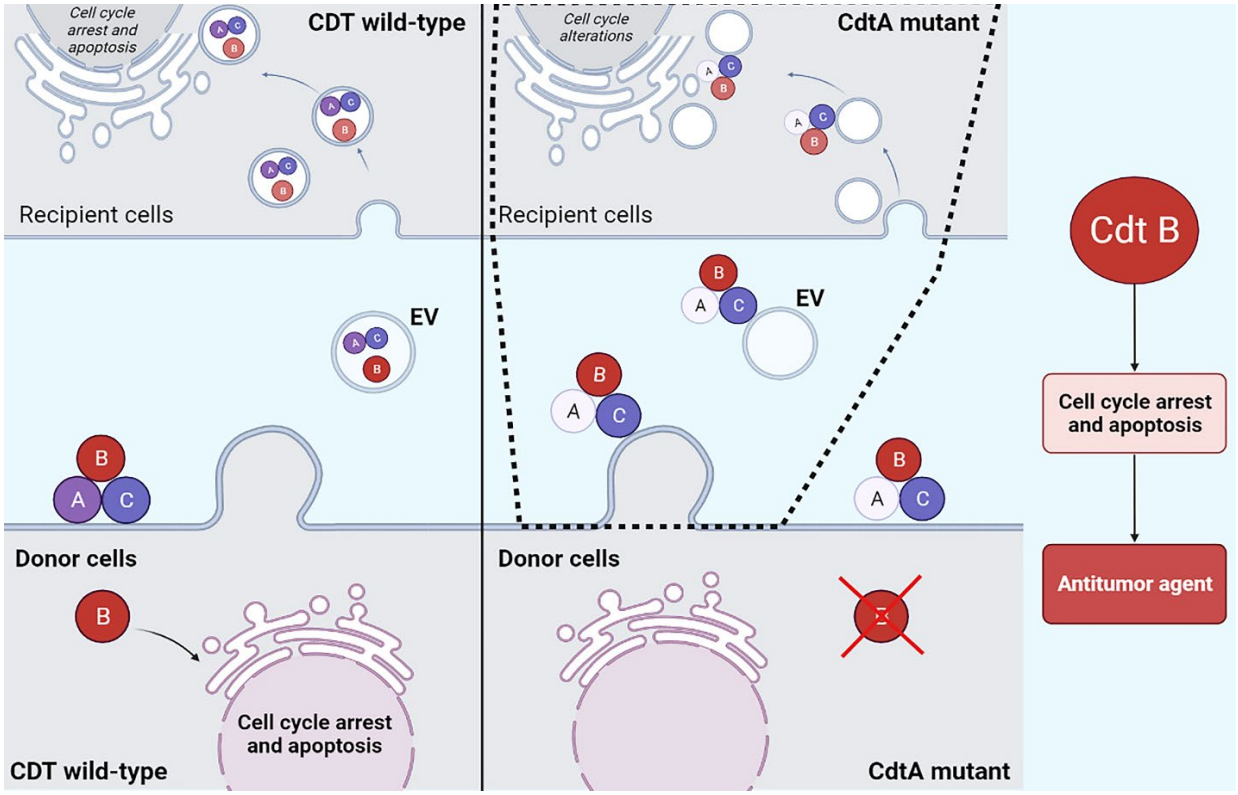


**Figure 26**: Scheme of activity of CDT-wild-type and CDT-CdtA mutant in donor cells. Hypothesis of EV release by CdtA mutant treated donor cell and mood of transmission in recipient cells (in the dashed area). Created in Biorender.com

In fact, mode of entry is likely cell type specific given that the Cdt binding subunit (CdtA-CdtC) must interact with a cell surface receptor. Nevertheless, recent evidence (Boesze-Battaglia *et al.*, 2020) suggests that this assertion is limiting because several CDT binding subunits interact directly with

cholesterol in the context of lipid rafts. In the case of CDT, surface association is dependent on the binding unit which is composed of both subunits CdtA and CdtC (Nesić, Hsu and Stebbins, 2004; Thelestam and Frisan, 2004; McSweeney and Dreyfus, 2005; Yamada *et al.*, 2006). Indeed, both CdtA and CdtC are required for maximal CdtB internalisation (Damek-Poprawa *et al.*, 2012; Boesze-Battaglia *et al.*, 2016).

Our mutant strain produces a toxin mutated for CdtA but not for CdtC: it is currently thought that CdtA remains on the plasma membrane (Dirienzo, 2014; Boesze-Battaglia *et al.*, 2016; Frisan, 2016; Taieb *et al.*, 2016), indeed, it was reported (Boesze-Battaglia *et al.*, 2016) that the CdtC subunit alone may not only target the holotoxin to a raft domain but also stabilise the association of the toxin with this domain.

## CONCLUSION

This study tries to better understand the relationship among the extracellular communication between gastric cells and immune cell trough, *C. jejuni* and Guillain-Barré syndrome. We used two different cell lines, Caco-2 as intestinal epithelial cells and U937 as myeloid cells. The immune competent Caco-2/U937-based model allowed the investigation of the extracellular communication during Caco-2 *C. jejuni* treated cells.

The significant effect of CDTs, nevertheless of the origin of bacteria, is its ability to cause DNA damage and to induce G2/M arrest in cell cycle progression.

The usage of *C. jejuni* CdtA mutant strains allowed us to investigate the role of the CDT in *C. jejuni* infection mechanisms. The fact that CDT produces some modifications in host cells after long time lapses (from 24 to 72 hours) might be essential for the onset of post-infectious sequelae such as the GBS.

Although mitochondrial modifications caused by *C. jejuni* CDT are associated to an activation of an intrinsic apoptotic pathway, recruitment of lysosomes can be associated to the activation of both the extrinsic apoptotic pathway and the autophagic pathway, two different pathways that meanwhile are strictly interconnected. Particularly interesting is the relationship between *C. jejuni* and lysosomes (Canonico *et al.*, 2018, 2020); we provided evidence about how much these organelles are important for *C. jejuni* infection. LAMP-1 upregulation, lysosomal destabilisation, autophagic-like vacuole increase occurred in our cell models suggesting that *C. jejuni* is particularly able to activate the endocytic pathway and the autophagic-secretory pathways.

After CDT enters and affects host cells, they release EVs carrying an altered profile of host-molecules, and even pathogen-derived proteins (Kuipers *et al.*, 2018). These *C. jejuni*-infected host cell EVs can have a variety of effects on gastric epithelial cells (Caco-2) and macrophages (U937), including changes in epithelial cell morphology (González *et al.*, 2021). Of note, after EV administration, we observed mitochondrial membrane potential alterations, lysosomes recruitment and cell cycle arrest in G2/M phase, in both recipient Caco-2 and U937 cells.

Therefore, *C. jejuni*-infected host cell EVs promote cellular alterations supporting the development and/or progression of inflammation/infection.

In conclusion, this work represents a novel approach to investigate the mechanisms particularly targeted by *C. jejuni* CDT, to cause the disease. Indeed, the ability of *C. jejuni* CDT not to be

completely degraded by the endo-lysosomal compartment and to remain active within intestinal cells, might have a critical role in GBS outset.

To this regard, *C. jejuni*-infected host cell EVs assume the role of transporters of the toxin to other cells, both belonging to the same lineage and to different lineages. Despite current knowledge on the biogenesis and uptake of EVs and their relevance in various medical areas as biomarkers, therapeutic targets, or biological vehicles for drug delivery, information on the fate of endocytosed EV content remains limited (Kanada *et al.*, 2015; Margolis and Sadovsky, 2019). In our model, we can consider the heterogeneity of EVs and the mechanism of cellular internalisation as factors determining the fate of EV content. Finally, in recently published manuscripts, CDTs from different bacterial sources (*A. actinomycetemcomitans, H. ducreyi, and C. jejuni)* (Bachran *et al.*, 2014; Faïs *et al.*, 2016; Pons *et al.*, 2020) are prospected as important molecules in the development of anti-tumor agent (Lin *et al.*, 2017; Kailoo, Shreya and Kumar, 2021; Keshtvarz *et al.*, 2021). Our data confirm these possibilities, nevertheless the lineage of the target cells should be carefully taken into account, due the nuclear events (observed in our models), such as pRb decrease in U937 and/or PCNA increase in Caco-2 cells that, at long term, could become an advantage for tumour cells (Ye *et al.*, 2020).

## MATERIALS AND METHODS

### *C. jejuni* cell lysate preparation

*C. jejuni* ATCC 33291 and *C. jejuni* 11168H CdtA mutant strains were grown in 50 ml Brucella broth (Oxoid) at 37°C in a shaking incubator under microaerophilic condition for 48 hours. The bacterial suspensions were adjusted spectrophotometrically to approximately $10^8$ bacteria/ml and centrifuged at 4,000 rpm for 10 min. The pellets were resuspended in 20 ml of Dulbecco's modified eagle medium (D-MEM) (Sigma-Aldrich) and lysed by sonication (2 x 30 s bursts with 30 s intervals between each burst) by using a sonicator (Sonifier 450, Branson, U.S.A). Cell debris and un-lysed bacterial cells were then removed by centrifugation at 4,000 rpm for 10 min. Aliquots of each lysate were sterilized by a 0.22 μm membrane filter (Millipore, Italy) and stored at -20°C before use.

### Cell Culture

U937 (human myelomonocytic cell line) cells (Sigma-Aldrich, St Louis, MO, USA) were grown in RPMI 1640 supplemented with 10% heat-inactivated fetal bovine serum (FBS), 2 mM glutamine, and 1% antibiotics, and was maintained at 37 ◦C in humidified air with 5% $CO_2$. Caco-2 cells were maintained at 37 ◦C in humidified air with 5% $CO_2$ in DMEM/F12 containing 10% heat-inactivated fetal bovine serum (FBS), 2 mM glutamine, and 1% antibiotics.

### Co-culture

Caco-2 cells were cultured in DMEM-F12 cell culture medium supplemented with 10% heat-inactivated FBS, 1% L-Glutamine and 1% Penicillin/Streptomycin at 37°C, 5% CO2. The U937 cells were cultured in RPMI 1640 substituted with 10% heat-inactivated FBS, 1% Penicillin/Streptomycin, 1% L-Glutamine at 37°C, 5% CO2. For co-cultures, the Caco-2 were seeded ($2.5 \times 10^5$ cells) on apical side of *trans-well inserts membrane* (0.4-μm pore-size membrane) for 9 day and allowed to form polarized cell monolayers (Yoshimoto, Okada and Hayashi, 2019). Media were changed every two days. At day 9 Caco-2 cells were treated with *C. jejuni* lysates (*C. jejuni* ATCC 33291, and *C. jejuni* 11168H CdtA mutant strains) for 24 h. At day 10 U937 cells were seeded ($10^6$) in the lower chambers (scheme of co-culture at Figure 9).

### Pre-Treatment of Cells with *C. jejuni* Lysates

U937 and Caco-2 cells were incubated for 24, 48, and 72 h with 2 mL of media enriched with *C. jejuni* lysates (1:100 and 1:50 dilution respectively) from ATCC 33291 and 11168H CdtA mutant strains previously prepared. Treated cells were analysed by means of flow cytometry and confocal

microscopy to evaluate different cellular parameters. For the negative control, cells were incubated with media only.

**Pre-Treatment of Cells with isolated EV-infected host cell**

U937 and Caco-2 cells were incubated for 24, 48, and 72 h with 1 mL of media enriched with $2x10^4$ PKH67-labeled EVs/cell isolated from medium of Caco-2 cells treated with ATCC 33291 and 11168H CdtA mutant (Gai *et al.*, 2017; Busatto *et al.*, 2020). EV treated cells were analysed by means of flow cytometry and confocal microscopy to evaluate different cellular parameters. For the negative control, cells were incubated with media only.

## Flow Cytometry (FCM) and Confocal Microscopy (CM) Staining

**Morphological Feature Evaluation**

To evaluate changes in cell morphology and size, both cytometry and confocal microscopy were used. In flow cytometry, populations that differed in size were distinguished by using their physical characteristics, forward scatter (FSC, cell size). Although a quantitative analysis was carried out by flow cytometry, a parallel microscopic evaluation of cell dimension was performed.

**Flow Cytometric Detection of Cell Death and Flow Cytometric Absolute Count**

Cell death features were evaluated using 7-amino-actino-mycin D (7AAD, Sigma-Aldrich) that is capable of binding and labelling DNA. No permeabilized cells were incubated 30 min in the dark with 1 μg/mL. Cells were washed with PBS and then analysed by flow cytometry. Absolute cell counting was performed by using Dako CytoCountTM beads (Thermo Fisher Scientific, Waltham, MA, USA). 200 μL of sample was carefully dispensed at the bottom of the tube and 50-μL beads were added. Samples were acquired by using a FACSCanto II cytometer (BD, Franklin Lakes, NJ, USA) within 60 min. Approximately 20,000 cell events were collected. Setup and calibration procedures were optimized for the absolute counting protocols (Brando *et al.*, 2000). Additionally, absolute count was performed by Omnicyt flow cytometer (Cytognos SL).

**Assessment of Lysosomal Involvement and Lysosomal exocytosis**

To label and trace lysosomes the acidotropic dye LysoTracker Deep Red (LTDR) (Thermo Fisher Scientific,Waltham, MA,USA) and the pH-sensitive dye Acridine Orange (AO; Sigma-Aldrich, St. Louis, MO,USA) 75 ng/ml for 30 min at 37 °C in 5%$CO_2$ were used. LysoTracker probes are fluorescent acidotropic probes for labelling and tracking acidic organelles in live cells: it means that the amount of fluorescence obtained from staining with LysoTracker is directly related to the volume

of lysosome-related organelles in a cell (Chazotte, 2011). Cells were cultured at 37 ◦C and resuspended in pre-warmed (37 ◦C) medium containing 100 nM of LysoTracker. After 45 min of incubation, red lysosomal fluorescence was detected by flow cytometry and confocal microscopy (Canonico *et al.*, 2016). AO is a cell-permeable fluorescent dye that, at its highest concentrations, stains the double stranded DNA red green and the cytoplasm bright green red. It can also enter acidic compartments, such as lysosomes and autolysosomes, where it becomes protonated and sequestered. In these compartments, at its lowest concentrations, in an acid environment, AO emits red fluorescence with an intensity proportional to the degree of acidity and/or to the acidic compartment volume (Canonico et al. 2018; Traganos and Darzynkiewicz 1994). Red lysosomal and green cytoplasmic fluorescence were acquired by flow cytometry using the FL3 and FL1 channels, respectively.

Cell surface CD107a (LAMP-1), which is found on lysosomes and intracellular lytic granules, was measured. LAMP-1 surface expression was used as a marker of lysosomal exocytosis (Andrews, 2017). CD107a-PeCy5 antibody (clone H4A3, BioLegend, London, UK) was added to 50 μL of cellular suspension at the concentration indicated in the manufacturer's instructions. The cells were incubated for 1 h at RT and analysed by flow cytometry.

**Determination of Mitochondria Membrane Potential (ΔΨm) and Mitochondrial Reactive Oxygen Species (ROS)**

Mitochondrial features were investigated by Tetramethylrhodamine ethyl ester perchlorate (TMRE) (Sigma-Aldrich, St. Louis, MO, USA) and MitoSOX Red (Thermo Fisher Scientific, Waltham, MA, USA).

TMRE is a ΔΨm-specific stain able to selectively enter the mitochondria depending on ΔΨm, producing red fluorescence. TMRE 40 nM was added to the samples 15 min before the acquisition time.

MitoSOX Red is a fluorigenic dye specifically targeted to mitochondria in live cells. Oxidation of this probe by superoxide that is contained in the mitochondria produces a red fluorescence. MitoSOX Red, 5 μM, was added to the samples 10 min before the time of acquisition. The samples were analysed by confocal microscopy and flow cytometry using the appropriate fluorescence channel (Canonico *et al.*, 2018, 2020).

**Autophagic-like vacuole detection**

Autophagic-like vacuoles were detected in flow cytometry by monodansylcadaverine (MDC) staining, a specific autophagolysosomes marker typically used to investigate the autophagic machinery (Vázquez and Colombo, 2009). Cells were incubated with 50μM MDC at 37°C for 15 minutes.

**Evaluation of Intracellular ROS content (mainly $H_2O_2$)**

Intracellular reactive oxygen species (ROS) content was measured with 5 μM 5-(and-6)-chloromethyl-2,7'-dichlorodihydrofluorescein diacetate acetyl ester (CM-H2DCFDA, DCFDA) (Molecular Probes, Eugene, OR) incubated for 30 min at 37°C (Eruslanov and Kusmartsev, 2010). Analyses were then performed by flow cytometry and confocal microscopy using the appropriate fluorescence channel.

**Surface expression of CD133**

Cells were trypsinized, collected, and stained with anti-CD133 PE-conjugated (clone 293C3, Miltenyi Biotec) as CSCs markers, as manufacturer's recommendation, for 20 mins at RT. Analyses were then performed by flow cytometry and confocal microscopy using the appropriate fluorescence channel.

**Cell cycle analysis**

The distribution of DNA in the cell cycle was investigated by flow cytometry. Cells were fixed by ice-cold ethanol (70%) and stored at +4°C until the analysis. For cell cycle analyses, samples were washed twice with PBS 1X and each pellet was resuspended in 440 μL of PBS 1X, to which 10 μL of 1 mg/mL PI (Sigma-Aldrich, St Louis, MO, USA) and 50 μL of 1 mg/ml RNAse (Sigma-Aldrich, St Louis, MO, USA) were added, to reach a final volume of 500 μL. The samples were well resuspended and incubated at 37°C for at least 1 h by flow cytometry.

**Intracellular Detection of Prb, NF-kB and PCNA**

Using flow cytometry, we can measure the intracellular content of these molecules with previous cellular fixation and permeabilization (FIX & PERM® cell fixation and cell permeabilization kit—Invitrogen). Cells were fixed and permeabilized, then fixed cells were stained with monoclonal anti-human antibodies anti-pRb PE-conjugated (clone G3-245) (BD) and NF-kB Alexa Fluor 488-conjugated (112A1021, Novus Biologicals) was added to samples at concentrations according to the manufacturer's instructions. Proliferating cell nuclear antigen expression was studied in cells fixed in 70% ethanol, using anti-PCNA FITC-conjugated (clone P10, Sigma-Aldrich).

**Extracellular Vesicle Detection**

In order to detect microparticles in the extracellular environment, without any preparation step of ultracentrifugation, we resuspended each sample (40 μL) in 0.22-filtered PBS 1X.

EVs from *C jejuni lysate* treated Caco-2 and co-culture medium were evaluated by means of LCD dye (BD Biosciences, USA, Custom kit. Cat. 626267), following flow cytometric protocols, both in mono culture and in co-culture condition (Brocco *et al.*, 2019; Simeone *et al.*, 2020). After an incubation of 60 min to ensure the binding of the monoclonal antibodies (anti-CD107a PerCP/Cy5.5-conjugated (clone H4A3, BioLegend, London, UK), anti-CD63 FITC-conjugated (clone TEA3/18, Immunostep) and anti-CD133 PE-conjugated (clone 293C3, Miltenyi Biotec) to the specific epitope, we proceeded with FC analyses. The flow cytometry approach consisted of acquiring samples mixed with beads of defined size (Ø 0.5 μm, 1 μm, 5.2 μm) to obtain a size calibration of small particles detected outside the scatter area of intact cells. Furthermore, it is important to specify that the FCS of the complete medium was ultracentrifuged to minimize contamination by serum microvesicles. Samples were acquired by a FACSCanto II flow cytometer and a FACSDiva™ software was used to analyse all data.

**Scanning Electron Microscopy**

Caco-2 cells from *trans-well inserts membrane* were cut from the supports and were fixed with 2.5% glutaraldehyde in 0.1 M phosphate buffer pH 7.2–7.4 for 1 h, postfixed with 1% osmium tetroxide (OsO4) in the same buffer for 2 h and, finally, dehydrated with graded ethanol (50%–100%, 5 min each). Critical point dried specimens were mounted on aluminum stubs. After 10 nm, gold sputter-coated samples were examined with a Philips scanning electron microscopy (SEM) at 20 kV (Burattini *et al.*, 2016).

**Extracellular vesicle isolation**

EV isolation was carried out following the guidelines reported in (Turchinovich, Weiz and Burwinkel, 2012). In brief, medium was first cleared by centrifugation for 15 min at 1000g to eliminate cell contamination. Supernatants were further centrifuged for 20 min at 12,000g and subsequently for 20 min at 18,000–20,000g. The resulting supernatants were filtered through a 0.22 μm filter and then EVs were pelleted by ultracentrifugation at 110,000g for 70 min. The EV pellets were washed in PBS, pelleted again and resuspended in PBS.

**Nanoparticle Tracking Analysis (NTA)**

Isolated EVs were diluted at 1:100 in PBS and stored at -20°C for further analysis. NTA measurements were performed with a NanoSight LM20 (NanoSight, U.K), equipped with a sample chamber with a 640-nm laser and a Viton fluoroelastomer O-ring. The samples were injected in the sample chamber with sterile syringes until the liquid reached the tip of the nozzle. All measurements were performed at RT.

**miRNA quantification**

The EV pellets were washed, pelleted again and resuspended in PBS for nanoparticle tracking assay before the lysis with Trizol for RNA extraction. The extraction of miRNA from the EV pellets was performed using the Total Exosome RNA & Protein Isolation Kit (Invitrogen, Milan, MI, Italy). Reverse transcription of RNA was performed using miRCURY LNA Universal RT microRNA PCR, Polyadenylation and cDNA synthesis kit II according to manufacturer's instructions (Exiqon, Milan, MI, Italy). Real-time quantitative PCR for the cDNA extracted from the EVs were performed in a StepOnePlus Real-Time PCR (Applied Biosystems, Monza, MB, Italy) using the ExiLENT SYBR® Green master mix and the miRCURY LNA miRNA PCR Assays (Exiqon, Milan, MI, Italy), specific for human miR-146a-5p and miR-16-5p (Guescini *et al.*, 2015).

**Extracellular vesicle PKH67 staining**

EVs released from Caco-2 treated by lysates were fluorescently labelled using PKH67 (Green Fluorescent Cell linker for General Cell Membrane) according to the manufacturer's instruction (Sigma-Aldrich). Briefly, PKH-67 green fluorescence was added at 2–4 μM EV suspension in diluent C and the mixture was incubated at room temperature for 5 min. Staining was stopped using 1% BSA and the EV suspension was subjected to ultracentrifugation at 100,000 g for 2 h.

**Cytometric Investigations**

Cytometric experiments were carried out with a FACSCanto II flow cytometer (BD, Franklin, Lakes, NJ, USA) equipped with an argon laser (Blue, Excitation 488 nm), a helium-neon laser (Red, Excitation 633 nm), and a solid-state diode laser (Violet, Ex 405 nm) and Omnicyt flow cytometer (Cytognos SL, Spagna). Analyses were performed with the FACSDivaTM software (BD) and the Infinicyt 2.0 software (Cytognos SL, Spagna); approximately 10,000 cell events were acquired for each sample.

**Confocal Microscopy**

Analyses Confocal microscopy analyses were applied by a Leica TCS SP5 II confocal microscope (Leica Microsystem, Germany) with 488, 543, and 633 nm illuminations and oil-immersed objectives. For confocal live imaging, cells were grown on MatTek glass bottom chambers (MatTek Corporation, Bratislava, Slovak Republic). The images were further processed and analysed in ImageJ software (NIH, Bethesda, MD, USA).

**Statistical Analyses**

Data are shown as mean (or percentage, as indicated) ± standard deviation (SD) of at least three independent experiments. Analyses of variance (ANOVA) approaches were used to compare values among more than two different experimental groups for data that met the normality assumption. One-way ANOVA or two-way ANOVA were followed by a Bonferroni post-hoc test. The means of two groups were compared by using a t test. The p values less than 0.05 were considered statistically significant. All statistical analyses were performed using GraphPad Prism 5.0 (GraphPad software, San Diego, CA, USA).

## ABBREVIATIONS

| | |
|---|---|
| *C. jejuni* | *Campylobacter jejuni* |
| CCV | Campylobacter-Containing Vacuole |
| CDT | Cytolethal distending toxin |
| CM | Confocal Microscopy |
| CSCs | Cancer Stem Cells |
| EAN | Experimental Autoimmune Neuritis |
| ER | Endoplasmic Reticulum |
| EVs | Extracellular vesicles |
| FCM | Flow Cytometry |
| GBS | Guillain Barré Syndrome |
| IECs | Intestinal Epithelial Cells |
| LPS | Lipopolysaccharide |
| LTDR | LysoTracker Deep Red |
| MFI | Mean Fluorescence Intensity |
| MVB | Multivesicular Body |
| NTA | Nanoparticle Tracking Analysis |
| OMVs | Outer Membrane Vesicles |
| PCNA | Proliferating Cell Nuclear Antigen |
| pRb | Retinoblastoma Protein |

## SUPPLEMENTARY MATERIALS

EV uptake on U937 cells was evaluated on live and fixed cells and relative data are shown in both **Figure S1A upper** and **Figure S1A below**. as shown in the graphics, the comparison of labelled EV treated samples and the untreated cells enable to set up a marker, distinguishing the EV+ population (**Figure S1A**). It must be remembered that ethanol fixation and the washing steps required by the protocol for DNA content evaluation, alter the fluorescence intensities. As expected, the level of EV uptake is sensibly lower, in the fixed U937 cells, than the level registered for live U937cells.

However, similar to what is described for CaCo-2 cells, EvM cells show an uptake lower than EvA and EvC cells and this trend is confirmed also on FRESH cells (Figure S1 A).

Changes in pRb (Figure S1 B) highlight an increase in ATCC and mutant-treated cells. Our data show an overexpression of pRb in cells after an incubation of 72 h with the EvA and EvM, compared with the EvC.

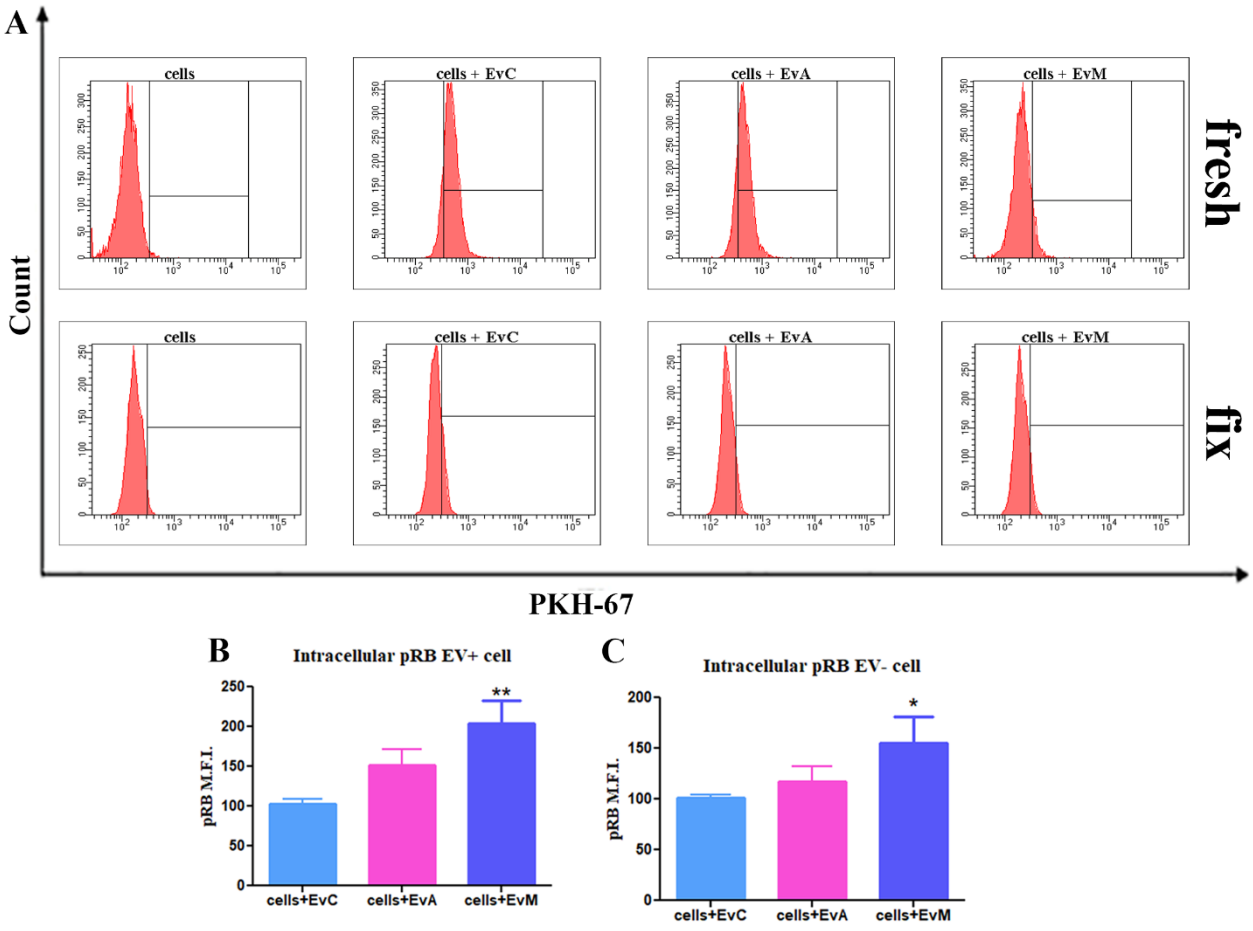


**Figure S1: (A)** Representative cytometric histograms of fresh (upper) and ethanol-fixed cells (below) for cells, cell +EvC, +EvA, +EvM. **(B)** Statistical histogram of pRB MFI on U937 cells EV+ at 72 h. Each value was expressed as a mean ± SD (Results from n ≥ 3 independent experiments). One-way ANOVA with Bonferroni's

multiple comparison test revealed * = $p < 0.05$, ** = $p < 0.01$, *** = $p < 0.001$ vs. cells+EvC and † = $p < 0.05$, †† = $p < 0.01$, ††† = $p < 0.001$ vs. cells+EvM. (**C**) Statistical histogram of pRB MFI on U937 cells EV- at 72 h. Each value was expressed as a mean ± SD (Results from $n \geq 3$ independent experiments). One-way ANOVA with Bonferroni's multiple comparison test revealed * = $p < 0.05$, ** = $p < 0.01$, *** = $p < 0.001$ vs. cells+EvC and † = $p < 0.05$, †† = $p < 0.01$, ††† = $p < 0.001$ vs. cells+EvM.

## REFERENCES


Abrami, L. *et al.* (2013) 'Hijacking Multivesicular Bodies Enables Long-Term and Exosome-Mediated Long-Distance Action of Anthrax Toxin', *Cell Reports*, 5(4), pp. 986–996. doi: 10.1016/j.celrep.2013.10.019.

Alaoui-El-Azher, M. *et al.* (2010) 'Role of the ATM-checkpoint kinase 2 pathway in CDT-mediated apoptosis of gingival epithelial cells', *PLoS ONE*, 5(7), pp. 1–10. doi: 10.1371/journal.pone.0011714.

Alvarez-Erviti, L. *et al.* (2011) 'Delivery of siRNA to the mouse brain by systemic injection of targeted exosomes', *Nature Biotechnology 2011 29:4*, 29(4), pp. 341–345. doi: 10.1038/nbt.1807.

Amon, P. *et al.* (2012) 'Analysis of Campylobacter jejuni isolates of various sources for loci associated with Guillain-Barré Syndrome.', *European journal of microbiology & immunology*, 2(1), pp. 20–3. doi: 10.1556/EuJMI.2.2012.1.4.

Amour, C. *et al.* (2016) 'Epidemiology and Impact of Campylobacter Infection in Children in 8 Low-Resource Settings: Results From the MAL-ED Study', *Clinical Infectious Diseases*, 63(9), pp. 1171–1179. doi: 10.1093/CID/CIW542.

Andrews, N. W. (2017) 'Detection of Lysosomal Exocytosis by Surface Exposure of Lamp1 Luminal Epitopes', *Methods in Molecular Biology*, 1594, pp. 205–211. doi: 10.1007/978-1-4939-6934-0_13.

Antonyak, M. A. and Cerione, R. A. (2018) 'The distinct traits of extracellular vesicles generated by transformed cells', *Small GTPases*, 9(5), pp. 427–432. doi: 10.1080/21541248.2016.1249044.

Babaei, G. *et al.* (2018) 'Application of sesquiterpene lactone: A new promising way for cancer therapy based on anticancer activity', *Biomedicine and Pharmacotherapy*, 106(February), pp. 239–246. doi: 10.1016/j.biopha.2018.06.131.

Bachran, C. *et al.* (2014) 'Cytolethal distending toxin B as a cell-killing component of tumor-targeted anthrax toxin fusion proteins', 5(1), pp. e1003–e1003. Available at: https://pubmed.ncbi.nlm.nih.gov/24434511/ (Accessed: 17 January 2022).

Bacon, D. J. *et al.* (2001) 'A phase-variable capsule is involved in virulence of Campylobacter jejuni 81-176', *Molecular microbiology*, 40(3), pp. 769–777. doi: 10.1046/J.1365-2958.2001.02431.X.

Bebelman, M. P. *et al.* (2018) 'Biogenesis and function of extracellular vesicles in cancer', *Pharmacology and Therapeutics*, 188, pp. 1–11. doi: 10.1016/j.pharmthera.2018.02.013.

Bezine, E., Vignard, J. and Mirey, G. (2014) 'The Cytolethal Distending Toxin Effects on Mammalian Cells: A DNA Damage Perspective', *Cells*, 3(2), pp. 592–615. doi: 10.3390/cells3020592.

Bhaumik, D. *et al.* (2008) 'Expression of microRNA-146 suppresses NF-κB activity with reduction of metastatic potential in breast cancer cells', *Oncogene*, 27(42), pp. 5643–5647. doi: 10.1038/onc.2008.171.

Bhaumik, D. *et al.* (2009) 'MicroRNAs miR-146a/b negatively modulate the senescence-associated inflammatory mediators IL-6 and IL-8.', *Aging*, 1(4), pp. 402–411. doi: 10.18632/aging.100042.

Bhunia, A. K. (2018) 'Campylobacter and Arcobacter', in *Foodborne Microbial Pathogens. Food Science Text Series.* Springer, New York, NY, pp. 289–299. doi: 10.1007/978-1-4939-7349-1_16.

Bisping, G. *et al.* (2001) 'Patients with inflammatory bowel disease (IBD) reveal increased induction capacity of intracellular interferon-gamma (IFN-γ) in peripheral CD8+ lymphocytes co-cultured with intestinal epithelial cells', *Clinical and Experimental Immunology*, 123(1), pp. 15–22. doi: 10.1046/j.1365-2249.2001.01443.x.

Bockman, D. E., Boydston, W. R. and Beezhold, D. H. (1983) 'The role of epithelial cells in gut-associated immune reactivity', *Annals of the New York Academy of Sciences*, 409(1), pp. 129–144. doi: 10.1111/j.1749-6632.1983.tb26864.x.

Boesze-Battaglia, K. *et al.* (2016) 'A Journey of Cytolethal Distending Toxins through Cell Membranes', *Frontiers in Cellular and Infection Microbiology*, 6, p. 81. doi: 10.3389/fcimb.2016.00081.

Boesze-Battaglia, K. *et al.* (2020) 'Internalization and Intoxication of Human Macrophages by the Active Subunit of the Aggregatibacter actinomycetemcomitans Cytolethal Distending Toxin Is Dependent Upon Cellugyrin (Synaptogyrin-2)', *Frontiers in Immunology*, 0, p. 1262. doi: 10.3389/FIMMU.2020.01262.

Brando, B. *et al.* (2000) 'Cytofluorometric methods for assessing absolute numbers of cell subsets in blood', *Cytometry*, 42(6), pp. 327–346. doi: 10.1002/1097-0320(20001215)42:6<327::AID-CYTO1000>3.0.CO;2-F.

Brocco, D. *et al.* (2019) 'Circulating Cancer Stem Cell-Derived Extracellular Vesicles as a Novel Biomarker for Clinical Outcome Evaluation', *Journal of Oncology*, 2019. doi: 10.1155/2019/5879616.

Bull, D. M. and Bookman, M. A. (1977) 'Isolation and functional characterization of human intestinal mucosal lymphoid cells', *Journal of Clinical Investigation*, 59(5), pp. 966–974. doi: 10.1172/JCI108719.

Burattini, S. *et al.* (2016) 'Melatonin action in tumor skeletal muscle cells: an ultrastructural study', *Acta histochemica*, 118(3), pp. 278–285. doi: 10.1016/J.ACTHIS.2016.02.004.

Busatto, S. *et al.* (2020) 'Brain metastases-derived extracellular vesicles induce binding and aggregation of low-density lipoprotein', *Journal of Nanobiotechnology*, 18(1), pp. 1–15. doi: 10.1186/S12951-020-00722-2/FIGURES/4.

Butkevych, E. *et al.* (2020) 'Contribution of Epithelial Apoptosis and Subepithelial Immune Responses in Campylobacter jejuni-Induced Barrier Disruption', *Frontiers in Microbiology*, 11(March), pp. 1–14. doi: 10.3389/fmicb.2020.00344.

Caggiu, E. *et al.* (2018) 'Differential expression of miRNA 155 and miRNA 146a in Parkinson's disease patients', *eNeurologicalSci*, 13, pp. 1–4. doi: 10.1016/J.ENSCI.2018.09.002.

Canonico, B. *et al.* (2014) 'Campylobacter jejuni cell lysates differently target mitochondria and lysosomes on HeLa cells', *Apoptosis*, 19(8), pp. 1225–1242. doi: 10.1007/s10495-014-1005-0.

Canonico, B. *et al.* (2016) 'Defective autophagy, mitochondrial clearance and lipophagy in niemann-pick type B lymphocytes', *PLoS ONE*. doi: 10.1371/journal.pone.0165780.

Canonico, B. *et al.* (2018) 'Monocyte response to different Campylobacter jejuni lysates involves endoplasmic reticulum stress and the lysosomal–mitochondrial axis: When cell death is better than cell survival', *Toxins*, 10(6). doi: 10.3390/toxins10060239.

Canonico, B. *et al.* (2020) 'Rapamycin re-directs lysosome network, stimulates er-remodeling, involving membrane CD317 and affecting exocytosis, in Campylobacter Jejuni-lysate-infected U937 cells', *International Journal of Molecular Sciences*, 21(6), p. 2207. doi: 10.3390/ijms21062207.

Card, T. *et al.* (2018) 'Post-infectious IBS: Defining its clinical features and prognosis using an internet-based survey', *United European Gastroenterology Journal*, 6(8), pp. 1245–1253. doi: 10.1177/2050640618779923.

Chazotte, B. (2011) 'Labeling lysosomes in live cells with LysoTracker.', *Cold Spring Harbor protocols*, 2011(2), p. pdb.prot5571. doi: 10.1101/pdb.prot5571.

Chen, C. *et al.* (2018) 'Visualization and intracellular dynamic tracking of exosomes and exosomal miRNAs using single molecule localization microscopy', *Nanoscale*, 10(11), pp. 5154–5162. doi: 10.1039/c7nr08800k.

Chen, M. L. *et al.* (2006) 'Disruption of tight junctions and induction of proinflammatory cytokine responses in colonic epithelial cells by Campylobacter jejuni', *Infection and Immunity*, 74(12), pp. 6581–6589. doi: 10.1128/IAI.00958-06.

Chen, Y. A. *et al.* (2021) 'Bacterial Genotoxin-Coated Nanoparticles for Radiotherapy Sensitization in Prostate Cancer', *Biomedicines 2021, Vol. 9, Page 151*, 9(2), p. 151. doi: 10.3390/BIOMEDICINES9020151.

Choi, K. *et al.* (2009) 'Oxidative Stress-Induced Necrotic Cell Death via Mitochondira-Dependent Burst of Reactive Oxygen Species', *Current Neurovascular Research*, 6(4), pp. 213–222. doi: 10.2174/156720209789630375.

Cohen, A. *et al.* (2018) 'Differential plasma microvesicle and brain profiles of microRNA in experimental cerebral malaria', *Malaria Journal*, 17(1). doi: 10.1186/s12936-018-2330-5.

Del Conde, I. *et al.* (2005) 'Tissue-factor-bearing microvesicles arise from lipid rafts and fuse with activated platelets to initiate coagulation', *Blood*, 106(5), pp. 1604–1611. doi: 10.1182/blood-2004-03-1095.

Cooper, J. M. *et al.* (2014) 'Systemic exosomal siRNA delivery reduced alpha-synuclein aggregates in brains of transgenic mice', *Movement Disorders*, 29(12), pp. 1476–1485. doi: 10.1002/mds.25978.

Corazza S. and Wade E.J. (2010) 'Chapter 10: Assay development Using Primary and Primary-Like Cells | Signed in', in *A Practical Guide to Assay Development and High-Throughput Screening in Drug Discovery*, pp. 169–182. Available at: https://www.scopus.com/record/display.uri?eid=2-s2.0-85028039903&origin=inward (Accessed: 5 January 2022).

Corbeil, D. *et al.* (2001) 'Prominin: a story of cholesterol, plasma membrane protrusions and human pathology', *Traffic (Copenhagen, Denmark)*, 2(2), pp. 82–91. doi: 10.1034/J.1600-0854.2001.020202.X.

Corbeil, D. *et al.* (2020) 'Uptake and Fate of Extracellular Membrane Vesicles: Nucleoplasmic Reticulum-Associated Late Endosomes as a New Gate to Intercellular Communication', *Cells*, 9(9). doi: 10.3390/cells9091931.

Cortes-Bratti, X. *et al.* (2001) 'The Haemophilus ducreyi Cytolethal Distending Toxin Induces Cell Cycle Arrest and Apoptosis via the DNA Damage Checkpoint Pathways', *Journal of Biological Chemistry*, 276(7), pp. 5296–5302. doi: 10.1074/jbc.M008527200.

Costa, D. and Iraola, G. (2019) 'Pathogenomics of emerging Campylobacter species', *Clinical Microbiology Reviews*, 32(4). doi: 10.1128/CMR.00072-18.

Cress, B. F. *et al.* (2014) 'Masquerading microbial pathogens: Capsular polysaccharides mimic host-tissue molecules', *FEMS microbiology reviews*, 38(4), p. 660. doi: 10.1111/1574-6976.12056.

Damek-Poprawa, M. *et al.* (2012) 'Localization of Aggregatibacter actinomycetemcomitans Cytolethal Distending Toxin Subunits during Intoxication of Live Cells', *Infection and Immunity*. Edited by J. B. Bliska, 80(8), pp. 2761–2770. doi: 10.1128/IAI.00385-12.

Davies, C. *et al.* (2019) 'Sodium Taurocholate Stimulates Campylobacter jejuni Outer Membrane Vesicle Production via Down-Regulation of the Maintenance of Lipid Asymmetry Pathway', *Frontiers in Cellular and Infection Microbiology*, 9(MAY), p. 177. doi: 10.3389/FCIMB.2019.00177/BIBTEX.

Dempe, J. S. *et al.* (2013) 'Metabolism and permeability of curcumin in cultured Caco-2 cells', *Molecular Nutrition and Food Research*, 57(9), pp. 1543–1549. doi: 10.1002/mnfr.201200113.

Dirienzo, J. M. (2014) 'Uptake and processing of the cytolethal distending toxin by mammalian cells', *Toxins*, 6(11), pp. 3098–3116. doi: 10.3390/toxins6113098.

Dlakic, M. (2001) 'Is CdtB a Nuclease or a Phosphatase?', *Science*, 291(5504), pp. 547a – 547. doi: 10.1126/science.291.5504.547a.

Du, H. *et al.* (2021) 'miRNA-146a-5p mitigates stress-induced premature senescence of D-galactose-induced primary thymic stromal cells', *Cytokine*, 137, p. 155314. doi: 10.1016/J.CYTO.2020.155314.

Du, T. *et al.* (2020) 'M1 Macrophage Derived Exosomes Aggravate Experimental Autoimmune Neuritis via Modulating Th1 Response', *Frontiers in Immunology*, 11, p. 1603. doi: 10.3389/fimmu.2020.01603.

Dubreuil, V. *et al.* (2007) 'Midbody and primary cilium of neural progenitors release extracellular membrane particles enriched in the stem cell marker prominin-1', *Journal of Cell Biology*, 176(4), pp. 483–495. doi: 10.1083/jcb.200608137.

Duell, B. L. *et al.* (2011) 'Epithelial cell coculture models for studying infectious diseases: Benefits and limitations', *Journal of Biomedicine and Biotechnology*, 2011. doi: 10.1155/2011/852419.

Durak-Kozica, M. *et al.* (2018) '3D visualization of extracellular vesicle uptake by endothelial cells', *Cellular and Molecular Biology Letters*, 23(1), pp. 1–9. doi: 10.1186/s11658-018-0123-z.

Eitan, E. *et al.* (2016) 'Impact of lysosome status on extracellular vesicle content and release', *Ageing Research Reviews*, 32, pp. 65–74. doi: 10.1016/j.arr.2016.05.001.

El-Aouar Filho, R. A. *et al.* (2017) 'Heterogeneous family of cyclomodulins: Smart weapons that allow bacteria to hijack the eukaryotic cell cycle and promote infections', *Frontiers in Cellular and Infection Microbiology*, 7(MAY), pp. 1–17. doi: 10.3389/fcimb.2017.00208.

Elmi, A. *et al.* (2016) 'Campylobacter jejuni outer membrane vesicle-associated proteolytic activity promotes bacterial invasion by mediating cleavage of intestinal epithelial cell E-cadherin and occludin', *Cellular Microbiology*, 18(4), pp. 561–572. doi: 10.1111/cmi.12534.

Elmi, A. *et al.* (2018) 'The bile salt sodium taurocholate induces Campylobacter jejuni outer membrane vesicle production and increases OMV-associated proteolytic activity', *Cellular Microbiology*, 20(3), pp. 1–14. doi: 10.1111/cmi.12814.

Elsharkasy, O. M. *et al.* (2020) 'Extracellular vesicles as drug delivery systems: Why and how?', *Advanced Drug Delivery Reviews*. Elsevier, pp. 332–343. doi: 10.1016/j.addr.2020.04.004.

Elsheikh, M. A. *et al.* (2018) 'Bioactive-Chylomicrons for Oral Lymphatic Targeting of Berberine Chloride: Novel Flow-Blockage Assay in Tissue-Based and Caco-2 Cell Line Models', *Pharmaceutical Research*, 35(1), pp. 1–15. doi: 10.1007/S11095-017-2307-Z/FIGURES/9.

Elwell, C. A. and Dreyfus, L. A. (2000) 'DNase I homologous residues in CdtB are critical for cytolethal distending toxin-mediated cell cycle arrest', *Molecular Microbiology*, 37(4), pp. 952–963. doi: 10.1046/j.1365-2958.2000.02070.x.

Eruslanov, E. and Kusmartsev, S. (2010) 'Identification of ROS using oxidized DCFDA and flow-cytometry', *Methods in Molecular Biology*, 594(1), pp. 57–72. doi: 10.1007/978-1-60761-411-1_4.

European Centre for Disease Prevention and Control (2019) 'Campylobacteriosis', *ECDC. Annual epidemiological report for 2017*, (April). Available at: https://www.ecdc.europa.eu/sites/default/files/documents/AER_for_2017-campylobacteriosis.pdf.

European Food Safety Authority and European Centre for Disease Prevention and Control (2019) 'The European Union One Health 2018 Zoonoses Report', *EFSA Journal*, 17(12). doi: 10.2903/j.efsa.2019.5926.

Fahrer, J. *et al.* (2014) 'Cytolethal distending toxin (CDT) is a radiomimetic agent and induces persistent levels of DNA double-strand breaks in human fibroblasts', *DNA Repair*, 18(1), pp. 31–43. doi: 10.1016/j.dnarep.2014.03.002.

Faïs, T. *et al.* (2016) 'Impact of CDT toxin on human diseases', *Toxins*, 8(7), pp. 18–20. doi: 10.3390/toxins8070220.

Fedele, A. O. *et al.* (2018) 'Lysosomal N-acetyltransferase interacts with ALIX and is detected in extracellular vesicles', *Biochimica et Biophysica Acta (BBA) - Molecular Cell Research*, 1865(10), pp. 1451–1464. doi: 10.1016/J.BBAMCR.2018.07.001.

Ferrandina, G. *et al.* (2009) 'Targeting CD133 antigen in cancer', *Expert Opinion on Therapeutic Targets*, 13(7), pp. 823–837. doi: 10.1517/14728220903005616.

Ferrero, R. L. and Lee, A. (1988) 'Motility of Campylobacter jejuni in a viscous environment: comparison with conventional rod-shaped bacteria.', *Journal of general microbiology*, 134(1), pp. 53–59. doi: 10.1099/00221287-134-1-53/CITE/REFWORKS.

Fleming, A. *et al.* (2014) 'The carrying pigeons of the cell: Exosomes and their role in infectious diseases caused by human pathogens', *Pathogens and Disease*, 71(2), pp. 109–120. doi: 10.1111/2049-632X.12135.

Friedman, C. R. *et al.* (2004) 'Risk Factors for Sporadic *Campylobacter* Infection in the United States: A Case-Control Study in FoodNet Sites', *Clinical Infectious Diseases*, 38(s3), pp. S285–S296. doi: 10.1086/381598.

Frisan, T. (2016) 'Bacterial genotoxins: The long journey to the nucleus of mammalian cells', *Biochimica et Biophysica Acta - Biomembranes*, 1858(3), pp. 567–575. doi: 10.1016/j.bbamem.2015.08.016.

Gai, C. *et al.* (2017) 'Protective Role of Stem Cell Derived Extracellular Vesicles in an In Vitro Model of Hyperglycemia-Induced Endothelial Injury Characterization of urinary Extracellular Vesicles in Transplanted Patients View project Protective Role of Stem Cell Derived Extracellular Vesicles in an In Vitro Model of Hyperglycemia-Induced Endothelial Injury', *Article in Journal of Cell Science & Therapy*. doi: 10.4172/2157-7013.1000264.

Galluzzi, L. *et al.* (2017) 'Molecular definitions of autophagy and related processes', *The EMBO Journal*, 36(13), pp. 1811–1836. doi: 10.15252/embj.201796697.

Gantier, M. P. *et al.* (2010) 'Genetic modulation of TLR8 response following bacterial phagocytosis', *Human Mutation*, 31(9), pp. 1069–1079. doi: 10.1002/humu.21321.

Ge, Z., Schauer, D. B. and Fox, J. G. (2008) 'In vivo virulence properties of bacterial cytolethal-distending toxin', *Cellular Microbiology*, 10(8), pp. 1599–1607. doi: 10.1111/j.1462-5822.2008.01173.x.

Gillespie, I. A. *et al.* (2002) 'A case-case comparison of Campylobacter coli and Campylobacter jejuni infection: A tool for generating hypotheses', *Emerging Infectious Diseases*, 8(9), pp. 937–942. doi: 10.3201/eid0809.010817.

Gisina, A. M. *et al.* (2019) 'Proliferative Activity of Colorectal Cancer Cells with Different Levels of CD133 Expression', *Bulletin of Experimental Biology and Medicine*, 167(4), pp. 541–545. doi: 10.1007/s10517-019-04569-y.

González, M. F. *et al.* (2021) 'Helicobacter pylori outer membrane vesicles and extracellular vesicles from helicobacter pylori-infected cells in gastric disease development', *International Journal of Molecular Sciences*, 22(9), p. 4823. doi: 10.3390/ijms22094823.

Groschwitz, K. R. and Hogan, S. P. (2009) 'Intestinal barrier function: molecular regulation and disease pathogenesis', *The Journal of allergy and clinical immunology*, 124(1), pp. 3–20. doi: 10.1016/J.JACI.2009.05.038.

Guerra, L. *et al.* (2011) 'The biology of the cytolethal distending toxins', *Toxins*, 3(3), pp. 172–190. doi: 10.3390/toxins3030172.

Guescini, M. *et al.* (2015) 'Muscle Releases Alpha-Sarcoglycan Positive Extracellular Vesicles Carrying miRNAs in the Bloodstream', *PLOS ONE*. Edited by F. Martelli, 10(5), p. e0125094. Available at: https://journals.plos.org/plosone/article?id=10.1371/journal.pone.0125094 (Accessed: 27 August 2020).

Hameed, A. *et al.* (2020) 'An Updated Classification System and Review of the Lipooligosaccharide Biosynthesis Gene Locus in Campylobacter jejuni', *Frontiers in Microbiology*, 11, p. 677. doi: 10.3389/FMICB.2020.00677/BIBTEX.

Han, L., Lam, E. W. F. and Sun, Y. (2019) 'Extracellular vesicles in the tumor microenvironment: Old stories, but new tales', *Molecular Cancer*, 18(1). doi: 10.1186/s12943-019-0980-8.

Hansen, M. S. *et al.* (2020) 'Specific and non-invasive fluorescent labelling of extracellular vesicles for evaluation of intracellular processing by intestinal epithelial cells', *Biomedicines*, 8(7). doi: 10.3390/BIOMEDICINES8070211.

Harrer, A. *et al.* (2019) 'Campylobacter jejuni enters gut epithelial cells and impairs intestinal barrier function through cleavage of occludin by serine protease HtrA', *Gut Pathogens*, 11(1), p. 4. doi: 10.1186/s13099-019-0283-z.

Harting, M. T. *et al.* (2018) 'Inflammation-Stimulated Mesenchymal Stromal Cell-Derived Extracellular Vesicles Attenuate Inflammation', *Stem Cells*, 36(1), pp. 79–90. doi: 10.1002/stem.2730.

Hassane, D. C., Lee, R. B. and Pickett, C. L. (2003) 'Campylobacter jejuni Cytolethal Distending Toxin Promotes DNA Repair Responses in Normal Human Cells', *Society*, 71(1), pp. 541–545. doi: 10.1128/IAI.71.1.541.

Hassanpour, M. *et al.* (2020) *The role of extracellular vesicles in COVID-19 virus infection*, *Infection, Genetics and Evolution*.

He, Z. *et al.* (2019) 'Campylobacter jejuni promotes colorectal tumorigenesis through the action of cytolethal distending toxin', *Gut*, 68(2), pp. 289–300. doi: 10.1136/gutjnl-2018-317200.

Herrmann, I. K., Wood, M. J. A. and Fuhrmann, G. (2021) 'Extracellular vesicles as a next-generation drug delivery platform', *Nature Nanotechnology*, 16(7), pp. 748–759. doi: 10.1038/s41565-021-00931-2.

Hessvik, N. P. and Llorente, A. (2018) 'Current knowledge on exosome biogenesis and release', *Cellular and Molecular Life Sciences*, 75(2), pp. 193–208. doi: 10.1007/s00018-017-2595-9.

Heusermann, W. *et al.* (2016) 'Exosomes surf on filopodia to enter cells at endocytic hot spots, traffic within endosomes, and are targeted to the ER', *Journal of Cell Biology*, 213(2), pp. 173–184. doi: 10.1083/jcb.201506084.

Hickey, T. E. *et al.* (2000) 'Campylobacter jejuni Cytolethal Distending Toxin Mediates Release of Interleukin-8 from Intestinal Epithelial Cells Campylobacter jejuni Cytolethal Distending Toxin Mediates Release of Interleukin-8 from Intestinal Epithelial Cells', 68(12), pp. 6535–6541. doi: 10.1128/IAI.68.12.6535-6541.2000.Updated.

Hofmann, K. *et al.* (2000) 'Cloning and characterization of the mammalian brain-specific, Mg2+-dependent neutral sphingomyelinase.', *Proceedings of the National Academy of Sciences of the United States of America*, 97(11), pp. 5895–900. doi: 10.1073/pnas.97.11.5895.

Huizinga, R. *et al.* (2015) 'Innate Immunity to Campylobacter jejuni in Guillain-Barré Syndrome', *Annals of neurology*, 78(3), pp. 343–354. doi: 10.1002/ANA.24442.

Hüser, J., Rechenmacher, C. E. and Blatter, L. A. (1998) 'Imaging the permeability pore transition in single mitochondria', *Biophysical Journal*, 74(4), pp. 2129–2137. doi: 10.1016/S0006-3495(98)77920-2.

Ijaz, U. Z. *et al.* (2018) 'Comprehensive longitudinal microbiome analysis of the chicken cecum reveals a shift from competitive to environmental drivers and a window of opportunity for Campylobacter', *Frontiers in Microbiology*, 9(OCT), p. 2452. doi: 10.3389/FMICB.2018.02452/BIBTEX.

Islam, Z. *et al.* (2012) 'Guillain-Barré Syndrome-Related Campylobacter jejuni in Bangladesh: Ganglioside Mimicry and Cross-Reactive Antibodies', *PLOS ONE*, 7(8), p. e43976. doi: 10.1371/JOURNAL.PONE.0043976.

Jeon, B., Itoh, K. and Ryu, S. (2005) 'Promoter Analysis of Cytolethal Distending Toxin Genes ( *cdtA, B* , and *C* ) and Effect of a *luxS* Mutation on CDT Production in *Campylobacter jejuni*', *Microbiology and Immunology*, 49(7), pp. 599–603. doi: 10.1111/j.1348-0421.2005.tb03651.x.

Jinadasa, R. N. *et al.* (2011) 'Cytolethal distending toxin: A conserved bacterial genotoxin that blocks cell cycle progression, leading to apoptosis of a broad range of mammalian cell lineages', *Microbiology*, 157(7), pp. 1521–1875. doi: 10.1099/mic.0.049536-0.

Johmura, Y. and Nakanishi, M. (2016) 'Multiple facets of p53 in senescence induction and maintenance', *Cancer Science*, 107(11), pp. 1550–1555. doi: 10.1111/cas.13060.

Joshi, B. S. *et al.* (2020) 'Endocytosis of Extracellular Vesicles and Release of Their Cargo from Endosomes', *ACS nano*, 14(4), pp. 4444–4455. doi: 10.1021/acsnano.9b10033.

Jutley, J. K. *et al.* (1987) 'Cytosolic retinoic acid-binding protein in human prostatic dysplasia and neoplasia', *The Prostate*, 11(2), pp. 127–132. doi: 10.1002/pros.2990110204.

Kailoo, S., Shreya and Kumar, Y. (2021) 'Cytolethal distending toxin: from genotoxin to a potential biomarker and anti-tumor target', *World Journal of Microbiology and Biotechnology*, 37(9), pp. 1–18. doi: 10.1007/s11274-021-03117-z.

Kalluri, R. and LeBleu, V. S. (2020) 'The biology, function, and biomedical applications of exosomes', *Science*, 367(6478). doi: 10.1126/science.aau6977.

Kämpfer, A. A. M. *et al.* (2017) 'Development of an in vitro co-culture model to mimic the human intestine in healthy and diseased state', *Toxicology in Vitro*, 45(May), pp. 31–43. doi: 10.1016/j.tiv.2017.08.011.

Kanada, M. *et al.* (2015) 'Differential fates of biomolecules delivered to target cells via extracellular vesicles', *Proceedings of the National Academy of Sciences of the United States of America*, 112(12), pp. E1433–E1442. doi: 10.1073/PNAS.1418401112.

Kang, M., Kim, S. and Ko, J. (2019) 'Roles of CD133 in microvesicle formation and oncoprotein trafficking in colon cancer', *The FASEB Journal*, 33(3), pp. 4248–4260. doi: 10.1096/FJ.201802018R.

Kang, S. W., Lee, S. and Lee, J. H. S. (2018) 'Cancer-Associated Function of 2-Cys Peroxiredoxin Subtypes as a Survival Gatekeeper', *Antioxidants 2018, Vol. 7, Page 161*, 7(11), p. 161. doi: 10.3390/ANTIOX7110161.

Kapperud, G. *et al.* (1992) 'Risk factors for sporadic Campylobacter infections: results of a case-control study in southeastern Norway.', *Journal of clinical microbiology*, 30(12), pp. 3117–21. Available at: http://www.ncbi.nlm.nih.gov/pubmed/1452694 (Accessed: 23 August 2018).

Keshtvarz, M. *et al.* (2021) 'Engineering of cytolethal distending toxin b by its reducing immunogenicity and maintaining stability as a new drug candidate for tumor therapy; an in silico study', *Toxins*, 13(11). doi: 10.3390/toxins13110785.

Ketley, J. M. (1997) 'Pathogenesis of enteric infection by', *Microbiology*, 143(1 997), pp. 5–21. doi: 10.1099/00221287-143-1-5.

Khalife, J. *et al.* (2019) 'MiR-16 regulates crosstalk in NF-B tolerogenic inflammatory signaling between myeloma cells and bone marrow macrophages', *JCI Insight*, 4(21). doi: 10.1172/jci.insight.129348.

Kowal, J., Tkach, M. and Théry, C. (2014) 'Biogenesis and secretion of exosomes', *Current Opinion in Cell Biology*, 29(1), pp. 116–125. doi: 10.1016/j.ceb.2014.05.004.

Krippeit-Drews, P., Düfer, M. and Drews, G. (2000) 'Parallel oscillations of intracellular calcium activity and mitochondrial membrane potential in mouse pancreatic B-cells', *Biochemical and Biophysical Research Communications*, 267(1), pp. 179–183. doi: 10.1006/bbrc.1999.1921.

Kuipers, M. E. *et al.* (2018) 'Pathogen-derived extracellular vesicle-associated molecules that affect the host immune system: An overview', *Frontiers in Microbiology*, 9(SEP), p. 2182. doi: 10.3389/FMICB.2018.02182/BIBTEX.

Kvietys, P. R. and Granger, D. N. (2010) 'Role of intestinal lymphatics in interstitial volume regulation and transmucosal water transport', *Annals of the New York Academy of Sciences*, 1207(SUPPL.1), pp. E29–E43. doi: 10.1111/J.1749-6632.2010.05709.X.

Lara-Tejero, M. and Galán, J. E. (2000) 'A bacterial toxin that controls cell cycle progression as a deoxyribonuclease I-like protein.', *Science (New York, N.Y.)*, 290(5490), pp. 354–7. Available at: http://www.ncbi.nlm.nih.gov/pubmed/11030657 (Accessed: 4 August 2018).

Lara-Tejero, M. and Galán, J. E. (2001) 'CdtA , CdtB , and CdtC Form a Tripartite Complex That Is Required for Cytolethal Distending Toxin Activity CdtA , CdtB , and CdtC Form a Tripartite Complex That Is Required for Cytolethal Distending Toxin Activity', *Infection and Immunity*, 69(7), pp. 4358–4365. doi: 10.1128/IAI.69.7.4358.

Lea, T. (2015) 'Caco-2 Cell Line', *The Impact of Food Bioactives on Health: In Vitro and Ex Vivo Models*, pp. 103–111. doi: 10.1007/978-3-319-16104-4_10.

Leonard, F., Collnot, E. M. and Lehr, C. M. (2010) 'A three-dimensional coculture of enterocytes, monocytes and dendritic cells to model inflamed intestinal mucosa in vitro', *Molecular Pharmaceutics*, 7(6), pp. 2103–2119. doi: 10.1021/mp1000795.

Liang, X. *et al.* (2016) 'MicroRNA-16 suppresses the activation of inflammatory macrophages in atherosclerosis by targeting PDCD4', *International Journal of Molecular Medicine*, 37(4), pp. 967–975. doi: 10.3892/ijmm.2016.2497.

Liaw, J. *et al.* (2019) 'The Campylobacter jejuni Type VI Secretion System Enhances the Oxidative Stress Response and Host Colonization', *Frontiers in Microbiology*, 10, p. 2864. doi: 10.3389/FMICB.2019.02864/BIBTEX.

Lilienblum, W. *et al.* (2008) 'Alternative methods to safety studies in experimental animals: Role in the risk assessment of chemicals under the new European Chemicals Legislation (REACH)', *Archives of Toxicology*, 82(4), pp. 211–236. doi: 10.1007/S00204-008-0279-9/TABLES/5.

Lin, H.-J. *et al.* (2017) 'Cytolethal Distending Toxin Enhances Radiosensitivity in Prostate Cancer Cells by Regulating Autophagy', *Frontiers in Cellular and Infection Microbiology*, 7(June), pp. 1–8. doi: 10.3389/fcimb.2017.00223.

Lindmark, B. *et al.* (2009) 'Outer membrane vesicle-mediated release of cytolethal distending toxin (CDT) from Campylobacter jejuni', *BMC Microbiology*, 9(1), p. 220. doi: 10.1186/1471-2180-9-220.

Liu, Y. *et al.* (2015) 'Targeted exosome-mediated delivery of opioid receptor Mu siRNA for the treatment of morphine relapse', *Scientific Reports*, 5(1), pp. 1–10. doi: 10.1038/srep17543.

Lombardo, G. *et al.* (2016) 'Activated Stat5 trafficking Via Endothelial Cell-derived Extracellular Vesicles Controls IL-3 Pro-angiogenic Paracrine Action', *Scientific Reports*, 6, pp. 1–14. doi: 10.1038/srep25689.

Lopes, G. V. *et al.* (2021) 'Virulence factors of foodborne pathogen Campylobacter jejuni', *Microbial Pathogenesis*, 161(October 2020), p. 105265. doi: 10.1016/j.micpath.2021.105265.

Maimaitiyiming, Y. *et al.* (2019) 'Selection and characterization of novel DNA aptamer against colorectal carcinoma Caco-2 cells', *Biotechnology and Applied Biochemistry*, 66(3), pp. 412–418. doi: 10.1002/BAB.1737.

Malumbres, M. and Barbacid, M. (2001) 'To cycle or not to cycle: A critical decision in cancer', *Nature Reviews Cancer*, 1(3), pp. 222–231. doi: 10.1038/35106065.

Mantel, P. Y. *et al.* (2016) 'Infected erythrocyte-derived extracellular vesicles alter vascular function via regulatory Ago2-miRNA complexes in malaria', *Nature Communications*, 7. doi: 10.1038/ncomms12727.

Margolis, L. and Sadovsky, Y. (2019) 'The biology of extracellular vesicles: The known unknowns', *PLoS biology*, 17(7). doi: 10.1371/JOURNAL.PBIO.3000363.

Marzesco, A. M. *et al.* (2009) 'Release of extracellular membrane vesicles from microvilli of epithelial cells is enhanced by depleting membrane cholesterol', *FEBS letters*, 583(5), pp. 897–902. doi: 10.1016/J.FEBSLET.2009.01.048.

Mashburn-Warren, L., McLean, R. J. C. and Whiteley, M. (2008) 'Gram-negative outer membrane vesicles: beyond the cell surface.', *Geobiology*, 6(3), pp. 214–9. doi: 10.1111/j.1472-4669.2008.00157.x.

Mathieu, M. *et al.* (2019) 'Specificities of secretion and uptake of exosomes and other extracellular vesicles for cell-to-cell communication', *Nature Cell Biology*, 21(1), pp. 9–17. doi: 10.1038/s41556-018-0250-9.

Maue, A. C. *et al.* (2013) 'The polysaccharide capsule of Campylobacter jejuni modulates the host immune response', *Infection and Immunity*, 81(3), pp. 665–672. doi: 10.1128/IAI.01008-12/ASSET/726DF6C6-F6B5-4EB2-B6ED-E8F10FBAAF71/ASSETS/GRAPHIC/ZII9990900080006.JPEG.

McSweeney, L. A. and Dreyfus, L. A. (2005) 'Carbohydrate-binding specificity of the Escherichia coli cytolethal distending toxin CdtA-II and CdtC-II subunits', *Infection and Immunity*, 73(4), pp. 2051–2060. doi: 10.1128/IAI.73.4.2051-2060.2005.

Mertins, S. *et al.* (2013) 'Role of motAB in adherence and internalization in polarized Caco-2 cells and in cecal colonization of Campylobacter jejuni', *Avian diseases*, 57(1), pp. 116–122. doi: 10.1637/10235-050412-RESNOTE.1.

Møller Nielsen, E., Engberg, J. and Madsen, M. (1997) 'Distribution of serotypes of Campylobacter jejuni and C. coli from Danish patients, poultry, cattle and swine', *FEMS Immunology & Medical Microbiology*, 19(1), pp. 47–56. doi: 10.1111/j.1574-695x.1997.tb01071.x.

Monteville, M. R., Yoon, J. E. and Konkel, M. E. (2003) 'Maximal adherence and invasion of INT 407 cells by Campylobacter jejuni requires the CadF outer-membrane protein and microfilament reorganization', *Microbiology (Reading, England)*, 149(Pt 1), pp. 153–165. doi: 10.1099/MIC.0.25820-0.

Moyes, S. M., Morris, J. F. and Carr, K. E. (2010) 'Macrophages increase microparticle uptake by enterocyte-like Caco-2 cell monolayers', *Journal of Anatomy*, 217(6), pp. 740–754. doi: 10.1111/j.1469-7580.2010.01304.x.

Müller, A. *et al.* (2014) 'Ultrastructure and complex polar architecture of the human pathogen Campylobacter jejuni', *MicrobiologyOpen*, 3(5), pp. 702–710. doi: 10.1002/mbo3.200.

Murphy, D. E. *et al.* (2019) 'Extracellular vesicle-based therapeutics: natural versus engineered targeting and trafficking', *Experimental and Molecular Medicine*, 51(3), pp. 1–12. doi: 10.1038/s12276-019-0223-5.

Nathens, A. B. *et al.* (1995) 'Intestinal epithelial cells down-regulate macrophage tumor necrosis factor-alpha secretion: A mechanism for immune homeostasis in the gut-associated lymphoid tissue', *Surgery*, 118(2), pp. 343–351. doi: 10.1016/S0039-6060(05)80343-5.

NEIMANN, J. *et al.* (2003) 'A case–control study of risk factors for sporadic campylobacter infections in Denmark', *Epidemiology and Infection*, 130(03), pp. 353–366. doi: 10.1017/S0950268803008355.

Nesić, D., Hsu, Y. and Stebbins, C. E. (2004) 'Assembly and function of a bacterial genotoxin.', *Nature*, 429(6990), pp. 429–33. doi: 10.1038/nature02532.

van Niel, G., D'Angelo, G. and Raposo, G. (2018) 'Shedding light on the cell biology of extracellular vesicles', *Nature reviews. Molecular cell biology*, 19(4), pp. 213–228. doi: 10.1038/NRM.2017.125.

Nyati, K. K. *et al.* (2013) 'Role of Campylobacter jejuni infection in the pathogenesis of Guillain-Barré syndrome: an update.', *BioMed research international*, 2013, p. 852195. doi: 10.1155/2013/852195.

Ofir-Birin, Y. *et al.* (2018) 'Monitoring extracellular vesicle cargo active uptake by imaging flow cytometry', *Frontiers in Immunology*, 9(MAY), p. 1011. doi: 10.3389/fimmu.2018.01011.

Ohara, M., Oswald, E. and Sugai, M. (2004) 'Cytolethal Distending Toxin: A Bacterial Bullet Targeted to Nucleus', *Journal of Biochemistry*, 136(4), pp. 409–413. doi: 10.1093/jb/mvh154.

Olson, C. K. *et al.* (2014) 'Epidemiology of Campylobacter jejuni Infections in Industrialized Nations', *Campylobacter*, pp. 163–189. doi: 10.1128/9781555815554.CH9.

Pan, B. T. *et al.* (1985) 'Electron microscopic evidence for externalization of the transferrin receptor in vesicular form in sheep reticulocytes', *Journal of Cell Biology*, 101(3), pp. 942–948. doi: 10.1083/jcb.101.3.942.

Pant, S., Hilton, H. and Burczynski, M. E. (2012) 'The multifaceted exosome: Biogenesis, role in normal and aberrant cellular function, and frontiers for pharmacological and biomarker opportunities', *Biochemical Pharmacology*, 83(11), pp. 1484–1494. doi: 10.1016/j.bcp.2011.12.037.

Parlesak, A. *et al.* (2004) 'Modulation of cytokine release by differentiated CACO-2 cells in a compartmentalized coculture model with mononuclear leucocytes and nonpathogenic bacteria', *Scandinavian Journal of Immunology*, 60(5), pp. 477–485. doi: 10.1111/j.0300-9475.2004.01495.x.

Parolini, I. *et al.* (2009) 'Microenvironmental pH is a key factor for exosome traffic in tumor cells', *Journal of Biological Chemistry*, 284(49), pp. 34211–34222. doi: 10.1074/jbc.M109.041152.

Patel, V. A. *et al.* (2009) 'Apoptotic and necrotic cells as sentinels of local tissue stress and inflammation: Response pathways initiated in nearby viable cells Review', *Autoimmunity*. Taylor & Francis, pp. 317–321. doi: 10.1080/08916930902832124.

Pickett, C. L. and Whitehouse, C. A. (1999) 'The cytolethal distending toxin family', *Trends in Microbiology*, 7(7), pp. 292–297. doi: 10.1016/S0966-842X(99)01537-1.

Pons, B. J. *et al.* (2020) 'Functional Study of Haemophilus ducreyi Cytolethal Distending Toxin Subunit B', *Toxins*, 12(9). doi: 10.3390/TOXINS12090530.

Quereda, V. *et al.* (2016) 'An essential role for Ink4 and Cip/Kip cell-cycle inhibitors in preventing replicative stress', *Cell Death and Differentiation*, 23(3), pp. 430–441. doi: 10.1038/cdd.2015.112.

Ren, F., Sheng, W. Q. and Du, X. (2013) 'CD133: a cancer stem cells marker, is used in colorectal cancers', *World journal of gastroenterology*, 19(17), pp. 2603–2611. doi: 10.3748/WJG.V19.I17.2603.

Robinson, L. *et al.* (2021) 'Bioinformatic Analysis of the Campylobacter jejuni Type VI Secretion System and Effector Prediction', *Frontiers in Microbiology*, 12, p. 1751. doi: 10.3389/FMICB.2021.694824/BIBTEX.

Röper, K., Corbeil, D. and Huttner, W. B. (2000) 'Retention of prominin in microvilli reveals distinct cholesterol-based lipid microdomains in the apical plasma membrane', *Nature Cell Biology*, 2(9), pp. 582–592. doi: 10.1038/35023524.

Sansonetti, P. (2001) 'Phagocytosis of bacterial pathogens: Implications in the host response', *Seminars in Immunology*, 13(6), pp. 381–390. doi: 10.1006/smim.2001.0335.

Santos, M. F. *et al.* (2018) 'VAMP-associated protein-A and oxysterol-binding protein–related protein 3 promote the entry of late endosomes into the nucleoplasmic reticulum', *Journal of Biological Chemistry*, pp. 13834–13848. doi: 10.1074/jbc.RA118.003725.

Sari Kovats, R. *et al.* (2005) 'Climate variability and campylobacter infection: An international study', *International Journal of Biometeorology*, 49(4), pp. 207–214. doi: 10.1007/s00484-004-0241-3.

Schnee, A. E. and Petri, W. A. (2017) 'Campylobacter jejuni and associated immune mechanisms: Short-term effects and long-term implications for infants in low-income countries', *Current Opinion in Infectious Diseases*, 30(3), pp. 322–328. doi: 10.1097/QCO.0000000000000364.

Shenker, B. J. *et al.* (1999) 'Induction of apoptosis in human T-cells by methyl mercury: Temporal relationship between mitochondrial dysfunction and loss of reductive reserve', *Toxicology and Applied Pharmacology*, 157(1), pp. 23–35. doi: 10.1006/taap.1999.8652.

Shenker, B. J. *et al.* (2007) 'A Novel Mode of Action for a Microbial-Derived Immunotoxin: The Cytolethal Distending Toxin Subunit B Exhibits Phosphatidylinositol 3,4,5-Triphosphate Phosphatase Activity', *Journal of immunology (Baltimore, Md. : 1950)*, 178(8), p. 5099. doi: 10.4049/JIMMUNOL.178.8.5099.

Shigematsu, M. *et al.* (1998) 'Spirochaete-like swimming mode of Campylobacter jejuni in a viscous environment', *Journal of Medical Microbiology*, 47(6), pp. 521–526. doi: 10.1099/00222615-47-6-521/CITE/REFWORKS.

Simeone, P. *et al.* (2020) 'Diameters and Fluorescence Calibration for Extracellular Vesicle Analyses by Flow Cytometry', *International Journal of Molecular Sciences*, 21(21), pp. 1–15. doi: 10.3390/IJMS21217885.

Sirirak, T. *et al.* (2019) 'Eleutherine americana extract inhibits adherence to and invasion of Caco-2 cells by commonly contaminated Campylobacter spp. in food', *Journal of Food Processing and Preservation*, 43(8), pp. 1–9. doi: 10.1111/jfpp.14007.

Skirrow, M. B. (1987) 'A demographic survey of campylobacter, salmonella and shigella infections in England. A Public Health Laboratory Service Survey', *Epidemiology and infection*, 99(3), pp. 647–657. doi: 10.1017/S0950268800066504.

Slodzinski, M. K., Aon, M. A. and O'Rourke, B. (2008) 'Glutathione oxidation as a trigger of mitochondrial depolarization and oscillation in intact hearts', *Journal of Molecular and Cellular Cardiology*, 45(5), pp. 650–660. doi: 10.1016/j.yjmcc.2008.07.017.

Smith, J. L. and Bayles, D. O. (2006) 'The Contribution of Cytolethal Distending Toxin to Bacterial Pathogenesis', *Critical Reviews in Microbiology*, 32(4), pp. 227–248. doi: 10.1080/10408410601023557.

Song, I. S. *et al.* (2021) 'The sulfiredoxin-peroxiredoxin redox system regulates the stemness and survival of colon cancer stem cells', *Redox Biology*, 48, p. 102190. doi: 10.1016/J.REDOX.2021.102190.

Statello, L. *et al.* (2018) 'Identification of RNA-binding proteins in exosomes capable of interacting with different types of RNA: RBP-facilitated transport of RNAs into exosomes', *PLoS ONE*, 13(4). doi: 10.1371/journal.pone.0195969.

Susewind, J. *et al.* (2016) 'A 3D co-culture of three human cell lines to model the inflamed intestinal mucosa for safety testing of nanomaterials', *Nanotoxicology*, 10(1), pp. 53–62. doi: 10.3109/17435390.2015.1008065.

Szymanski, C. M. *et al.* (1995) 'Campylobacter jejuni motility and invasion of Caco-2 cells', *Infection and Immunity*, 63(11), pp. 4295–4300. doi: 10.1128/IAI.63.11.4295-4300.1995.

Taganov, K. D. *et al.* (2006) 'NF-κB-dependent induction of microRNA miR-146, an inhibitor targeted to signaling proteins of innate immune responses', *Proceedings of the National Academy of Sciences of the United States of America*, 103(33), pp. 12481–12486. doi: 10.1073/pnas.0605298103.

Taieb, F. *et al.* (2016) 'The Enterobacterial Genotoxins: Cytolethal Distending Toxin and Colibactin', *EcoSal Plus*, 7(1). doi: 10.1128/ecosalplus.esp-0008-2016.

Taïeb, N. *et al.* (2009) 'The first extracellular domain of the tumour stem cell marker CD133 contains an antigenic ganglioside-binding motif', *Cancer letters*, 278(2), pp. 164–173. doi: 10.1016/J.CANLET.2009.01.013.

Tanoue, T. *et al.* (2008) 'In vitro model to estimate gut inflammation using co-cultured Caco-2 and RAW264.7 cells', *Biochemical and Biophysical Research Communications*, 374(3), pp. 565–569. doi: 10.1016/j.bbrc.2008.07.063.

Thelestam, M. and Frisan, T. (2004) 'A. actinomycetemcomitans Cytolethal Distending Toxin', *The Journal of Immunology*, 172(10), pp. 5813–5813. doi: 10.4049/JIMMUNOL.172.10.5813.

Tremblay, W. *et al.* (2021) 'Cytolethal Distending Toxin Promotes Replicative Stress Leading to Genetic Instability Transmitted to Daughter Cells', *Frontiers in Cell and Developmental Biology*, 9. doi: 10.3389/fcell.2021.656795.

Turchinovich, A., Weiz, L. and Burwinkel, B. (2012) 'Extracellular miRNAs: the mystery of their origin and function', *Trends in biochemical sciences*, 37(11), pp. 460–465. doi: 10.1016/J.TIBS.2012.08.003.

Turturici, G. *et al.* (2014) 'Extracellular membrane vesicles as a mechanism of cell-to-cell communication: Advantages and disadvantages', *American Journal of Physiology - Cell Physiology*, 306(7). doi: 10.1152/ajpcell.00228.2013.

Ugarte-Ruiz, M. *et al.* (2015) 'Prevalence of Type VI Secretion System in Spanish Campylobacter jejuni Isolates', *Zoonoses and public health*, 62(7), pp. 497–500. doi: 10.1111/ZPH.12176.

Vafadar, A. *et al.* (2020) 'In Silico Design and Evaluation of scFv-CdtB as a Novel Immunotoxin for Breast Cancer Treatment', *International Journal of Cancer Management 2020 13:1*, 13(1). doi: 10.5812/IJCM.96094.

Vázquez, C. L. and Colombo, M. I. (2009) 'Assays to Assess Autophagy Induction and Fusion of Autophagic Vacuoles with a Degradative Compartment, Using Monodansylcadaverine (MDC) and DQ-BSA', *Methods in Enzymology*. doi: 10.1016/S0076-6879(08)03606-9.

Vojdani, A. and Vojdani, E. (2019) 'Reaction of antibodies to *Campylobacter jejuni* and cytolethal distending toxin B with tissues and food antigens', *World Journal of Gastroenterology*, 25(9), pp. 1050–1066. doi: 10.3748/wjg.v25.i9.1050.

Vu, L. T. *et al.* (2020) 'microRNA exchange via extracellular vesicles in cancer', *Cell Proliferation*, 53(11), p. e12877. doi: 10.1111/CPR.12877.

Wachira, V. K., Peixoto, H. M. and de Oliveira, M. R. F. (2019) 'Systematic review of factors associated with the development of Guillain–Barré syndrome 2007–2017: what has changed?', *Tropical Medicine and International Health*, 24(2), pp. 132–142. doi: 10.1111/TMI.13181.

Wassenaar, T. M., Bleumink-Pluym, N. M. C. and Van Der Zeijst, B. A. M. (1991) 'Inactivation of Campylobacter jejuni flagellin genes by homologous recombination demonstrates that flaA but not flaB is required for invasion.', *The EMBO Journal*, 10(8), pp. 2055–2061. doi: 10.1002/J.1460-2075.1991.TB07736.X.

Wäster, P. *et al.* (2020) 'Extracellular vesicles released by melanocytes after UVA irradiation promote intercellular signaling via miR21', *Pigment Cell & Melanoma Research*, 33(4), pp. 542–555. doi: 10.1111/PCMR.12860.

Whitehouse, C. A. *et al.* (1998) 'Campylobacter jejuni Cytolethal Distending Toxin Causes a G 2 -Phase Cell Cycle Block', 66(5), pp. 1934–1940.

Wijdicks, E. F. M. and Klein, C. J. (2017) 'Guillain-Barré Syndrome', *Mayo Clinic Proceedings*, 92(3), pp. 467–479. doi: 10.1016/J.MAYOCP.2016.12.002.

Willms, E. *et al.* (2018) 'Extracellular vesicle heterogeneity: Subpopulations, isolation techniques, and diverse functions in cancer progression', *Frontiers in Immunology*, 9(APR), p. 738. doi: 10.3389/fimmu.2018.00738.

Wira, C. R. *et al.* (2005) 'Innate and adaptive immunity in female genital tract: cellular responses and interactions', *Immunological Reviews*, 206(1), pp. 306–335. doi: 10.1111/J.0105-2896.2005.00287.X.

Woith, E., Fuhrmann, G. and Melzig, M. F. (2019) 'Extracellular Vesicles-Connecting Kingdoms', *International journal of molecular sciences*, 20(22). doi: 10.3390/IJMS20225695.

Wottrich, R., Diabaté, S. and Krug, H. F. (2004) 'Biological effects of ultrafine model particles in human macrophages and epithelial cells in mono- and co-culture', *International Journal of Hygiene and Environmental Health*, 207(4), pp. 353–361. doi: 10.1078/1438-4639-00300.

Xu, J. and Xu, Y. (2017) 'The lncRNA MEG3 downregulation leads to osteoarthritis progression via miR-16/SMAD7 axis', *Cell and Bioscience*, 7(1). doi: 10.1186/s13578-017-0195-x.

Yamada, T. *et al.* (2006) 'Variation of loop sequence alters stability of cytolethal distending toxin (CDT): crystal structure of CDT from Actinobacillus actinomycetemcomitans.', *Protein science : a publication of the Protein Society*, 15(2), pp. 362–72. doi: 10.1110/ps.051790506.

Yaniv, Y. *et al.* (2010) 'Matching ATP supply and demand in mammalian heart: In vivo, in vitro, and in silico perspectives', *Annals of the New York Academy of Sciences*, 1188(410), pp. 133–142. doi: 10.1111/j.1749-6632.2009.05093.x.

Yao, Z. *et al.* (2018) 'Exosomes Exploit the Virus Entry Machinery and Pathway To Transmit Alpha Interferon-Induced Antiviral Activity', *Journal of Virology*, 92(24). doi: 10.1128/jvi.01578-18.

Ye, X. *et al.* (2020) 'Clinical significance of high expression of proliferating cell nuclear antigen in non-small cell lung cancer', *Medicine*, 99(16), p. e19755. doi: 10.1097/MD.0000000000019755.

Yoshimoto, S., Okada, K. and Hayashi, O. (2019) 'Immuno-regulatory and anti-inflammatory actions of phycocyanin on Caco-2/U937 cells co-culture as a model of the intestinal barrier', *Functional Foods in Health and Disease*, 9(7), p. 466. doi: 10.31989/ffhd.v9i7.611.

You, C. *et al.* (2016) 'Deregulation of the miR-16-KRAS axis promotes colorectal cancer', *Scientific Reports*, 6(1), pp. 1–12. doi: 10.1038/srep37459.

Young, K. T., Davis, L. M. and DiRita, V. J. (2007) 'Campylobacter jejuni: molecular biology and pathogenesis', *Nature Reviews Microbiology*, 5(9), pp. 665–679. doi: 10.1038/nrmicro1718.

Yuana, Y., Sturk, A. and Nieuwland, R. (2013) 'Extracellular vesicles in physiological and pathological conditions', *Blood Reviews*, 27(1), pp. 31–39. doi: 10.1016/j.blre.2012.12.002.

Zaborowski, M. P. *et al.* (2015) 'Extracellular Vesicles: Composition, Biological Relevance, and Methods of Study', *BioScience*, 65(8), pp. 783–797. doi: 10.1093/BIOSCI/BIV084.

Zamzami, N. *et al.* (1995) 'Sequential reduction of mitochondrial transmembrane potential and generation of reactive oxygen species in early programmed cell death', *Journal of Experimental Medicine*, 182(2), pp. 367–377. doi: 10.1084/jem.182.2.367.

Zeng, X., Zhang, Y. and Nyström, A. M. (2012) 'Endocytic uptake and intracellular trafficking of bis-MPA-based hyperbranched copolymer micelles in breast cancer cells', *Biomacromolecules*, 13(11), pp. 3814–3822. doi: 10.1021/bm301281k.

Zhang, Y. *et al.* (2019) 'Alantolactone exhibits selective antitumor effects in HELA human cervical cancer cells by inhibiting cell migration and invasion, G2/M cell cycle arrest, mitochondrial mediated apoptosis and targeting Nf-kB signalling pathway', *Journal of B.U.ON.*, 24(6), pp. 2310–2315.

Zhang, Y., Li, G. and Ji, C. (2018) 'Inhibition of human cervical cancer cell growth by Salviolone is mediated via autophagy induction, cell migration and cell invasion suppression, G2/M cell cycle arrest and downregulation of Nf-kB/m-TOR/PI3K/AKT pathway', *Journal of B.U.ON.*, 23(6), pp. 1739–1744.

Zorov, D. B. *et al.* (2000) 'Reactive oxygen species (ROS)-induced ROS release: A new phenomenon accompanying induction of the mitochondrial permeability transition in cardiac myocytes', *Journal of Experimental Medicine*, 192(7), pp. 1001–1014. doi: 10.1084/jem.192.7.1001.

Zorov, D. B., Juhaszova, M. and Sollott, S. J. (2014) 'Mitochondrial reactive oxygen species (ROS) and ROS-induced ROS release', *Physiological Reviews*. American Physiological Society, pp. 909–950. doi: 10.1152/physrev.00026.2013.

Zorova, L. D. *et al.* (2018) 'Mitochondrial membrane potential', *Analytical Biochemistry*, 552, pp. 50–59. doi: 10.1016/j.ab.2017.07.009.

**ACKNOWLEDGMENTS**

I would like to acknowledge my advisor Prof Francesca Luchetti for giving me the opportunity to grow professionally.

Moreover, I would like to extend my gratitude to my co-advisor Prof Barbara Canonico for lovingly teaching me her scientific knowledge and for the continuous motivation during my Ph.D study.

I would like to thank Prof Stefano Papa, Prof Claudio Ortolani and Prof Loris Zamai to always make me participate in the fantastic world of flow cytometry.

I would like to express my acknowledgement to Prof Michele Guescini for his significant contribution to the research.

I wish to thank Doctor Sabrina Burattini, Doctor Caterina Ciacci and Doctor Raffaella Campana for their support.

I also would like to thank Doctor Federica Sola for support and friendship during this journey.

I would like to give a special thanks to Doctor Erica Cesarini, who has been a fundamental source of inspiration and for her precious support.

I would like to thank Prof Ozan Gundogdu for his critical and constructive contribution.

Lastly, my sincere thanks go to all my family and all my friends who never let me give up and constantly motivated.